NASA Technical Memorandum 86548

Space Processing Applications Rocket (SPAR) Project

SPAR X Final Report

JULY 1986

NASA

NASA Technical Memorandum 86548

Space Processing Applications Rocket (SPAR) Project

SPAR X Final Report

R. Poorman, *Compiler*
George C. Marshall Space Flight Center
Marshall Space Flight Center, Alabama

NASA
National Aeronautics
and Space Administration
Scientific and Technical
Information Branch
1986

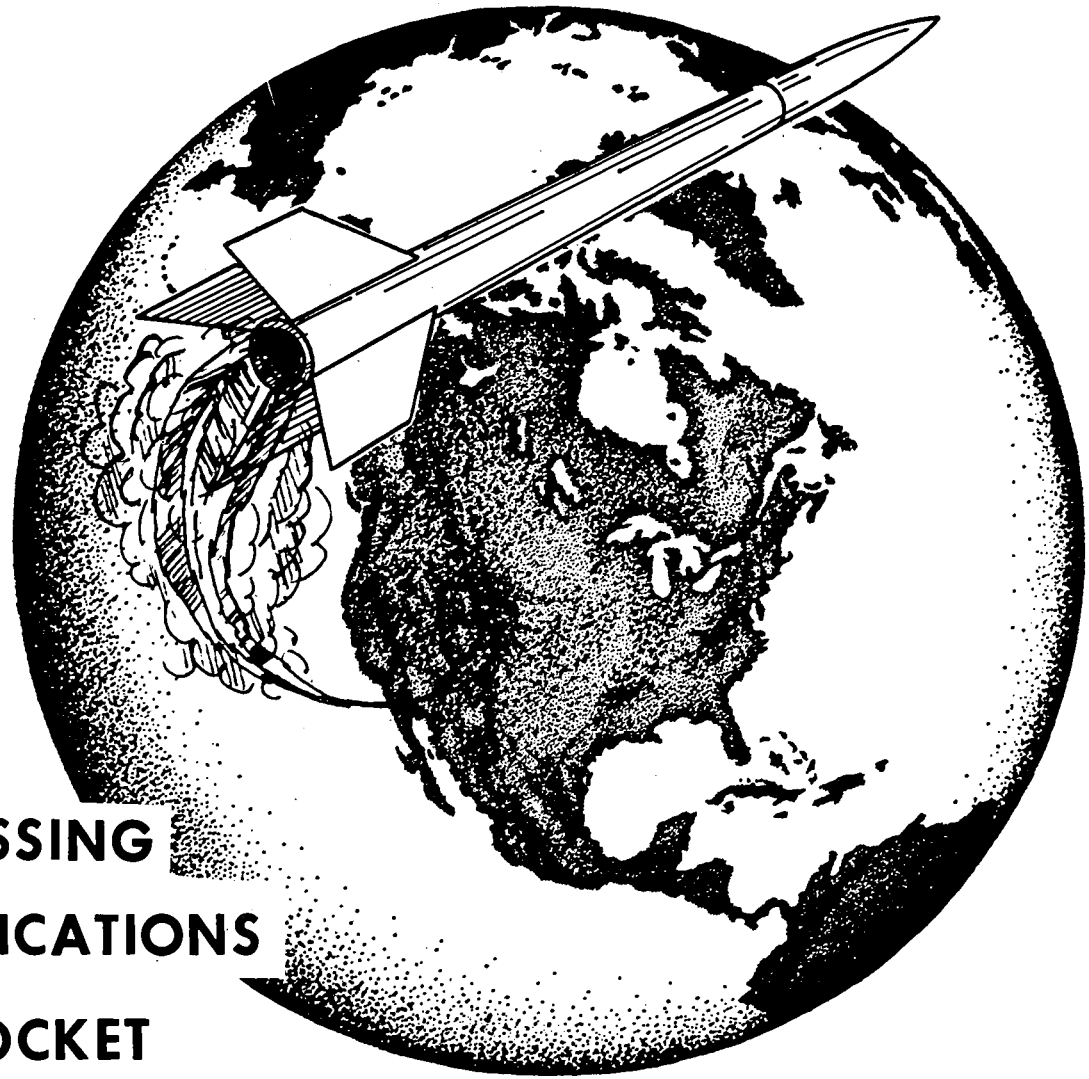

SPACE PROCESSING APPLICATIONS ROCKET

ACKNOWLEDGEMENTS

The Applications Payload Projects Office would like to acknowledge some of the major contributors to SPAR X (R-20) payload integration, checkout, and launch activities. They are:

MSFC:
- Carl Gibson
- John Noel
- Roy Darrell
- Ricky Welch
- Bill Smoot
- Bill Sutherland
- Ben Ondrak
- Bill Cobb

GSFC:
- Val Maksimovic
- George Kraft

WSMR:
- Gunner Briggs

TABLE OF CONTENTS

TECHNICAL MEMORANDUM

SPACE PROCESSING APPLICATIONS ROCKET (SPAR) PROJECT

SPAR X (R-20) - FINAL REPORT

SECTION I. INTRODUCTION

The unique low-g environment of space affords an opportunity for exploring and developing techniques for processing a variety of materials without the constraining gravitational influences as evidenced with the processing of liquid phase materials or melts on Earth. The Materials Processing in Space (MPS) program is directed toward the stimulation and development of the associated science and technology required to pursue these investigations. This NASA activity is undertaken in cooperation with the scientific community and includes follow-on studies of specific areas of scientific research emphasizing those selected investigations of materials and processes which best demonstrate potential benefit from the enhanced sensitivity of the controlled processing in a low-g environment. Examples of interest in the program are the reduction and/or elimination of adverse thermal effects such as convection, sedimentation of heavy particles, buoyancy rise and positioning aspects of bubbles in liquids or melts, and the stratification effects of particulates of variable densities in solution. These and similar studies are considered to be the means to expand the limiting frontier in the development of new materials and processes which are envisioned ultimately to be of benefit to mankind. As complementary to the research and technological nature of the investigations, the evolving emphasis is being directed, with the advent of the Shuttle and increased payload potential, toward the development of self-sustaining programs yielding direct product benefit.

The initial precursory zero-g demonstrations and investigations associated with this family of scientific experiments were proposed and developed for the Apollo flights beginning in the late 1960's and continued with Skylab and Apollo-Soyuz flights through the mid-1970's. During the period between the close of that era and the orbital space flights on the Space Shuttle in the 1980's, the Space Processing Applications Rocket (SPAR) project has provided the only viable flight opportunity for low-g scientific investigations for experimenters, and has served in a precursory role for planned and approved Shuttle investigations.

The SPAR project is part of the MPS program of the Office of Space Science and Applications (OSSA) which is responsible for directing research into the scientific effects of materials processing in the unique environment of space. This effort involves participation and interaction from various disciplines of the scientific community, government-supported laboratories, universities, and industrial organizations, in addition to foreign participation.

The Black Brant VC (BBVC) sounding rocket series, which is currently the carrier vehicle for the scientific payloads, with a Nike-boosted configuration available for heavier payloads, provides the opportunity to process materials in a low-g environment for periods up to 5 min in duration during a sub-orbital flight.

The rocket flights, which are conducted at White Sands Missile Range (WSMR) in New Mexico, afford experimenters and apparatus developers a flight opportunity

for a proof-of-concept verification and/or refinement of equipment operation and procedures prior to the longer duration, more sophisticated Shuttle flights.

This SPAR flight, mission 27.072, which is the tenth in a planned series of rocket flights, occurred on June 17, 1983, and carried four experiments. The investgations for the experiments comprising the payload manifest are managed and coordinated by the Application Payload Projects Office of the Marshall Space Flight Center (MSFC).

Previous experiments flown on the SPAR flights include the measurement of liquid mixing due to spacecraft motion; the dispersion of normally immiscible materials in the area of fluid dynamics; solidification experiments involving gravitational effects on dendritic growth, epitaxial growth, and solidification of eutectic materials with widely differing densities; and, solidification studies of interactions between second-phase particles and an advancing crystal-liquid interface and gravity-induced convection on cast microstructures. In the area of multiphase particle interaction, various experiments were conducted on the migration and coalescence of bubbles and particles, closed-cell metal foam, and the dispersion strengthening of composites.

The SPAR project has been increasingly active in supporting research in the promising area of containerless processing with previous flights, including experiments on cast beryllium and the processing of amorphous ferro-magnetic materials in an electromagnetic field, and control of liquid droplets by an acoustic field in the furtherance of the state-of-the-art of acoustic containerless processing technology.

The SPAR flights have, through an evolutionary program addressed experiments of increasing complexity and refinement and have afforded additional flight opportunities consistent with the maturity of each investigation. The payloads selected for this SPAR X flight manifest were based on the advanced state-of-the-preparedness of their ground-based research activity.

The following experiments are included in this report:

- "Comparative Alloy Solidification" (Experiment No. 76-36) investigating casting phenomena of metal alloys, solidifying aluminum-copper.
- "Foam Copper" (Experiment 77-9) investigating a closed cell metal foamed in low-gravity.
- "Containerless Processing Technology" (Experiment No. 76-20), illustrating stability, oscillation, and rotation as the three major aspects of containerless processing technology in space.
- "Directional Solidification of Magnetic Composites" (Experiment 76-22), searching for unique magnetic properties.

The post-flight results and analyses of each experiment flown on SPAR X as prepared by the respective flight investigators, in addition to an engineering report on the performance of the SPAR X Science Payload, are contained in separate sections of this technical memorandum. With the successful completion of this flight and subsequent data analysis, much useful data and information were accumulated for directing and developing experimental techniques and investigations toward an expanding, beneficial program of materials processing in the Shuttle era.

SECTION II. SPAR X POST-FLIGHT ENGINEERING REPORT

1.0 SUMMARY

The SPAR X (R-20) Nike-Black Brant VC rocket was launched from White Sands Missile Range (WSMR), New Mexico, at 9:00 a.m. MST on June 17, 1983. The 470 kg (1034 lb) gross payload achieved an apogee of 211.6 km (131.5 statute miles); and a low-g period of 302 sec. The launch was successful and the payload was recovered intact.

2.0 SPAR X (R 20) PAYLOAD CONFIGURATION

The SPAR X (R-20) science payload consisted of four materials experiments, the Experiment Support Module (ESM), and the Abbreviated Measurement Module (AMM). The SPAR X experiments are:

76-22/3 Directional Solidification of Magnetic Composties

76-36/3 Comparative Alloy Solidification

77-9 Foam Copper

76-20/3 Containerless Processing Technology

The orientation of the experiments within the SPAR X rocket vehicle is shown in Figure 2-1.

3.0 ROCKET PERFORMANCE

3.1 Flight Sequence

The SPAR X flight profile is shown in Figure 2-2. The actual sequence of events are shown as a function of flight time.

3.2 Low Gravity

The low-g (10^{-4} or less) period was 302 sec. The minimum low-g period required by experiments was 292 sec. The gross payload weight was 470 kg (1034 lbs).

4.0 PAYLOAD SUPPORT

4.1 Payload Sequence of Events

Experiment 76-36 and 76-22 required preheat power prior to launch that was supplied by ground power, beginning at T-90 min and T-30 min, respectively. Experiment 77-9 was activated at T-70 sec. At T-0, a lift-off signal was given which activated a timer within all experiments for control of events during the flight. The power removal to all experiments occurred at 727 sec. All payload events sequenced as planned.

SPAR X R20
SCIENCE PAYLOAD

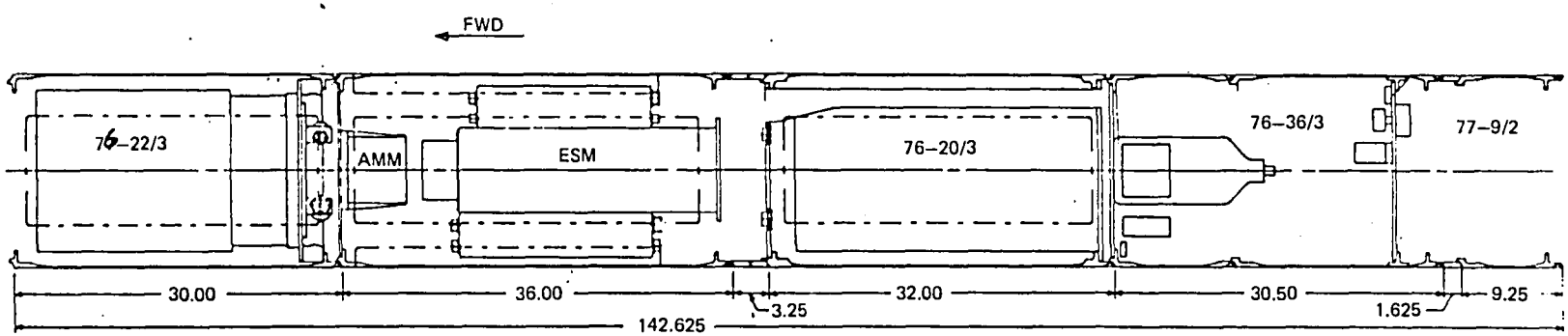

Figure 2-1. Experiment arrangement within the payload.

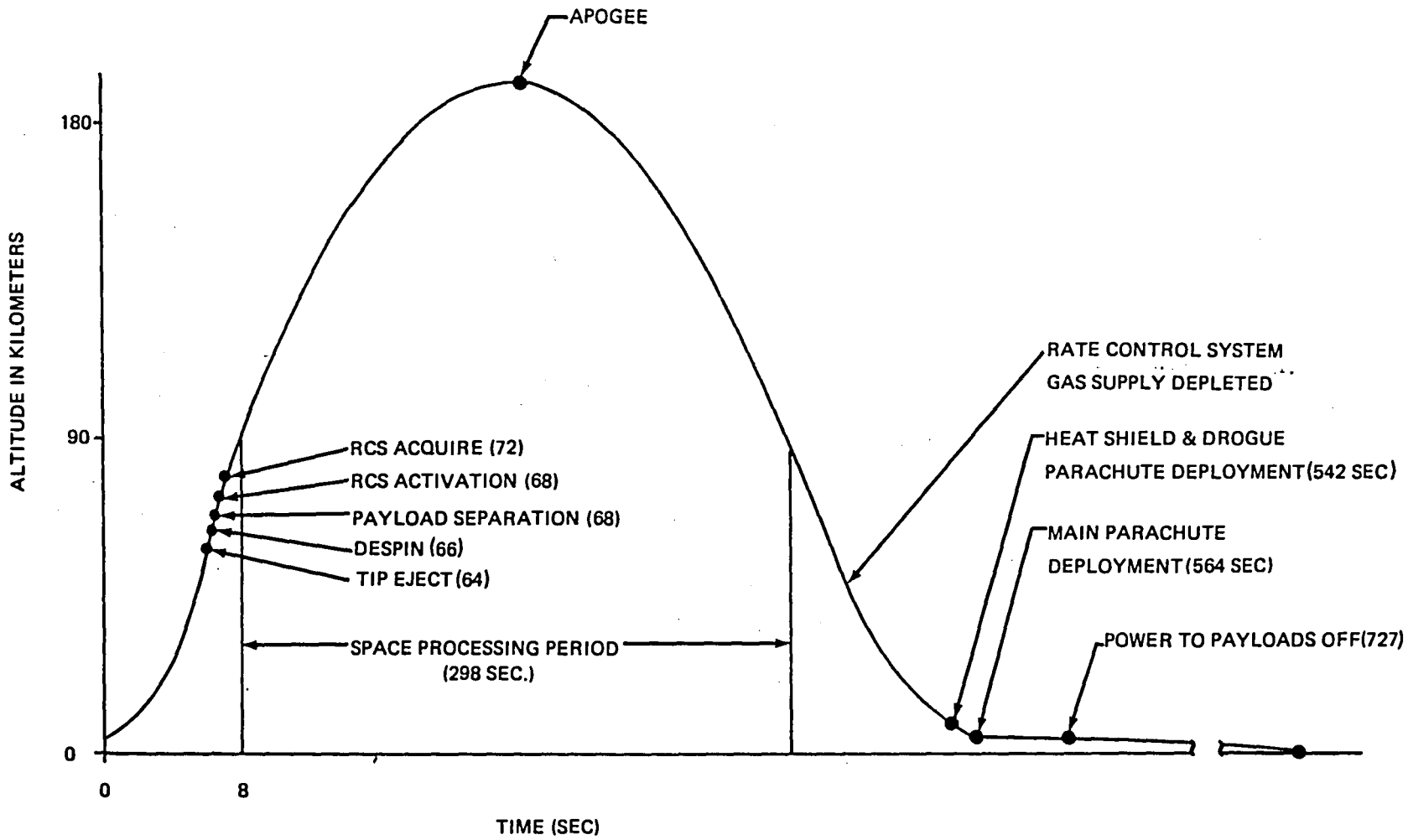

Figure 2-2. Flight profile and events.

4.2 Payload Power

Transfer of electrical power from ground support equipment to the flight battery was accomplished at 2 min prior to launch. The science payload battery, located in the Experiment Service Module (ESM), supplied power to all experiments. Battery voltage measurement (M001-SM) indicates that the battery voltage was 35.0 v at lift-off. The bus voltage remained within allowable limits throughout the flight. Both voltage and amperages were as planned in the flight timelines.

It might be noted that the battery at flight time was several months past its normal shelf life. However, preflight testing and detailed storage temperature history indicated it to be satisfactory for this flight power load. Its flight preformance was very satisfactory.

5.0 EXPERIMENTS

5.1 Experiment 76-22/3: Directional Solidification of Magnetic Composites

This experiment utilizes four furnaces, each traveling along an experiment sample which is mounted on the furnace axis. The objectives are:

1) Determine whether low-g processing offers substantial improvement over one-g processing in the development of high coercive force magnetic composites.

2) Determine whether terrestrial analytical theory is inadequate and should be amended.

3) Determine whether the processed $(G/R)^{-\frac{1}{2}}$ functionality is significant to the performance of magnetic composites or whether it is simply an interface stability criterion.

4) Test the existing theories of directional solidification against experimental data in the region where the theoretical predictions diverge.

5) Determine whether gravitational level plays a role in the dendritic to cooperative growth transition.

6) Determine whether gravitational level influences interparticle spacing and particle diameter for eutectic and off-eutectic compositions.

7) Determine the effect of gravity reduction on particle ripening for off-eutectic compositions.

There had been two previous flights of this experiment hardware configuration. In preparing for these two flights, there has been a continuing problem in ground tests wherein slower than planned or erratic furnace travel speeds occurred after long hardware storage periods. On such occasions, the moving parts were then cleaned and/or relubricated and the problem seemed to have been resolved in each case. In the SPAR X prelaunch testing between January 1983 and launch, June 17, 1983, these problems became more persistant. The symptoms appeared even more pronounced when the furnace was hot. Efforts were made to use improved lubricants. However, a more detailed look at the problem showed the furnace drive shaft torque requirement to be very temperature dependent. It was later measured to be 64 g cm

(12 in./oz) at 20°C and 13,961 h vm (180 in./oz) at 73°C. There was drive belt slippage at the 12,961 g cm (180 in./oz) value.

Based on the discovery of temperature dependence of the drive shaft torque, MSFC recommended a 20 min prelaunch furnace heat period instead of the 120 min planned preheat. The Principal Investigator (PI) agreed to change his requirement of 120 min preheat to 30 min; the 30 min preheat was actually used and the in-flight data and furnace apparatus appears normal.

Post-flight furnace drive shaft torque tests were made and the data given to the hardware developer for use in preparing a hardware modification so that this procedural workaround used on SPAR X would not be necessary for future flights of the ADSF.

5.2 Experiment 76-36/2: Comparative Alloy Solidification

This experiment used aluminum and 5 percent copper to continue the low-g study of casting phenomena by investigating the solidification of selected metal alloys during the weightless period of a SPAR sounding rocket flight. Other objectives of this experiment included the verification of the conclusions of SPAR Experiment 74-21 by solidifying metallic alloys in the 76-36 hardware and obtaining quantitative segregation data as a function of gravity. All inflight data appears normal.

5.3 Experiment 77-9/IR, "Foam Copper"

This experiment utilized a newly developed "Low Gravity Exothermic Heating/Cooling Apparatus," U.S. Patent Number 4,513,810. It was initiated some 70 sec before launch. The "Foam Copper" sample was heated from ambient to 1050°C. Melting took place after the low gravity period of the flight started, T = 86 sec. Peak temperature of the sample was planned to be 1200 to 1300°C and the sample was to resolidify before the low gravity period ended, T = 397. Preliminary examination of the flight sample by the principal investigator indicated these flight requirements were met.

5.4 Experiment 76-20/3: Containerless Processing Technology

This experiment utilized the Jet Propulsion Laboratory (JPL) Acoustic Levitation Space Processing Rocket Instrument (ALSP) for the purpose of investigating the stability and manipulability of a liquid drop. The primary objectives of this flight were to:

1) Demonstrate the transport capability of the acoustic chamber for collision and coalescence of quiescent drops.

2) Study the mixing effects generated by collision and coalescence of oscillating drops.

3) Study the shift of natural frequencies of drop oscillation as a function of oscillation amplitude.

Telemetry data indicates all program sequences operated as planned, except the on-board camera failed at about T + 107 sec. This is 20 sec after the camera was started. All preflight checks had shown normal camera operation; it had operated

for about four complete flight sequences in ground checks since January 1983. During final prelaunch preparations in the launch tower, the camera was successfully cycled three times for 5 sec each.

Post-flight failure analyses indicated the film take-up spool had malfunctioned and film had jammed in the camera. Flight film development showed all functions normal before the film jammed and was torn at the film advance sprocket.

6.0 INSTRUMENTATION

6.1 Low-G Acclerations

The low-g data indicates that a low-g environment considerably less than 1×10^{-4} g was achieved in all three axes (Figs. 2-3, 2-4, and 2-5). The X-axis Linear Acceleration Measurement (A02-MM) indicates that low-g entry in that axis was at about T + 85 sec and exit at about T+ 395 sec with the g-levels during this period ranging from -0.9 to 0.4×10^{-4} g. The Y-axis (A03-MM) had low-g entry at T + 77 sec and exit at T + 388 sec. The Z-axis Linear Acceleration Measurement (A04-MM) indicates the low-g entry in that axis as 86 sec and exit at 397 sec. These values indicate a total low gravity period (less than 1×10^{-4} g's in all axis) of 302 sec.

6.2 Pressures and Temperatures

All on-board pressures and engineering temperatures were normal and comparable to earlier SPAR flights.

7.0 PAYLOAD RECOVERY

The R-20 payload landed approximately 82 km (51 miles) and on a 341 deg magnetic radial from the launch site. The landing site was flat sand. The payload landed on its aft end, sinking approximately 15 cm into the semi-soft gypsum. The payload fell to the northwest and came abruptly to rest on the flat soil. The parachute was stretched out northwest of the payload. There appeared to be no major visible damage to the payload. The electrical safing box was used to ensure the payload was de-energized.

The parachute lines were then detached from the four webbed risers and the payload was separated between Experiment 76-20 and the ESM. The two sections of the payload were lifted by a cargo helicopter and transported back to the Vertical Assembly Building of Launch Complex 36.

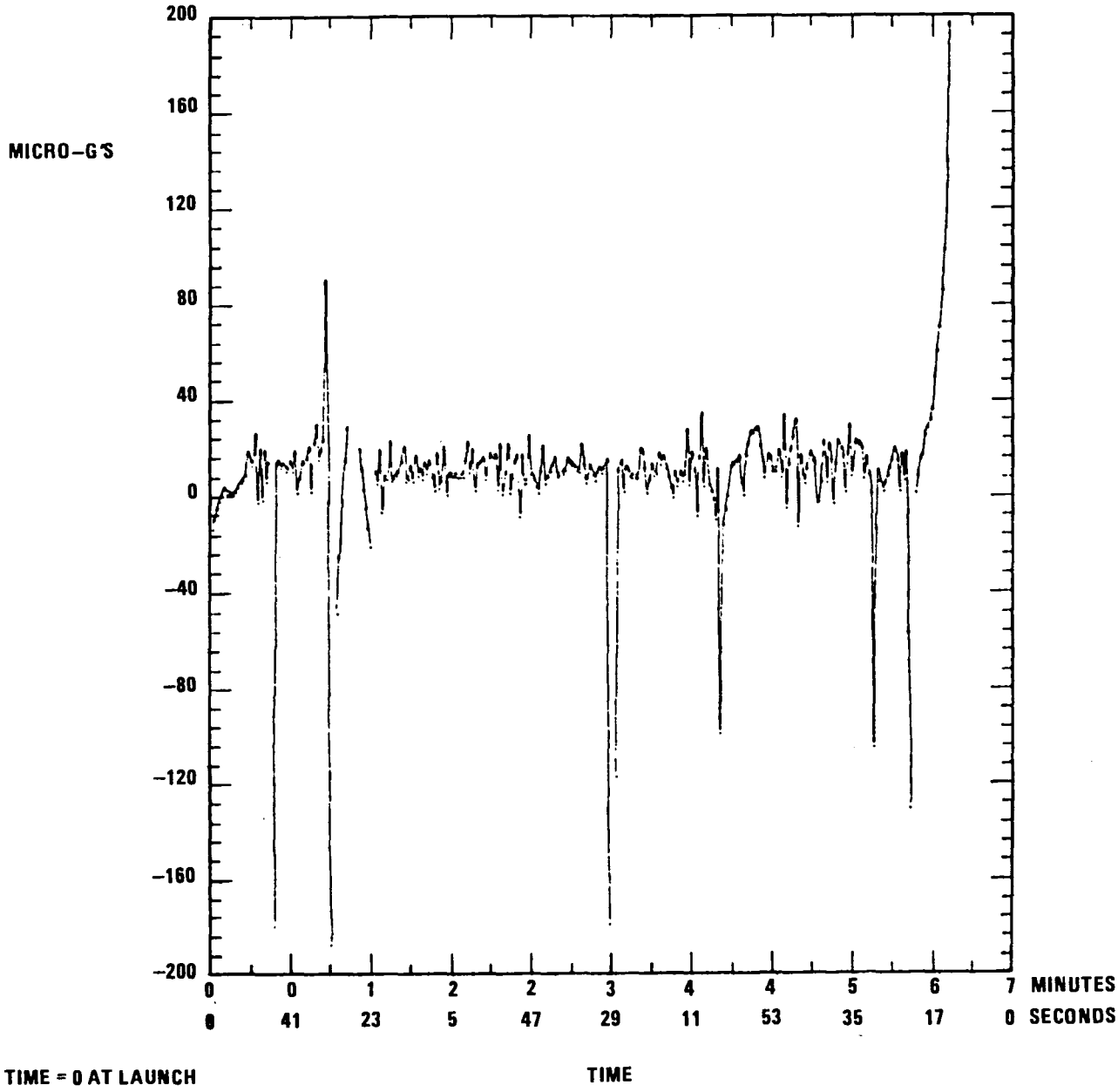

Figure 2-3. SPAR-X (R-20) accelerations, axis: -A 02-MM

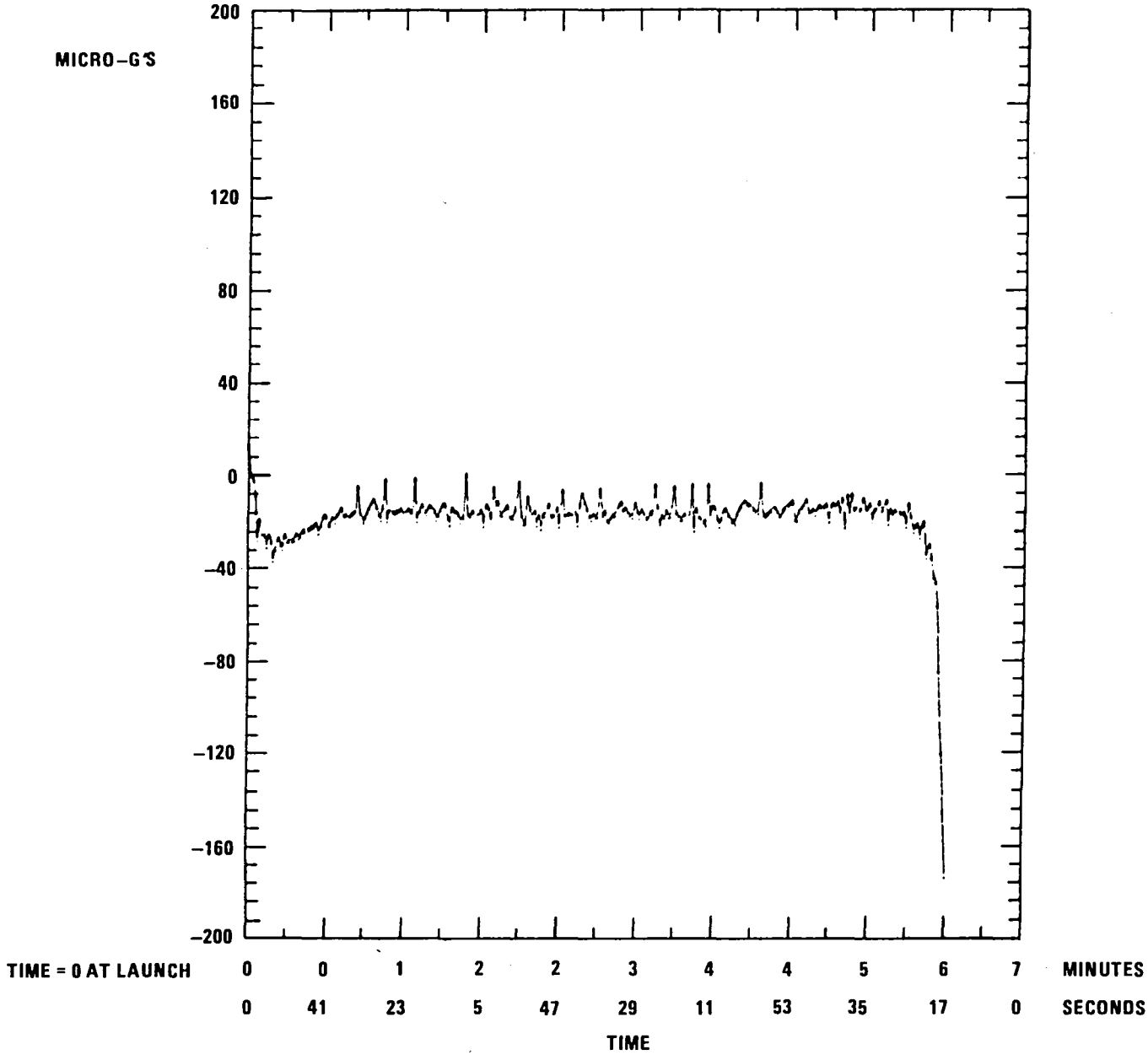

Figure 2-4. SPAR-X (R-20) accelerations, axis: -A 03-MM

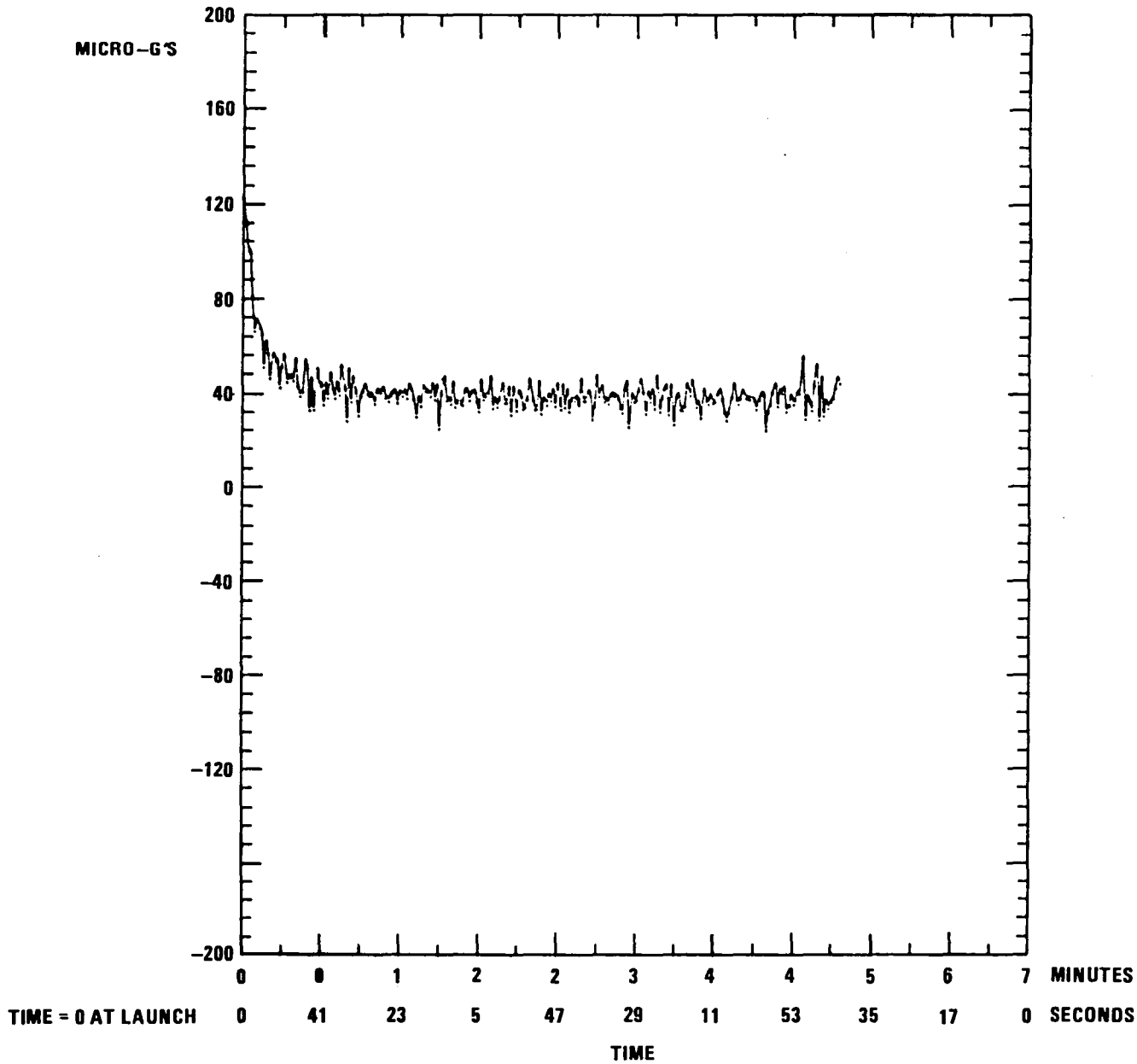

Figure 2-5. SPAR-X (R-20) accelerations, axis: -A 04-MM

SECTION III.

REPORT RE-691

SPAR X TECHNICAL REPORT FOR EXPERIMENT 76-22 DIRECTIONAL SOLIDIFICATION OF MAGNETIC COMPOSITES

NOVEMBER 1984

Post-Flight Technical Report on Contract NAS8-322119

prepared by

James Bethin

Materials & Structural Mechanics Directorate

Research and Development Center
Grumman Aerospace Corporation
Bethpage, New York 11714

prepared for

George C. Marshall Space Flight Center
National Aeronautics and Space Administration
Marshall Space Flight Center, Alabama 35812

ABSTRACT

The effects of gravity on Bridgman-Stockbarger directional solidification of off-eutectic Bi/MnBi has been studied in reduced gravity ($10^{-4} g_e$) aboard the SPAR X flight and compared to normal-gravity investigations and previous eutectic Bi/MnBi SPAR flight experiments. The directional solidification of off-eutectic Bi/MnBi results in either a dendritic structure connected with local cooperative growth or, with the proper solidification conditions, a coupled low volume fraction faceted/nonfaceted aligned rod eutectic whose Mn macrosegregation, MnBi rod size, interrod spacing, thermal and magnetic properties are sensitive functions of the solidification processing conditions.

Two hypoeutectic and two hypereutectic samples were solidified during 605 sec of furnace travel, with an initial 265 sec low-gravity interval, at a growth rate 11 cm/h. Comparison Earth-gravity samples were solidified in the same furnace assembly under identical processing conditions. Macrosegregation in the low-$\bar{g}$ samples determined by magnetic measurements, microstructural analysis, X-ray fluorescence, and chemical spectrophotometric absorbance, was consistent with a metastable increase in Mn solubility in the Bi matrix, in partial agreement with previous Bi/MnBi SPAR findings of MnBi volume reduction. Smaller mean rod diameter and interrod spacing were found in solidification in low gravity, as compared to Earth gravity, in agreement with previous SPAR findings. In addition, in normal gravity, Mn macrosegregation results for the hypoeutectic samples suggest that the thermal instability led to greater convection than did the induced solutal instability. Convection in Earth gravity is suggested as an explanation of morphological differences between normal- and low-gravity solidification. This explanation is consistent with a possible change in the equilibrium solid solubility limit of Mn in Bi observed in low gravity.

INTRODUCTION

This work compares the Bridgman-Stockbarger directional solidification of the Bi/MnBi off-eutectic system in low gravity to that in Earth gravity. Low gravity provides both a scientifically-revealing and potentially advantageous modification of controlled directional solidification of binary alloys in Earth gravity. In alloys where the melt density depends on temperature and on solute concentration, convection which consequently occurs in the melt in Earth gravity is substantially reduced in low gravity. Of particular interest is the role of convection in solute macrosegregation and in the aligned morphology observed in off-eutectic cooperatively grown systems.

Controlled plane-front directional solidification near the Bi/MnBi eutectic (2.7 a/o or 0.72 w/o Mn) produces an aligned (cooperatively grown) array of highly magnetic MnBi rods, which are often faceted and chevron-shaped in cross section and have very large aspect ratios, in a Bi-matrix which appears unfaceted. The morphology (and therefore the magnetic properties) and the thermal history during growth have been shown [3-1 - 3-5] to be sensitively dependent on the growth parameters and the degree of convection. For example, in an Earth-gravity study of the solidification of the Bi/MnBi off-eutectic system, different orientations of the solidification direction with respect to the gravity vector have resulted in different degrees of thermal and solutal convective flow as reflected in macrosegregation curves. Previous low-gravity experiments [3-3 and 3-4] conducted on SPAR flights VI and IX

have shown reduced interrod spacing and rod diameters in low-gravity processed samples. In addition, a lower volume fraction of the MnBi phase and a larger interfacial undercooling, i.e., a lower solidification temperature, was found for low-gravity compared to Earth-gravity samples. It appears unlikely that either a modified temperature gradient [3-6] or a fluctuating interface speed induced by convective flow [3-7 and 3-8] will account for the reduction in the interrod spacings. The lack of understanding of the convective, thermal, and morphological effects of low-gravity processing have led to this directional solidification experiment in low and one gravity for the Bi/MnBi off-eutectic system.

Samples of 0.49 w/o and 0.90 w/o Mn were grown up and down with respect to the gravity vector, providing different degrees of thermal and solutal convection on the ground. The nominal value of the furnace velocity was 11 cm/h and that of the thermal gradient in the liquid ahead of the interface was 140°C/cm. This moderate furnace velocity was chosen to reach a balance between the desire to obtain a cooperative morphology using a low velocity and the need to solidify a useful length of sample in the low-gravity period of 5 min. Also, the highest possible thermal gradient was used to maintain a planar freezing interface and thus maximize the extent of the cooperative region in each sample. The objectives of this investigation included:

1) Determining the effect of a reduction in gravity on the macrosegregation of Mn, the thermal history during growth (cooling rate and undercooling), and the morphology of cooperatively grown off-eutectic smaples.

2) Determining the extent to which a reduction in gravity may alter the degree to which cooperative growth may be further stabilized.

3) Determining areas of special interest or problems associated with the Bi/MnBi off-eutectic system or hardware in preparation for longer periods of low-gravity Bi/MnBi processing experiments aboard the space shuttle.

BACKGROUND

OFF-EUTECTIC SOLIDIFICATION

Gravity-induced Mn macrosegregation throughout the length of a plane-front solidified Bi/MnBi sample has its origin in the thermal and/or solutal convection in the melt during the growth of the solid. When solidification of a sample in the Bridgman-Stockbarger method proceeds with the cold zone below the hot zone, a relative thermal stability is achieved (growth up). An unstable thermal situation is obtained in growth down, when the hot zone is below the cold zone, which induces thermal convective flow. It is also expected that a Bi-rich sample will exhibit solutal convection during solidification in the growth-up configuration in Earth gravity. This is expected because a Bi-rich sample rejects Mn from the solidification front as growth proceeds, up to the point where no Mn gradient exists in the liquid (i.e., the bulk liquid composition equals the eutectic composition). Similarly, a Mn-rich sample will reject Bi at the front resulting in a solutally unstable situation for growth down in Earth gravity giving rise to solutal convection. These types of convection give rise to macrosegregation in the Bi/MnBi off-eutectic system which has been treated theoretically with a simplified model by Verhoeven and Homer [3-9]. The result is an analytical expression describing the average solid composition as a

function of the fraction of the sample solidified. For a cooperatively grown, directionally solidified sample, the parameters from the fit to the experimental macrosegregation data give a measure of the degree of convective versus diffusive control over the solute redistribution.

A third source of macrosegregation which must be dealt with in this system is that arising from what is here termed gravity-driven Stokes migration. In $1\text{-}\bar{g}$ growth up of a Mn-rich sample, MnBi dendrites, which will form at the interface if the dendritic to cooperative transition has not been reached (see below), may be sheared off by convective flow or thermal instabilities and float toward the top of the melt, driven by buoyancy. Dendrites may also grow in the melt near the interface in the presence of constitutional supercooling and float toward the top of the melt. These migrated dendrites may re-dissolve or remain and possibly nucleate further dendrites as the interface again approaches. Thus, Stokes migration or flow could lead to a gross disturbance of the Mn macrosegregation in these cases. Stokes migration effects have been noted previously, for example, in monotectic solidification [3-10 and 3-11] and in dendritic growth in the SnPb system [3-12].

A previous study of the solidification of the Bi/MnBi off-eutectic system in Earth gravity has shown that under certain solidification conditions samples solidify first with MnBi dendrites (hypereutectic) or with Bi solid solution dendrites (hypoeutectic) and undergo a transition to cooperative growth as the solidification proceeds [3-1]. A quantitative description of the position at which dendrites disappear is possible. Some inconsistencies in the experimental results of Table 1 of Reference 3-1 have been corrected and a reevaluation of those results have led us to replace Figure 7 of Reference 3-1 with Figure 3-1 here. The solid lines for Bi-rich and Mn-rich cases are based on the assumption of dendritic growth for even negligible constitutional supercooling. The zero constitutional supercooling criterion [3-13] is described by

$$G/V = -m(C_E - C_S)/D \qquad (3\text{-}1)$$

where G is the thermal gradient in the liquid, V is the interface velocity, m is the slope of the appropriate liquidus, C_E is the eutectic composition, C_S is the average solid composition at a particular cross-sectional position, and D is the diffusivity of Mn in the melt, assumed to be 2×10^{-5} cm^2/sec. In the Bi-rich region the disappearance of dendrites is described well by equation (3-1). Although scatter is large in the Mn-rich system, it seems clear that the criterion of no constitutional supercooling with the currently used value of D underestimates the cooperative compositional range. This trend has been noted by other workers [3-14] and might be better accounted for by a competitive growth model [3-15 and 3-16]. This theory finds that a finite constitutional undercooling is possible at the interface before plane front growth becomes unstable. The dashed line is a linear least squares fit of the Mn-rich data which has been constrained to go through the eutectic composition and $G/V = 0$ point. In order to directionally solidify an entire sample without dendrites, G and V must be chosen to place the entire Mn composition profile, including the effects of convective flow on macrosegregation, above the data in Figure 3-1.

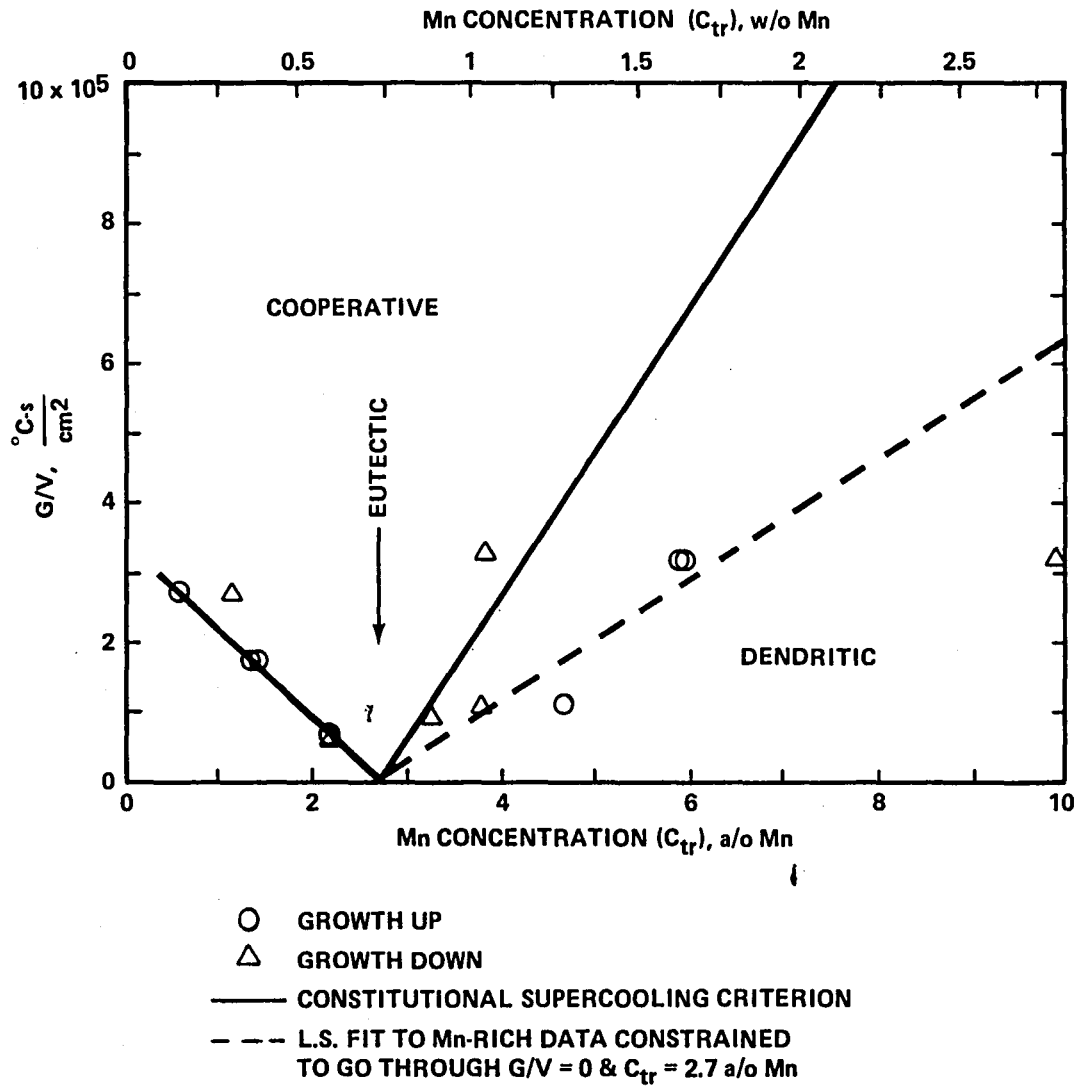

Figure 3-1. G/V versus average Mn composition at the position of dendritic-to-cooperative transition (C_{tr}) in 1-$\bar{g}$.

EUTECTIC SOLIDIFICATION

Low-gravity solidification of eutectic Bi/MnBi has been studied previously aboard the SPAR VI and SPAR IX flight experiments [3-3 and 3-4] with very interesting results which have significance for the solidification of the off-eutectic system. These results were contrasted to Earth-gravity solidification results and revealed:

- o A decrease in the mean MnBi rod diameter, d, and interrod spacing, λ, by almost 50 percent aboard SPAR IX and 40 percent in SPAR VI.
- o Lower volume fraction of MnBi by about 8 percent in SPAR IX and about 7 percent in SPAR VI.
- o Bi-rich like macrosegregation in low-gravity solidification of "eutectic" compositions.
- o Increased interfacial undercooling, ΔT, i.e., lower solidification temperature, in low-gravity solidification aboard SPAR IX, by about 5°C.

Quenisset and Naslain [3-17] have developed a theoretical approach to lamellar eutectic growth which includes the effect of gravitationally induced convection parallel to the solidification interface. The artificial, simplifying assumption of a stagnant boundary layer is dropped, with the new model leading to a characteristic diffusional length, $\Lambda/2$, smaller than found in other growth models. This model predicts a decrease in λ and an increase in ΔT as the fluid flow velocity decreases, such as is expected in low gravity. Baskaran et al. [3-8] found a similar result. This is in qualitative agreement with the previous SPAR experimental eutectic findings.

An effect of an increased undercooling in low gravity would be an adjustment in the phase diagram near the eutectic and the solid solubility limit of Mn in Bi. Metastable extensions of the various phase lines to accommodate the lower freezing temperature could change both the eutectic composition and the solid solubility limit. These compositional changes may be substantial since this eutectic system has a rather low minor phase volume fraction. Therefore, samples with 0.72 w/o Mn (eutectic in Earth gravity) might conceivably directionally solidify in space as perceptibly Bi-rich, off-eutectic compositions, with a Bi solid solution phase enriched in Mn. Decreased MnBi volume fraction and Bi-rich type macrosegregation were observed experimentally, and will be commented on later. Of course, any low-gravity induced phase diagram changes will also be reflected in solidification of nominal off-eutectic compositions.

The total undercooling of the eutectic interface in any of the numerous analyses is a function of interface velocity, V, (for example, Reference 3-17):

$$\Delta T = K_1 V\lambda + \frac{K_2}{\lambda} + \Delta T(V) \qquad (3\text{-}2)$$

where K_1 and K_2 are constants and $\Delta T(V)$ is a kinetic undercooling term. The first term is the constitutional undercooling and the second term is the curvature undercooling due to the Gibbs-Thompson effect. For regular eutectics, which grow with a minimum undercooling, this reduces to $\Delta T = 2(K_3K_4)^{1/2}V^{1/2}$, with $\lambda^2 V = K_4/K_3$.

An argument previously suggested to explain the SPAR Bi/MnBi eutectic experiments [3-4] notes that temperature fluctuations in the melt, caused by turbulent convection when the thermal gradient exceeds a critical value, may induce nonsteady-state interface motion. It was argued that if the eutectic nucleation or branching proceeds more slowly than MnBi rod termination, then the mean interface growth velocity might decrease in the presence of this supercritical convection. By the above equations it can be seen that if this supercritical convection is achieved at Earth gravity, then λ will be larger and ΔT will be smaller in Earth gravity compared to low gravity. This will also account for the observed phenomena in the previous SPAR experiment. This explanation, however, now seems somewhat less likely with the finding that the MnBi rod spacing was able to adapt more rapidly than the freezing rate could be changed in a recent experiment [3-7]. Therefore, in the present and upcoming experiments, we would particularly like to test the idea of an increased undercooling in low gravity which modifies the phase diagram in the Bi/MnBi system.

EXPERIMENTAL PROCEDURE

SAMPLE PREPARATION AND DIRECTIONAL SOLIDIFICATION PROCESSING

Off-eutectic Bi/MnBi ingots of 0.90 and 0.49 w/o Mn were made using commercially pure Mn (99.9 w/o) and high purity Bi (99.999 w/o) by induction heating in evacuated and sealed 4 mm inner-diameter quartz tubes and quenching by turning off the coil power. Ingot lengths were about 2.5 cm. A 1/4-mm diameter hole was drilled about 1 cm deep to place one 0.004 cm bead-diameter chromel-alumel thermocouple in each ingot. Each starting ingot was encapsulated in an evacuated 4 mm inner diameter quartz ampoule as described previously [3-2 and 3-3].

Samples were directionally solidified using the Bridgman-Stockbarger technique in furnace assemblies built by General Electric [3-18]. The same unit with identical parameters was used for both low-gravity and Earth-gravity comparison solidifications. The apparatus, referred to as the ADSS, Automatic Directional Solidification System, consisted of four furnace assemblies mounted symmetrically with their longitudinal axes parallel. Opposite assembly pairs moved in unison and in the opposite direction from the other furnace pair to keep total apparatus momentum equal to zero. On the ground, this feature was used to solidify compositions parallel and antiparallel to the gravity vector in order to create differing amounts of convection in the melt. For both flight and ground-based solidification, furnaces No. 1 and 2 contained samples No. 1 and 2 of composition 0.90 w/o Mn and furnaces No. 3 and 4 contained samples No. 3 and 4 of composition 0.49 w/o Mn. On the ground, furnaces No. 1 and 3 solidified samples up (antiparallel to the gravity vector) and furnaces No. 2 and 4 solidified samples down (parallel to the gravity vector).

The furnace assemblies were capable of producing a planar solidification interface near the equilibrium solidification temperature of 265°C with gradients of 20 to about 150°C/cm and furnace velocities of 0.3 to 5 cm/h. For this experiment, nominal values of 140°C/cm and 11 cm/h were chosen. The furnace translated along the stationary tubular quartz sample ampoule described above. A description of the methods of monitoring the furnace and sample temperatures and velocities during solidification has been given previously [3-19].

EARTH-GRAVITY AND FLIGHT EXPERIMENTS

Off-eutectic Bi/MnBi samples were directionally solidified in low gravity aboard the SPAR X flight on June 17, 1983. Prior to the launch, persistent problems with ground-based tests using the flight furnace assembly extended over several months, preventing a flight-comparison, ground-based solidification experiment (referred to as the All-Systems Test) from being run prior to the launch. A post-launch solidification experiment with SPAR X processing parameters was performed on the ground at Marshall Space Flight Center for comparison to the low-gravity results. One sample of each composition was solidified up and one down with respect to the gravity vector.

The SPAR X flight experiment began on the ground with a 30 min furnace warmup, reduced from the originally desired 120 min by the same prelaunch problems of persistently erratic furnace motion. Before previous SPAR launches using this assembly, cleaning and relubrication of moving parts had alleviated any problems with erratic furnace velocity. This same problem was noted before the SPAR X launch but was found to become critical when the furnace was hot. Prelaunch experiments suggested that reducing the warmup time from 120 to 30 min should be adequate for the furnaces to reach the desired maximum temperature and would allow the furnace motion to become more regular. It is noted here that this problem has been repaired for the space shuttle apparatus by the use of low thermal expansion, metal-impregnated nylon drive bushings. After launch, directional solidification began 38 sec after $10^{-4} g_e$ was obtained. The solidification time interval in low gravity was 265 sec (approximately 0.81 cm furnace travel) and furnaces were stopped after 604 sec of total furnace travel time.

Ground-based sample No. 2 solidified in a fashion to be described later which was inadequate for study. Therefore, a replacement sample was solidified in our laboratories at Grumman Aerospace Corporation using a furnace built by GE as a prototype to the ADSS flight furnaces and conditions which were nominally identical to those of the flight.

POST-SOLIDIFICATION SAMPLE HANDLING

Each SPAR X ground-based and flight sample was first polished shallowly lengthwise to inspect for solidification irregularities and dendritic growth. Samples were scribed on one side for identification and were then partitioned into pieces about 0.3 cm long by a low speed cutoff wheel with a 0.035 cm thick diamond-impregnated copper blade. This resulted in about eight sections per sample. Sections were labeled according to flight or ground-based processed, furnace number, and position in sample, starting with the letter "A" at the first solidified end of the sample. Each section was cleaned, weighed, and its length measured. Sections were then ready for mounting for measurement of their magnetization.

Sections were prepared for microstructural examination by polishing the cross-sectional surface of each section away from the first solidified end (except for the last section). Sections were mounted in a cold plastic mounting compound, polished in a sequence ending with 0.05 μm Al_2O_3, and etched lightly with a 10 percent solution of acetic acid in water. A morphological analysis was then conducted for each sample. A few selected sections were broken out of mounts and then heat treated at

250°C for 36 to 48 hr, and reexamined magnetically and microstructurally. All sections in plastic mounts were given a light refinishing on 600 paper to remove the etched surface layer and were then examined by X-ray fluorescence. In addition, two sections were broken out of their plastic mounts, cleaned in acetone, and destructively chemically analyzed.

MAGNETIC PROPERTY, MORPHOLOGICAL, CHEMICAL AND THERMAL ANALYSIS

Magnetic properties were determined for each section from the measured magnetizations, which were measured as a function of the applied magnetic field at the Francis Bitter National Magnet Laboratory. Measurements were made parallel to the aligned microstructure at room temperature in applied fields typically up to 150 kOe using a low frequency vibrating-sample magnetometer. At room temperature three magnetic phases have been shown previously to coexist in directionally solidified Bi/MnBi [3-2, 3-5 and 3-20]. The matrix, Bi solid solution, is diamagnetic with a (negative) susceptibility which is weakly dependent on Mn concentration. The expected equilibrium MnBi phase is strongly ferromagnetic and is referred to as the low temperature phase (LTP). A new, second MnBi phase, referred to as the high coercivity phase (HC) due to its large intrinsic coercivity at cryogenic temperatures where it is ferromagnetic, was found to be metastable and paramagnetic at room temperature. These three phases are magnetically additive at room temperature which allows the separation of the effects of each phase. The ferromagnetic character of the equilibrium MnBi phase can provide a measure of the effect of solidification processing on MnBi rod size and alignment. For example, as the rod diameter approaches the magnetic domain size, the resistance to demagnetization or intrinsic coercivity of a sample containing only LTP MnBi approaches the theoretical maximum of 35 kOe [3-4]. Also, dendritic samples will exhibit a decreased remanent magnetization and intrinsic coercivity. In previous work, the separate hysteresis curves of the LTP and HC phases at 77 K were used to determine the amount of each magnetic phase and hence the total volume fraction of MnBi [3-21] or the composition of samples in an off-eutectic experiment [3-1]. Using the parameters for the magnetic phases found in this previous work and the assumption of 0.11 w/o Mn in the Bi solid solution, the magnetization at room temperature has been used to determine magnetic phase and chemical composition of each sample in this study. This involved an iterative approach in which the volume fraction MnBi was first calculated. A first approximation of the amount of Bi solid solution was then returned with its diamagnetic contribution into the calculation of the volume fraction MnBi, the process being repeated until self-consistency was achieved. Figure 3-2 illustrates the separation of the magnetic MnBi phases from the magnetization data for flight sample No. 2 section A. Figure 3-2(a) shows the magnetization data normalized to sample weight, including a linear least squares fit to the data between 80 and 150 kOe where the hysteresis curve saturates. This fit was used to obtain the representation of the magnetization due to LTP and HC phases for this section as shown in Figure 3-2(b). Small section size meant that significant noise was present in the magnetization data which resulted in a typical uncertainty of ±5 percent in Mn composition values.

Microstructural and quantitative MnBi rod diameter and interrod spacing analyses were performed using a computer-aided Leitz particle analysis system. Approximately 2000 rods in 10 to 20 different views of a section surface were analyzed directly from a live video camera image, which allowed great control over focus, contrast, magnification, and lighting adjustments to produce the most representative image of the surface. Mean rod diameters, $\langle d \rangle$, mean interrod spacings, $\langle \lambda \rangle$, and standard deviations of the distributions were determined by either of two techniques.

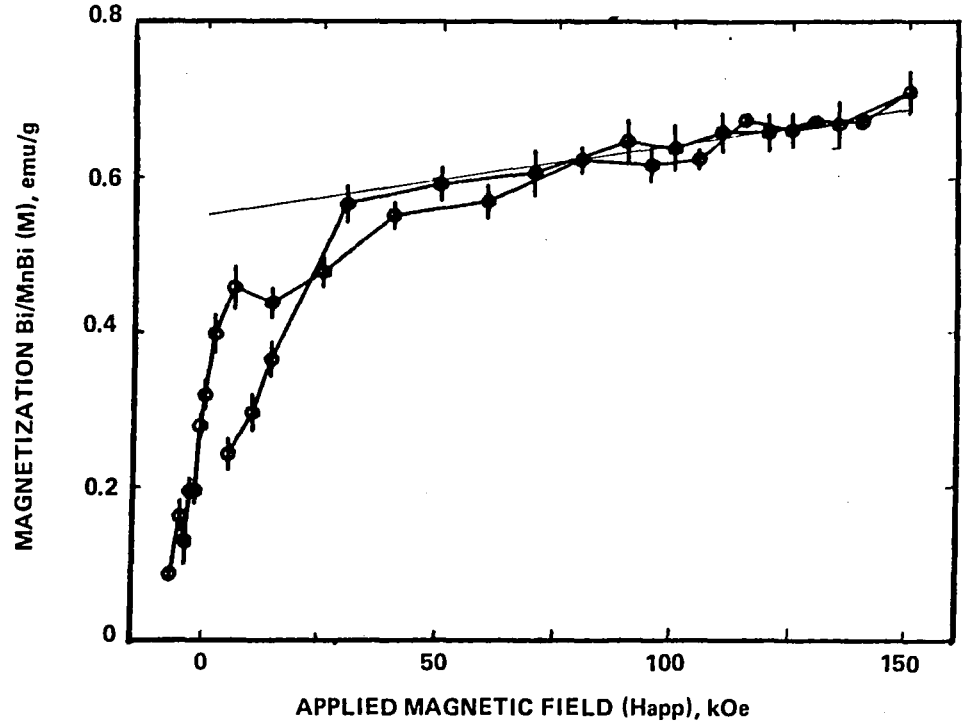

a. Data With Straight Line Representing L.S. Fit to Data Between About 80 & 150 kOe

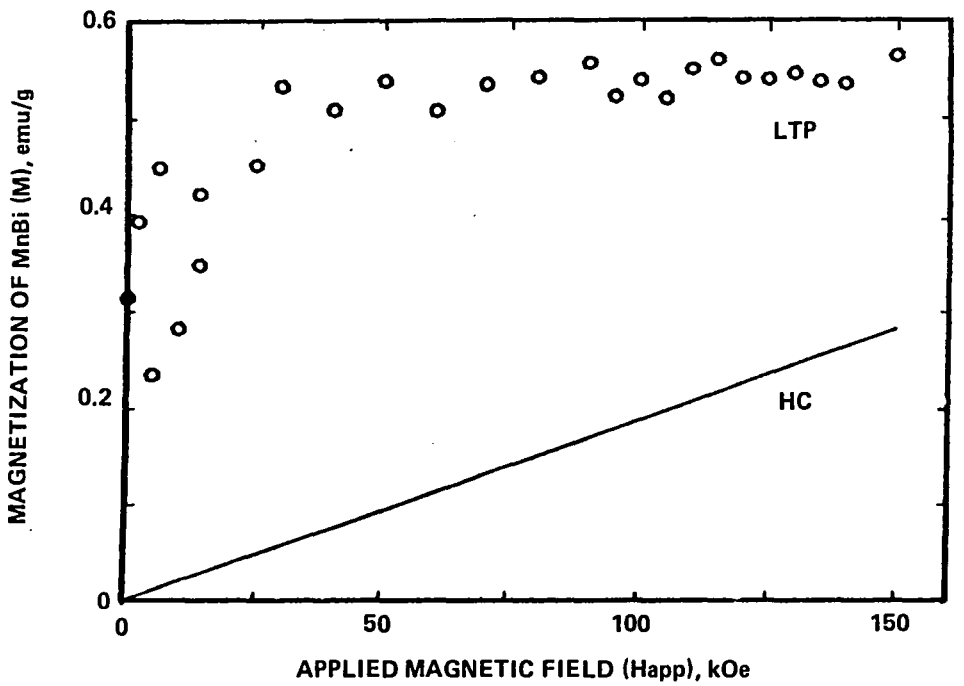

b. Deconvolution of Magnetization into MnBi LTP & HC Phases After Elimination of Bi Solid Solution Contribution

Figure 3-2. Room temperature magnetization of flight sample No. 2 section A

Histograms of the variable could be smoothed by hand and the mean extracted with half width at half maximum taken as the standard deviation. A more analytical approach was to fit a histogram with a modified Poisson distribution by minimizing χ^2, and to use the modified Poisson parameters to obtain the mean and standard deviation. In addition, MnBi volume fraction and Mn concentration (assuming 0.11 w/o in solid solution) were calculated directly from the camera images by the computer.

In order to check the accuracy of the Mn concentration values from magnetic and optical measurements and, in addition, to assess the correctness of the assumed value of the Mn concentration in Bi solid solution, X-ray fluorescence determinations of the total Mn concentrations near the surfaces of most of the sections of the samples were made. Measurements were performed by Fairfield Testing/LabTech, Inc. using Cu radiation. Three pieces each, of five Bi/MnBi cast ingots, of compositions 0.0, 0.4, 0.6, 0.7, and 0.9 w/o Mn in Bi were used to calibrate the Mn/Bi count ratios. The precision for these determinations was about 0.1 w/o Mn.

As the most reliable but destructive technique for measuring the bulk total Mn concentration of a Bi/MnBi section, chemical spectrophotometric absorbance (CSA) was used for a limited number of samples [3-22]. This technique had a sensitivity of ±0.05 w/o Mn.

Thermal measurements from the in situ thermocouple in each sample and two reference block thermistors were made as functions of elapsed solidification time at a rate of about one reading per second for each furnace assembly. These measurements were transmitted via telemetry and recorded both in digital and analog form. It was convenient to digitize the analog traces via a digitizing pad connected to a computer. Voltages representing the resistance of the thermistors were converted to temperatures [3-18] with a fourth-order polynomial and subsequently these temperature were converted to equivalent K-type reference junction voltages by an eighth order polynominal representation of the μV-T curve [3-23]. These voltages were added to the thermocouple voltages as a function of the elapsed time and the summed voltages were converted to sample temperature profiles with a fourth-order polynomial [3-24]. Due to a lack of point-to-point gounding in the ADSS apparatus, resolution of the in situ thermocouple measurements was limited to ±0.07 mV (±1.9°C).

RESULTS

LOW-GRAVITY EXPERIMENT - GENERAL OBSERVATIONS

On June 17, 1983, SPAR X was successfully launched form White Sands Missile Range and The payload was recovered later the same day. The ampoules were promptly removed and reached Grumman on June 21, 1983.

The Bi/MnBi off-eutectic samples in all ampoules were completely intact. As is shown in Figure 3-3, the end of each glass ampoule opposite from the thermocouple was broken off. The unoxidized state of each sample indicated that the breakage occurred when the rocket hit the desert floor.

X-ray radiographs of the flight ampoules are shown in Figure 3-4 and detail exact shapes of samples and slight leakby, but reveal no internal porosity. Photographs of the removed samples, with thermocouples and a graphite plug in place, are

shown in Figure 3-5. Sample No. 1 separated into two distinct pieces during its molten period due to the free volume created by leakby and contraction on melting. Sample No. 2 separated into two pieces about 3 mm from the first-solidified end of the sample, but the two pieces remained touching. Sample No. 3 looked perfect in form, as did sample No. 4, except the latter sample was fractured into two pieces at some time following solidification. This did not affect analysis of sample No. 4.

Evaluation of the telemetry data indicates that coolant pumps were funcitoning adequately to maintain the coolant temperatures within requirements, and reference transistors, cold junction thermistors, furnace thermocouples, and furnace assemblies appeared to operate properly. An occasional abrupt jump in the sample temperatures was evident in the data and was smoothed in the temperature plotting when it was believed to be too abrupt to be real. A more serous problem was the fact that the sample temperatures appeared to never reach the solidification temperature within the furnace travel time (Fig. 3-6), despite the fact that the thermocouple tip was located only 1 cm into the sample and that the end of the sample was believed to have been placed at the face of the chill block. There are three possible explanations for this problem. One is that the telemetry data drifted from the true temperature values as the assembly and electronics temperature increased. This is supported by the alignment of the MnBi rods parallel to the sample axis and the apparent directional solidification to the last solidified end of each sample. The temperature profiles of the post-flight ground-based comparison experiments, shown in Figure 3-7, provide additional information about this problem. A distinct break in the temperature profile of sample No. 4 at about 310 sec corresponds well to the expected time for the solidification front to reach the thermocouple tip. In addition, no break in this profile is visible near 265°C where the gradient should change rapidly to the value in the solid. A second possible explanation of the temperature profiles assumes the data is correct and the end of each sample was positioned incorrectly by about 1 cm from the initial position of the solidification front near the chill block. The third possibility is that, again, the data is correct, but each sample was positioned near the chill block and at these high furnace temperatures the initial position of the freezing isotherm was about 1 cm within the chill block. Since it is unlikely that the freezing isotherm could be moved a distance of 1 cm by a relatively small increase in temperature, this last suggestion is dismissed. Given the difficulty of choosing between the two remaining explanations, the problem is left to be resolved later and the analysis of the experiment will continue cautiously.

In spite of the last moment prelaunch furnace velocity difficulties, the velocity telemetry data indicated, within the noise signal, stable furnace motion except for furnace No. 2 the velocity profile of which is shown in Figure 3-8. The average speeds for furnaces No. 1, 2, 3, and 4 were 11.1, 11.4, 10.3, and 11.5 cm/h respectively with a noise level of ±0.7 cm/h, as seen in Table 3-1.

All flight samples and most ground-based samples had microstructural banding in the first solidified portions of the samples. A typical example is seen in Figure 3-9. The extent of banding ranged from less than 0.2 cm in the first piece of flight sample No.2 to about 1.5 cm in the ground-based sample No. 4, with most samples in the lower part of the range. The most probable cause of this is slightly unsteady furnace motion, with velocity changes within the noise signal of the velocity data.

The furnace thermocouples showed an unusually wide spread in hot zone temperatures, as seen in Table 1. Also, the higher furnace hot zone temperatures in low gravity observed previously [3-4] were not recorded in this work. The causes of these observations, if real, are unknown.

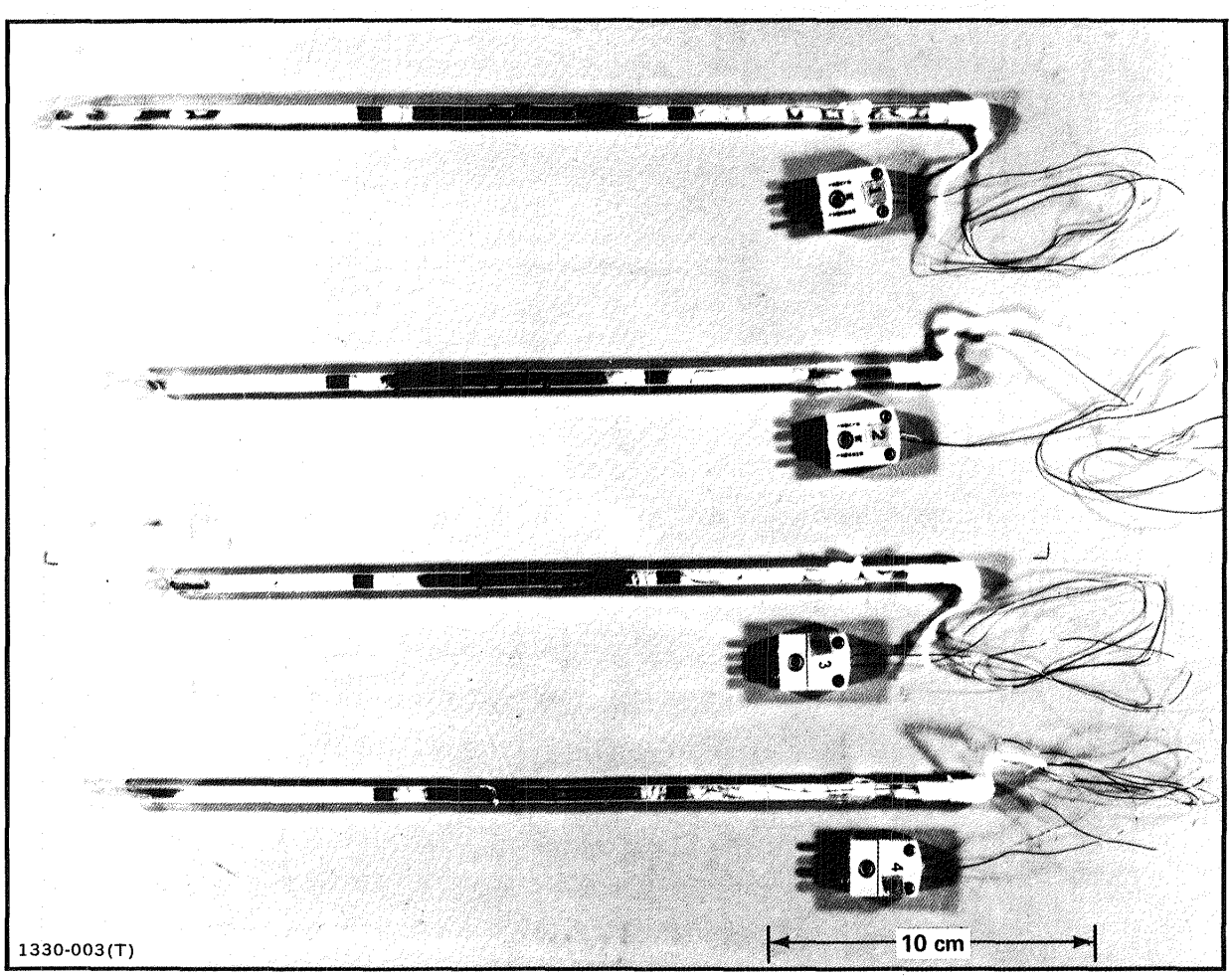

Figure 3-3. SPAR X flight ampoules as received after the low-gravity flight experiment

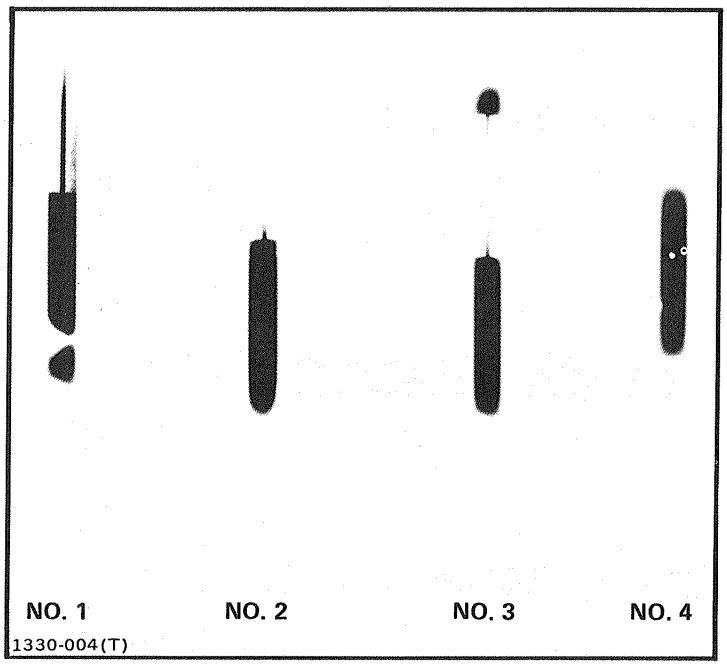

Figure 3-4. X-ray radiographs of flight samples before removal from ampoules

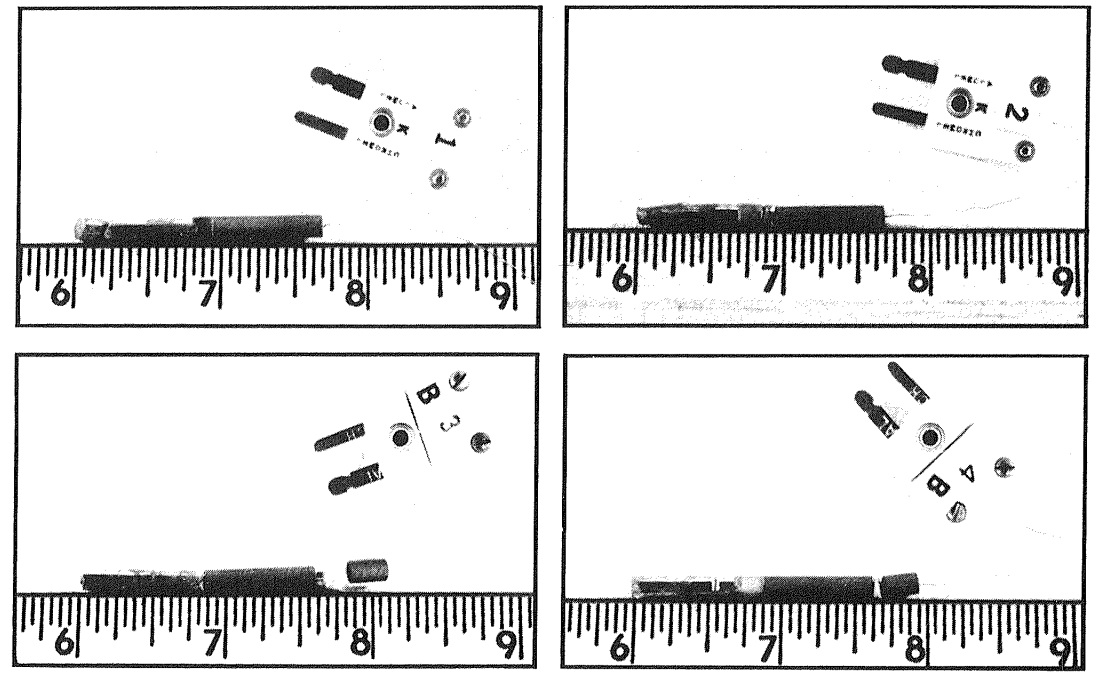

Figure 3-5. Photographs of flight samples after removal from ampoules

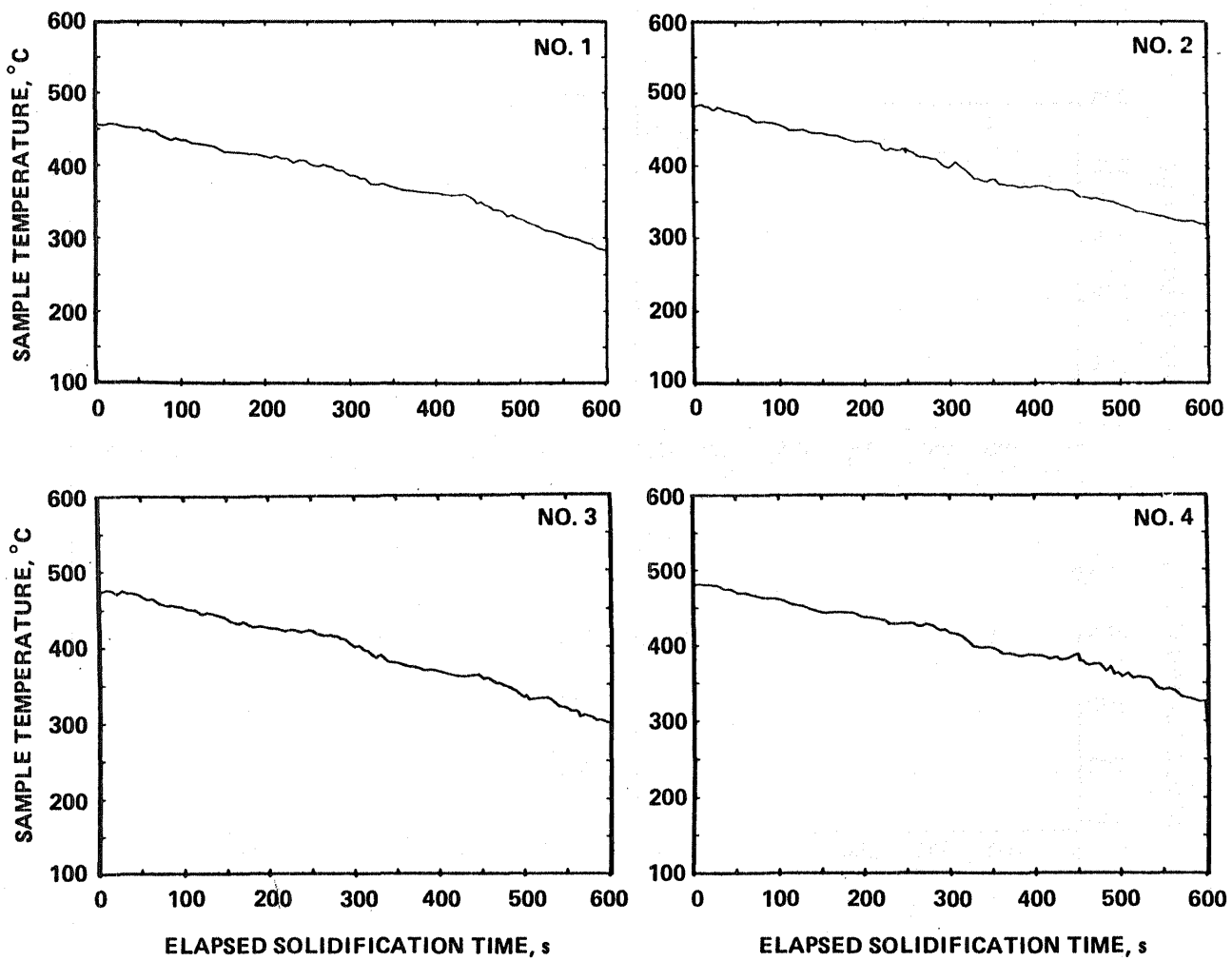

Figure 3-6. Temperature profiles of flight samples No. 1-4 at Thermocouples

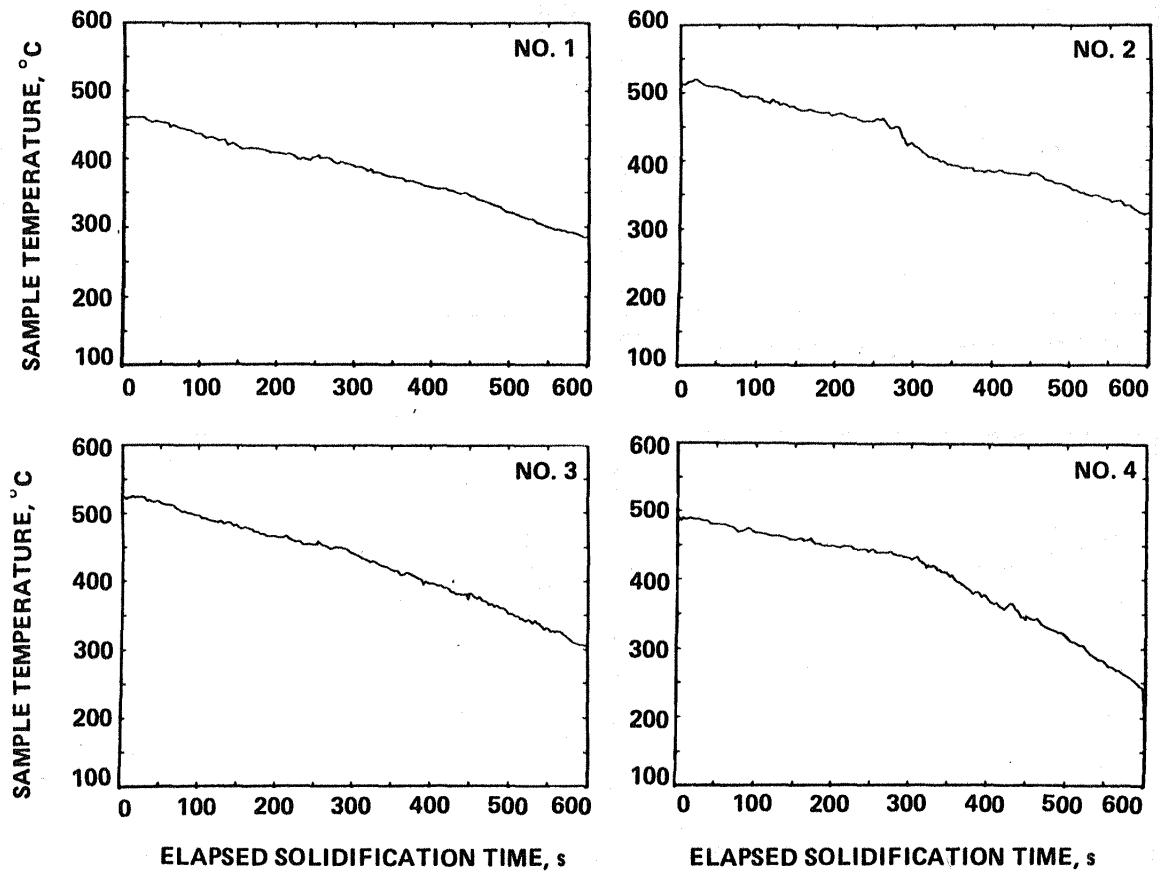

Figure 3-7. Temperature profiles of ground-based comparison samples No. 1-4 at thermocouples

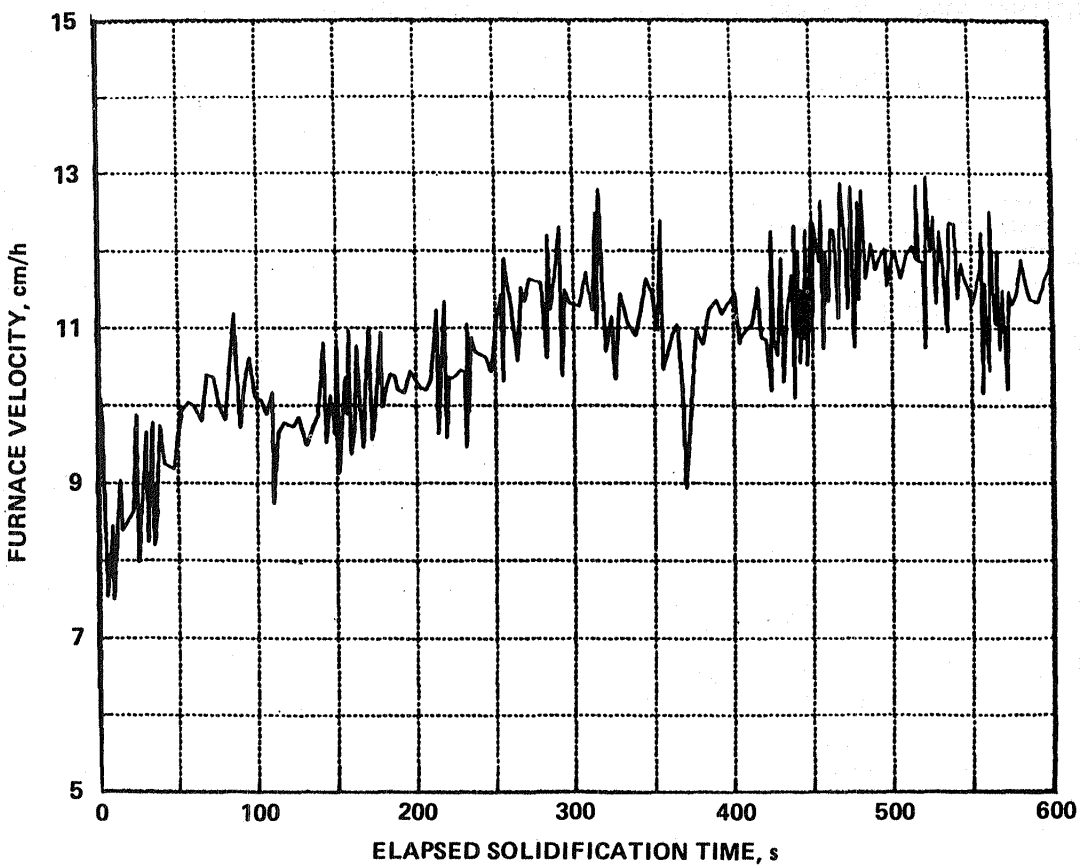

Figure 3-8. Velocity profile of flight furnace No. 2

TABLE 1 COMPARISON OF THERMAL PROPERTIES FOR SAMPLES GROWN DURING SPAR X AND GROUND-BASED COMPARISON EXPERIMENTS. VELOCITIES ARE AVERAGE AND THERMAL MEASUREMENTS WERE TAKEN AT 1 cm FURNACE TRAVEL

EXPERIMENTAL MEASUREMENT OR CONDITION	SPAR X FLIGHT (10^{-4} g) FURNACE ASSEMBLY NO.				GROUND-BASED COMPARISON FURNACE ASSEMBLY NO.			
	1	2	3	4	1	2	3	4
NOMINAL INITIAL BULK COMPOSITION, w/o Mn	0.90		0.49		0.90		0.49	
SOLIDIFICATION GEOMETRY	–	–	–	–	UP	DOWN	UP	DOWN
FURNACE VELOCITY, x 10^{-3} cm/s	3.08 ±0.3	3.17 ±0.3	2.86 ±.03	3.19 ±0.3	3.25 ±0.3	3.11 ±0.3	2.78 ±0.3	3.19 ±0.3
FURNACE HOT ZONE TEMP, °C	481 ±3	521 ±3	587 ±3	583 ±3	506 ±3	544 ±3	608 ±3	584 ±3
FURNACE CHILL BLOCK TEMP, °C	38 ±1	38 ±1	38 ±1	38 ±1	36 ±1	36 ±1	36 ±1	36 ±1
1330-017(T)								

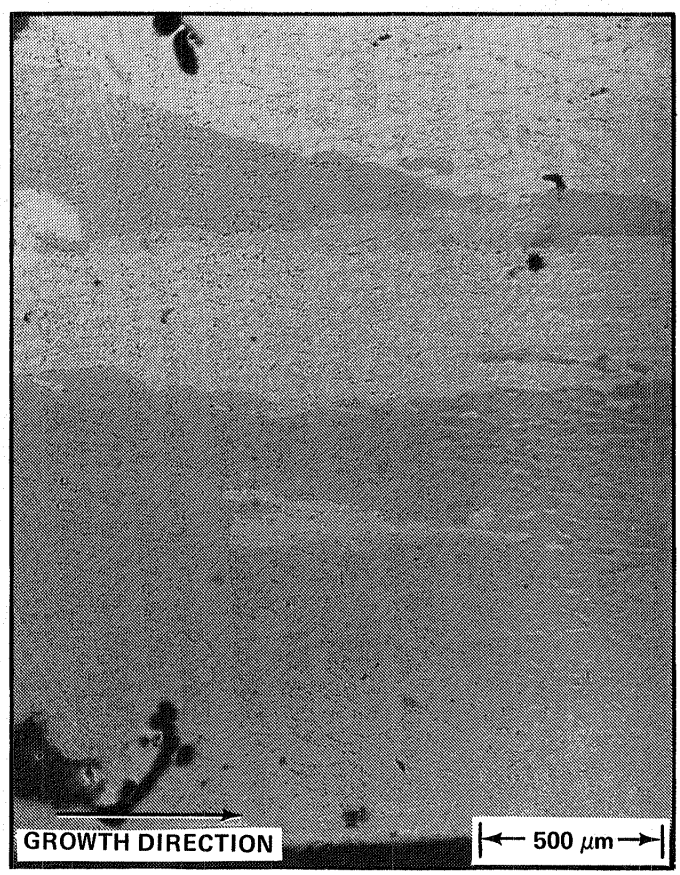

1330-009(T)

Figure 3-9. Microstructural banding in flight sample No. 4, longitudinal view

NORMAL-GRAVITY OBSERVATIONS

Ground-based comparison samples were solidified at Marshall Space Flight Center after the SPAR X launch, with the same furnace system and nominal processing parameters as for the flight experiment. These samples were received at Grumman on July 5, 1983. Table 3-1 lists the directional solidification conditions of these experiments and Figure 3-7, which shows the thermal profiles of the solidifications, indicates the same problem for the ground-based experiment as occurred in the flight experiment thermal profile.

Sample No. 1 was observed to have separated from the graphite plug by about 0.5 cm at the last-solidified end. Sample No. 2 was pulled into two pieces in the liquid state. A second sample No. 2 was processed later at MSFC with identical results. Therefore, a sample of identical composition was solidified at Grumman with the same nominal processing parameters to replace this particular sample. Samples No. 3 and 4 were well formed in outer appearance, although during removal from the ampoule, sample No. 4 broke into two pieces, which did not impact the analysis.

Particular sections of samples were annealed in an evacuated quartz tube at 250°C for 36 to 48 hr to simplify the magnetic analysis for those sections to that involving only the two equilibrium phases. The effect of heat treatment on the aligned-growth microstructures of samples solidified in this experiment is visible in Figure 3-10. Chevron and triangular rod cross sections annealed to circular cross sections in every sample examined in this study. This finding is in contrast to previous work [3-25] which did not find rod shape changes. Preliminary quantitative analysis of average rod areas and interrod spacings of annealed sections suggests that "coarsening" of rods did not take place and that the average rod area remained unchanged as the rod shape changed. One interesting possibility is that interfacial energies of the HC phase are lower than those of the LTP. This new finding of a shape change will be studied further at a later date.

Sections of the ground-based comparison samples were examined microstructurally on cross-sectional faces to determine the morphology of the MnBi phase on each face. Magnetic measurements and X-ray fluorescence measurements were made on sample sections to determine Mn content of the solid bulk and local cross-sectional surface, respectively. We begin to examine the results with sample No. 3. Sample No. 3 was Bi-rich and contained a few small areas of Bi solid solution cells or dendrites throughout most of the length of the sample, the remainder of the volume being an aligned MnBi rod-Bi solid solution matrix structure. Although this sample contained dendrites, a quantitative fit of the longitudinal macrosegregation for sample No. 3 was attempted and illustrated in Figure 3-11. As described in the background section of this report, such a quantitative description of macrosegregation for directional plane-front, off-eutectic composite growth, including the effect of convection, has been developed by Verhoeven and Homer [3-9] using a Burton-Prim-Slichter type stagnant film analysis. The average solid composition in a/o Mn, C_S, as a function of fraction solidified, f, is given by

$$C_S = C_E - \frac{C_E - C_o}{1-\exp(-p\delta)} (1-f)^{-1/(1-\exp(p\delta))} \qquad (3-3)$$

where C_E is the eutectic composition, C_o is the starting composition, p is the inverse of the Stefan length or solute boundary layer distance, and δ is the characteristic

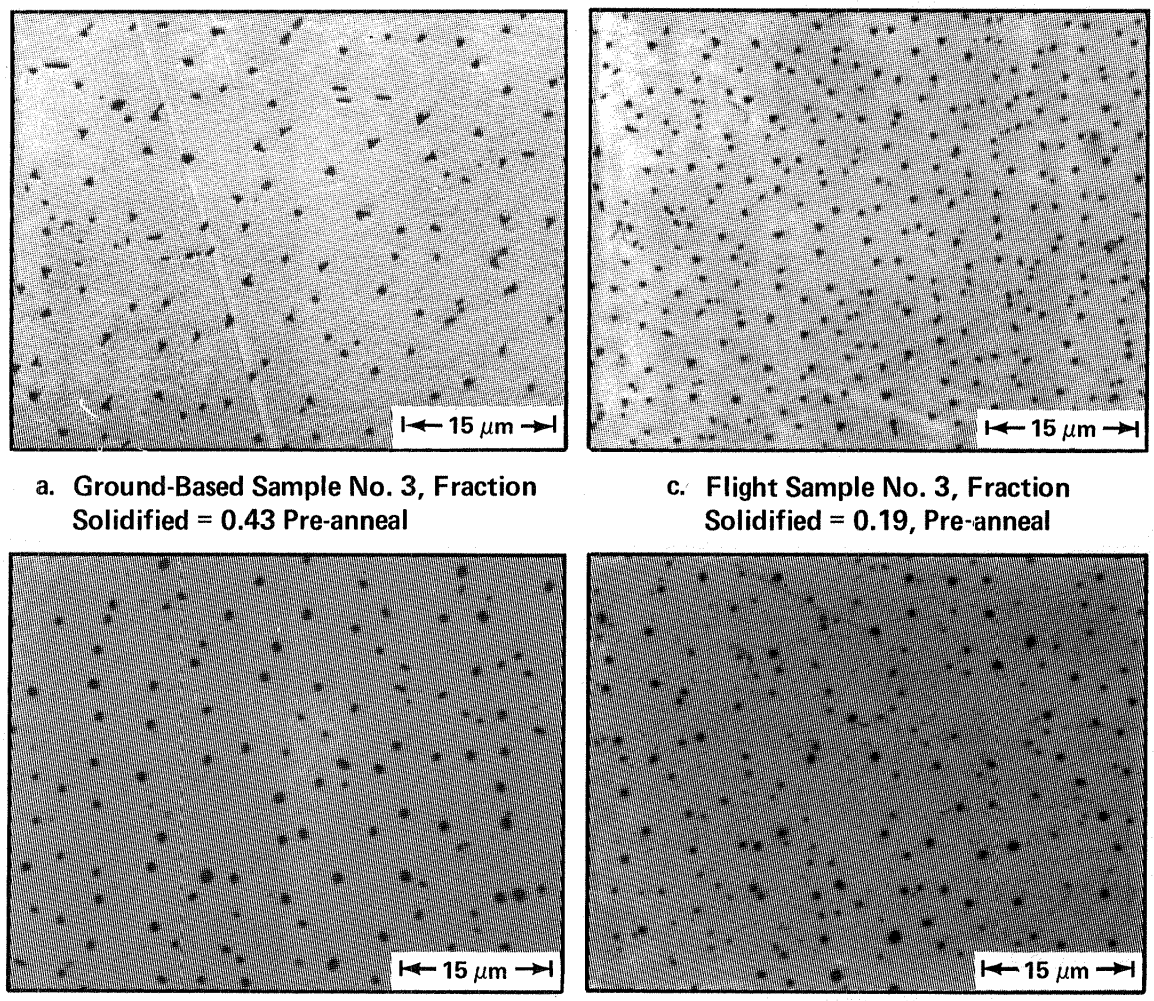

a. Ground-Based Sample No. 3, Fraction Solidified = 0.43 Pre-anneal

c. Flight Sample No. 3, Fraction Solidified = 0.19, Pre-anneal

b. Same as (a), but Post-anneal

d. Same as (c), but Post-anneal

1330-010(T)

Figure 3-10. Comparison of microstructures transverse to solidification direction in the as-grown state and after heat treatment at 250°C for 36 to 48 hr

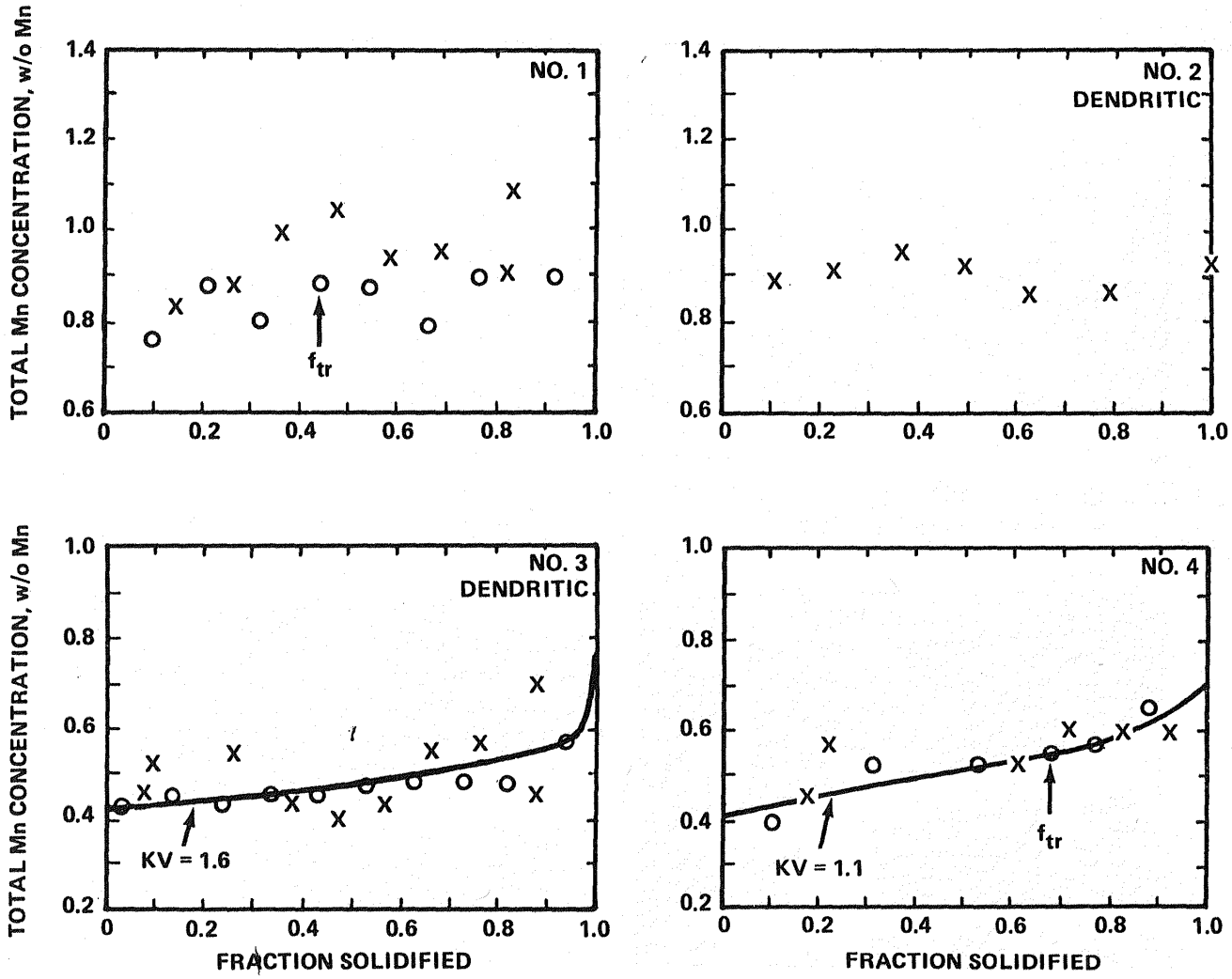

Figure 3-11. Total Mn composition versus fraction solidified for ground-based samples

stagnant film length. This form of their equation neglects thermotransport and is used here because of the relatively high growth rate for this experiment. Previously, it was reported for the Bi/MnBi off-eutectic system that this equation fit the macrosegregation data even when the growth was partially dendritic [3-1]. This might be because in this system with the processing conditions used, the growth may possibly still proceed with a macroscopically planar solidification isotherm. The relatively few dendrites may perturb the macrosegregation only slightly. In addition, the above equation has a very general Scheil-equation form so that although $p\delta$ may not be the proper exponential parameter, the equation still fits the data for this experiment. For the cases here, where a substantial length of the sample contained dendrites or cells, KV is substituted for $p\delta$ in equation (3-3), where K is the effective distribution coefficient. Figure 11 shows a best fit to the macrosegregation data of sample No. 3, where KV = 1.6. Sample No. 4 was also Bi-rich and contained dendrites or cells up to $f_{tr} = 0.67$ where the morphology became completely aligned (Fig. 3-12). Results of quantitative analysis of the aligned microstructure of a section of sample No. 4 are shown in Table 3-2. It is noted here that the normal-gravity equilibrium value of 0.11 w/o Mn in the Bi solid solution was assumed for the calculations of composition. Figure 3-11 displays the macrosegregation of sample No. 4 and includes a fit of equation (3-3) with KV = 1.1.

Sample No. 1 was Mn-rich and underwent a dendritic-to-cooperative transition at $f_{tr} = 0.44$. Table 3-2 lists the quantitative microsturctural analysis results for two cooperative sections of sample No. 1. Solutal macrosegregation (Fig. 3-11) appears to be minimal, although there is wide scatter in the compositional results, due in part to the very small size of the analyzed sections. Minimal macrosegregation implies in this case that KV > 1.6. In initial ground-based studies of growth up of Mn-rich compositions, Stokes flow was observed - that is, flotation of MnBi dendrites to the top of the melt, causing gross macrosegregation distrubances. This was particularly a problem with sample composition greater than 0.9 w/o Mn, and appears to have been successfully minimized in sample No. 1. Sample No. 2, as discussed previously, is a Grumman-solidified sample. The entire sample was scattered with MnBi dendrites, although Figure 3-11 shows that, similarly to sample No. 1, no macrosegregation of Mn appears to have taken place, again implying KV > 1.6.

The percentage of the MnBi which is in the HC phase for the ground-based samples No. 1, 3 and 4 is shown in Figure 3-13. Results generally fall in the 60 to 70 percent range and show only very weak dependence on the fraction solidified, f, or the Mn composition. HC phase percentages are this high because of the moderately high solidification velocity and the high gradient [3-4].

FLIGHT RESULTS AND NORMAL-GRAVITY PROPERTY COMPARISON

Flight samples No. 3, 4, and 1 were dendritic in the initial (proposed) low-$\bar{g}$ portions of the samples. Figure 3-14 shows resultant macrosegregation and Figure 3-15 the fraction MnBi in the HC phase for these samples. Within the scatter, after approximately the initial f = 0.37 in low-$\bar{g}$, both the macrosegregation and fraction HC phase curves are similar to those of the ground-based samples in Figure 3-11 and 3-13. Quantitative analysis of microstructures in non-low-$\bar{g}$ cooperatively grown sections of flight samples No. 3 and 4 are represented in Table 3-2 and show $\langle d \rangle$-values somewhat larger than the results from ground-based sample No. 4. This may be due to gravity levels in excess of normal Earth gravity at the latter stage of solidification. Values of $\langle \lambda \rangle$ were statistically identical.

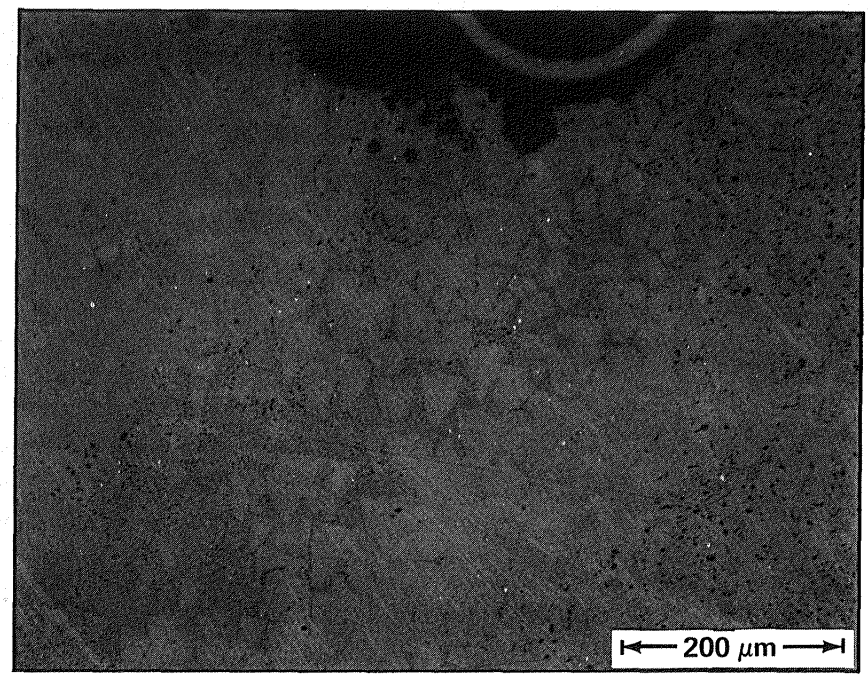

Dendrites Near Thermocouple at f = 0.19

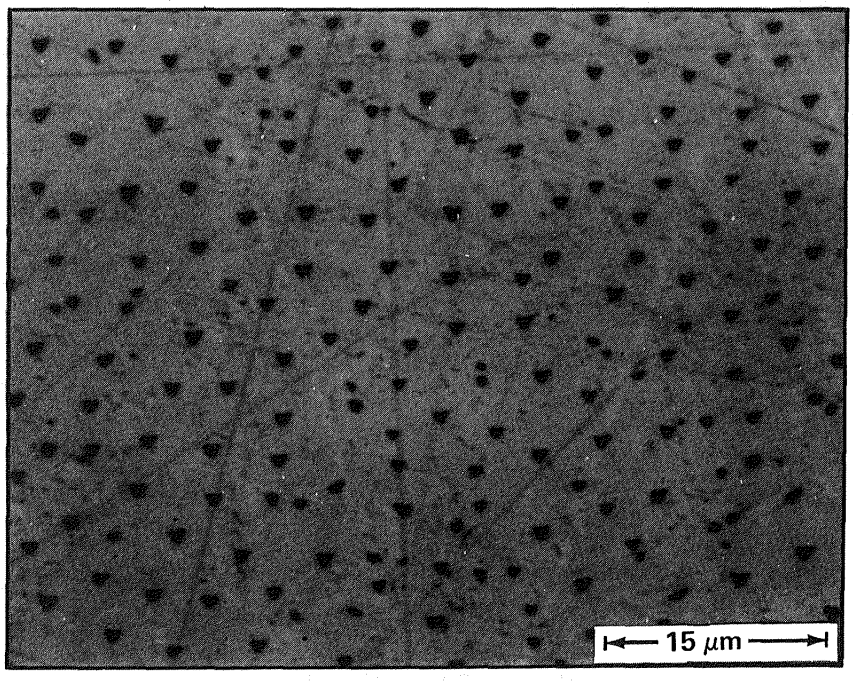

Cooperative Structure at f = 0.75

1330-012(T)

Figure 3-12. Microstructures representative of ground-based sample No. 4. Dendritic-to-cooperative transition is at $f_{tr} = 0.67$

TABLE 3-2 RESULTS OF QUANTITATIVE ANALYSIS OF COOPERATIVE MICROSTRUCTURES FROM SECTIONS OF SAMPLES GROWN DURING GROUND-BASED COMPARISON AND SPAR X FLIGHT EXPERIMENTS

SAMPLE NO.	f	$\langle d \rangle$, ±0.05 μm	σ, μm	$\langle \lambda \rangle$, ±0.3 μm	σ, μm	C_{Mn}, w/o	C^*_{Mn}, w/o
GROUND-BASED							
4	0.916	0.62	0.16	2.9	1.1	0.62	0.64
1	0.468	0.93	0.16	3.1	1.0	1.10	0.90
1	0.797	0.65	0.18	2.5	1.1	0.81	0.90
FLIGHT							
3 (ANNEALED)	0.980	0.77	0.17	3.2	1.1	0.74	0.72
4	0.840	0.69	0.18	3.3	1.4	0.59	0.54
2	0.195	0.50	0.18	2.3	1.1	0.61	0.62
2	0.445	0.77	0.19	3.2	1.4	0.69	0.72

C_{Mn} = Mn CONCENTRATION DETERMINED BY MICROSTRUCTURAL ANALYSIS

C^*_{Mn} = BULK Mn CONCENTRATION EXTRAPOLATED FROM MAGNETIC MEASUREMENT DETERMINATIONS

1330-018(T)

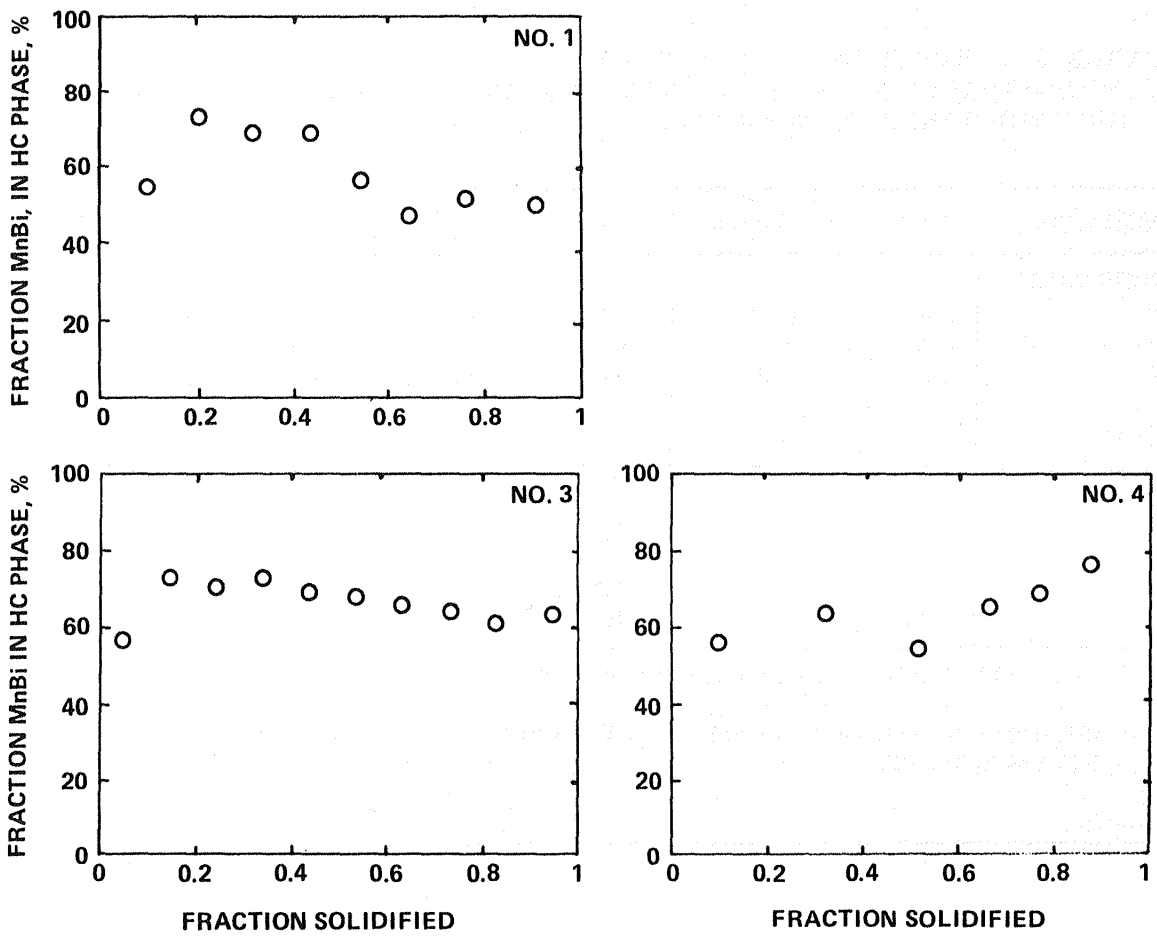

Figure 3-13. Fraction of MnBi in the HC phase versus fraction solidified for ground-based samples

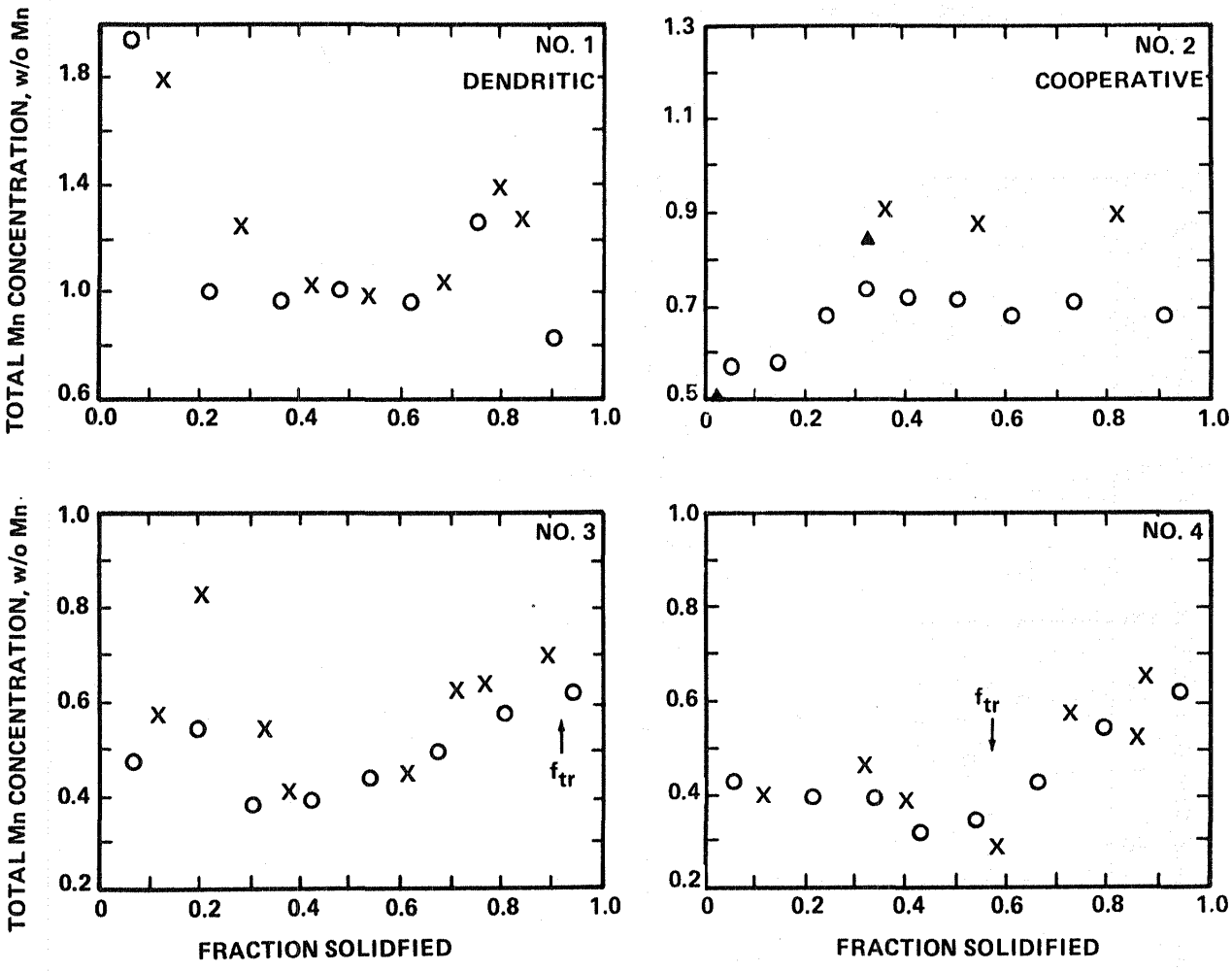

Figure 3-14. Total Mn composition versus fraction solidified for flight samples

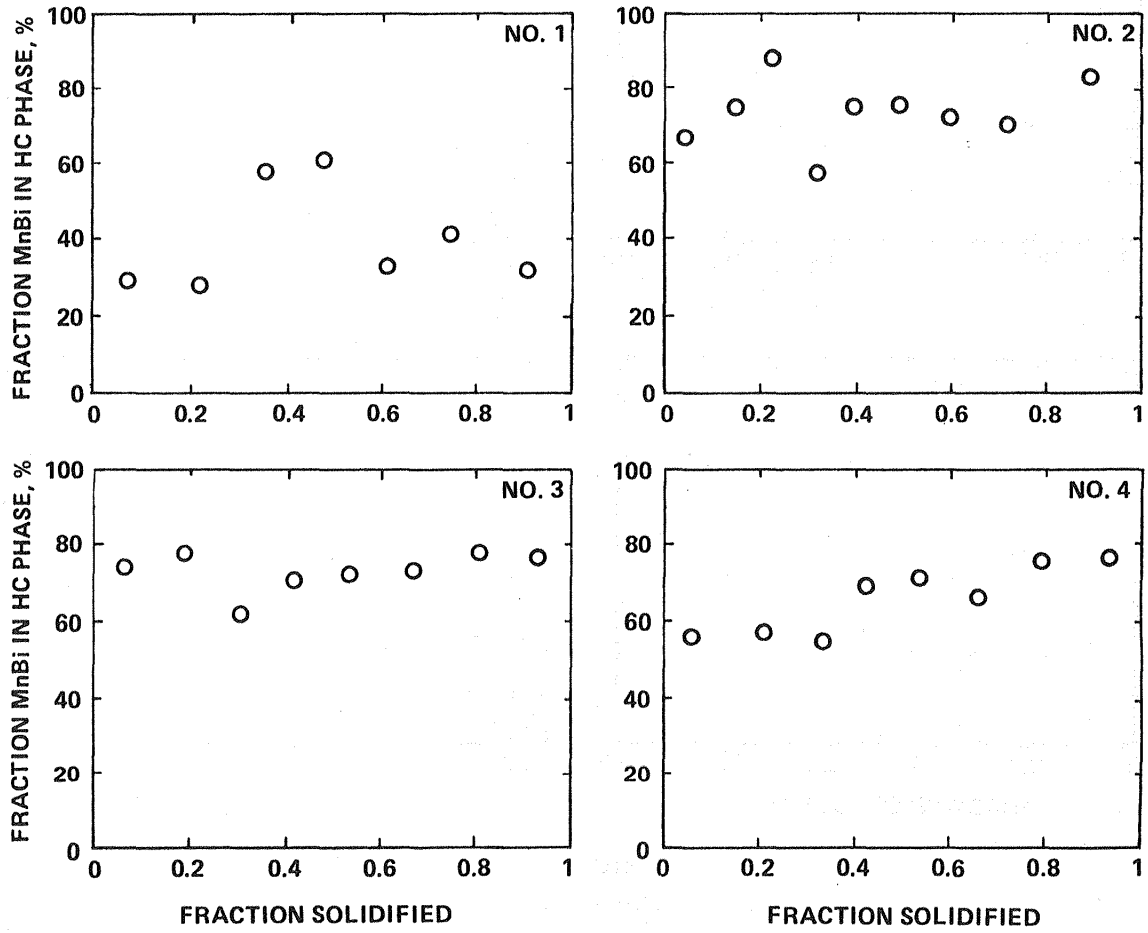

Figure 3-15. Fraction of MnBi in the HC phase versus fraction solidified for flight samples

Flight sample No. 2 is an interesting Mn-rich sample which solidified cooperatively over its entire length. Figure 3-14 shows the macrosegregation of this sample over its length and presents an unusual situation. X-ray fluorescence and magnetic measurement determinations of the Mn concentration do not agree. Unfortunately, complete fluorescence determinations could not be made due to unresolved measurement problems. Chemical spectrophotometric absorbance measurements were used as the most reliable test of total bulk Mn concentration for two samples. In addition, Table 3-2 includes Mn concentration values for two sections of flight sample No. 2 determined by microstructural analysis. Both this last technique and magnetic measurement technique use the assumption of the normal-gravity, equilibrium value of 0.11 w/o Mn in the Bi solid solution in their calculation of the total Mn content and are therefore insensitive to any solid solution Mn content changes. This is the possible source of the differences shown in Figure 3-14. Whereas the microstructurally and magnetically derived Mn concentrations are identical, these results disagree with X-ray fluorescence and chemical results. The first magnetic data point and chemical data point of Figure 3-14 lie in an initial transient section of this sample, but the next three magnetic data points result from sections solidified in the proposed low-$\bar{g}$ period. In this region of sample No. 2, the chemical and fluorescence results give statistically equivalent values, the average of which is 0.89 w/o Mn, quite different from the magnetic and microstructural value of 0.72 w/o Mn. Therefore, while the given limited evidence is not conclusive, it is suggested that a metastable, higher Mn content in the Bi solid solution in low-$\bar{g}$ would be consistent with these results. More will be said about this later.

Table 3-2 indicates a considerably smaller mean rod diameter, $\langle d \rangle = 0.50 \pm 0.05$ μm, and mean interrod spacing, $\langle \lambda \rangle = 2.3 \pm 0.3$ μm, in the proposed low-$\bar{g}$ region than in high-$\bar{g}$, $\langle d \rangle = 0.77 \pm 0.05$ μm and $\langle \lambda \rangle = 3.2 \pm 0.3$ μm. Micrographs comparing the morphology of these two analyzed cross sections are seen in Figure 3-16. Similar reductions in both $\langle d \rangle$ and $\langle \lambda \rangle$ seen previously in low-$\bar{g}$ experiments [3-3 and 3-4] are consistent with the proposal in the present experiment that the first 0.37 fraction solidified of flight sample No. 2 was indeed solidified in the low-$\bar{g}$ portion of the SPAR X flight, as intended.

DISCUSSION

Figure 3-1 allows the position of the dendritic-to-cooperative transition in samples soldified in the Bi/MnBi off-eutectic system to be predicted for a specific G/V ratio. For the SPAR X experiment, the nominal value of this ratio is $G/V = 0.46 \times 10^5$ °C-s/cm^2. Based on this value, Bi-rich samples should be cooperative for the average solid Mn composition of a section of a sample, C_S, greater than 0.60 w/o Mn, while Mn-rich samples should be cooperative for $C_S \leq 0.87$ w/o Mn. From Figure 3-11, a value of the transition composition, C_{tr}, equal to 0.55 ± 0.02 w/o Mn is reasonably consistent with the results and expectations for both Bi-rich ground-based samples No. 3 and 4. The Mn-rich samples No. 1 and 2 display no discernable macrosegregation in Figure 3-11, so that the actual fractional position of the transition in these samples is sensitively dependent on the exact G/V ratio. Sample No. 1 underwent the transition to cooperative growth at $C_{tr} = 0.92 \pm 0.04$ w/o Mn, whereas sample No. 2 was totally dendritic. The ground-based results for this experiment are found to be reasonably consistent with the previous experiments represented in Figure 3-1.

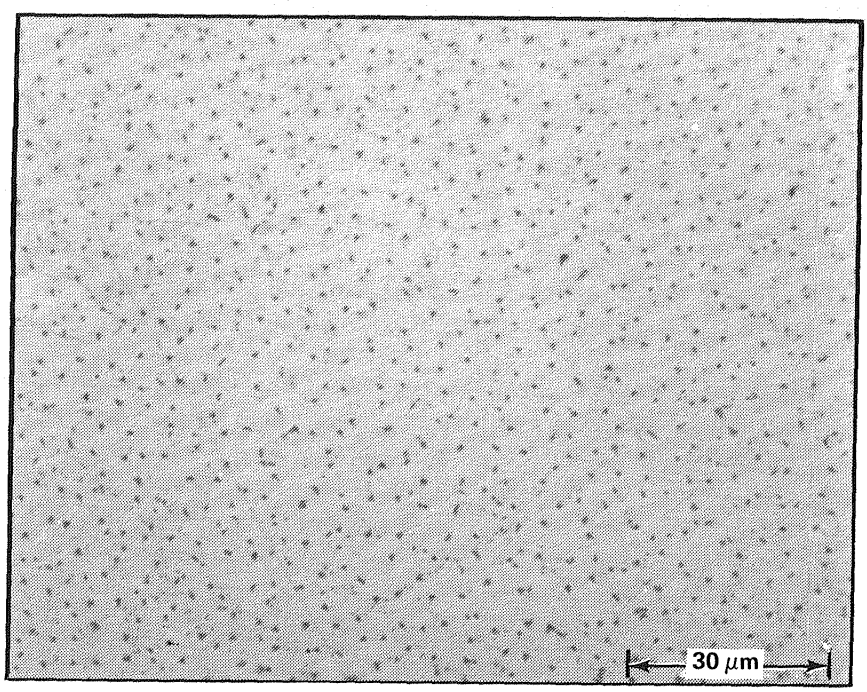

Figure 3-16. Comparison of representative cooperative microstructures of flight sample No. 2 from early and later portions of sample.

In previous work [3-1], Mn macrosegregation was able to be described by the model of Verhoeven and Homer, represented by equation (3-3). Here, as discussed in the text following equation (3-3), KV is substituted for $p\delta$. If it is noted for ground-based samples No. 3 and 4 that No. 4 shows greater solute redistribution, then a new situation is indicated. With a simplistic argument, the macrosegregation results show, since Mn was rejected at the solidification fronts of these two samples, that the growth down case of sample No. 4, which was unstable thermally but stable solutally, had greater convection in the melt than sample No. 3, which was stable thermally but unstable solutally. This implies that the thermal instability which was present was more important than the induced solutal instability in $1\text{-}\bar{g}$ with these particular solidification processing conditions. This finding is in contrast to the opposite result found in Reference 3-1 for lower velocities and gradients and may be due to a decrease in the role of thermal convection relative to solutal convection in $1\text{-}\bar{g}$ as the solidification velocity or thermal gradient increases, or may be an artifact caused by attempting to apply identical convection-solute redistribution arguments to composite and dendritic growth.

In the SPAR IX [3-4] Bi/MnBi eutectic flight experiment, a reduced volume fraction of MnBi was found in the low-gravity processed portion of all samples. That is, sections of the samples grown in low gravity contained 2.95 v/o MnBi, which would correspond to 0.67 w/o Mn, with the normal-gravity processing assumption of 0.11 w/o Mn in the Bi solid solution. Four of these sections have recently been analyzed by chemical spectrophotometric absorbance and found to contain 0.72 ± 0.03 w/o Mn, therefore supporting the suggestion that metastable extensions of the equilibrium normal-gravity phase diagram are operative in low-gravity processing due to interfacial undercooling. With this new result and assuming the densities of the "eutectic" and MnBi remain similar, it can be shown that these sections of SPAR IX samples contained 0.16 w/o Mn in the Bi solid solution, a 41 percent increase from the $1\text{-}\bar{g}$ equilibrium value. Calculated from the metastable linear extension of the solid solution limit and $\Delta T = 5°C$, a value of 0.18 w/o Mn is obtained. To complete the analysis, however, the metastable, low-gravity processed "eutectic" value cannot be found from SPAR IX results since the solidification of the samples was not completed in low gravity. From the trend of the volume fraction MnBi versus fraction solidified data of the SPAR IX experiment, however, it could be suggested that such a metastable eutectic value would be equal to or greater than the equilibrium value. While the SPAR X results can indicate nothing about a metastable eutectic value since only the first 0.37 fraction of flight sample No. 2 solidified in low gravity, the limited results, specifically, the different composition values found by magnetic and chemical techniques, do support the idea of an increased Mn solubility in the Bi matrix.

At the present time, the concept of a metastable extension of the phase diagram in low gravity seems to account best for MnBi volume fraction changes. Quenisset and Naslain's model, discussed earlier, predicts the necessary increased undercooling in low-gravity processing, as a consequence of reduced convective fluid velocity. Additional undercooling might also be possible from a kinetic term in equation (3-2).

SUMMARY AND FUTURE EXPERIMENTS

The effects of gravity on Bridgman-Stockbarger directional solidification of off-eutectic Bi/MnBi has been studied in reduced gravity aboard the SPAR X flight experiment and compared to normal-gravity investigations and previous eutectic Bi/MnBi SPAR flight experiments. The results included:

- Macrosegregation data are consistent with a metastable increase in Mn solubility in the Bi matrix in low-$\bar{g}$, in agreement with previous SPAR findings of MnBi volume reduction.

- Smaller mean rod diameter and interrod spacing were found in low-gravity compared to Earth-gravity solidification.

- Dendritic-to-cooperative growth transitions in Earth gravity agree with a revised supercooling criterion based on previous 1-$\bar{g}$ data.

- For these processing conditions, thermal instability led to more convection than the induced solutal instability in Earth gravity.

- Heat treatment of samples at 250°C for 36 to 48 hr resulted in rod shape change from chevron to circular.

Possible mechanisms involving gravity-induced convective fluid flow and metastable phase diagram extensions were proposed to explain the flight experiment findings.

This SPAR X off-eutectic Bi/MnBi solidification experiment was a high risk experiment, based on the very limited low-gravity time period available for processing, and was troubled with additional experimental problems. A longer-term low-gravity, off-eutectic Bi/MnBi solidification experiment is planned for the space shuttle, which will not be subject to severe time limitations and accompanying difficulties. This experiment will be a low velocity, high gradient experiment with two hypoeutectic and two hypereutectic compositions, which will, for the most part, solidify cooperatively on the ground and on the space shuttle. The objectives of this investigation will be to examine the role of convection in solidification of off-eutectics by determining the effect of low gravity and differing levels of convection on Mn macrosegregation, undercooling, the equilibrium phase diagram, and the detailed accommodation of the Mn content change in rod diameter and interrod spacing.

ACKNOWLEDGMENTS

The author wishes to thank D. Larson, P. Adler, and R. Pirich of Grumman for technical advice. Thanks also go to Grumman staff of B. Dressler for magnetic property characterization, W. Poit for sample preparation, and A. Trost for metallographic preparation. The author is indebted to B. Brandt and L. Rubin of Francis Bitter National Magnet Laboratory for their expert assistance. Finally, the author thanks J. Noel and F. Reeves of the Marshall Space Flight Center for their efforts to produce a successful SPAR X experiment.

REFERENCES

3-1. Pirich, R. G.: Gravitationally Induced Convection During Directional Solidification of Off-Eutectic Mn-Bi Alloys. In Matl. Proc. in the Reduced Gravity Envir. of Space, ed. Guy E. Rindone, Elsevier Science Publishing Company, New York, NY, p. 593, 1982.

3-2. Pirich, R. G., Larson, D. J., and Busch, G.: Studies of Plane-Front Solidification and Magnetic Properties of Bi/MnBi. AIAA J., Vol. 19, 1981, p. 589.

3-3. Pirich, R. G. and Larson, D. J.: SPAR VI Technical Report for Experiment 76-22 - Directional Solidification of Magnetic Composites. Grumman R&D Center Report RE-602, 1980.

3-4a. Pirich, R. G.: SPAR IX Technical Report for Experiment 76-22 - Directional Solidification of Magnetic Composites. Grumman R&D Center Report RE-642, 1982.

3-4b. Pirich, R. G. and Larson, D. J.: Influence of Gravity Driven Convection on the Directional Solidification of Bi/MnBi Eutectic Composites. In Matl. Proc. in the Reduced Gravity Envir. of Space, ed. Guy E. Rindone, Elsevier Science Publishing, New York, NY, 1982, p. 523.

3-5. Pirich, R. G., Larson, D. J., and Adler, P. N.: Characterization of the Effects of Plane-Front Solidification and Heat Treatment on the Magnetic Properties of Bi/MnBi Composites. Grumman R&D Center Report RE-663, 1983.

3-6. Ravishankar, P. S., Wilcox, W. R., and Larson, D. J.: The Microstructure of MnBi/Bi Eutectic Alloys. Acta Met., Vol. 28, 1980, p. 1583.

3-7. Wilcox, W. R., Doddi, K., Nair, M., and Larson, D. J.: Infleunces of Freezing Rate Changes on MnBi-Bi Eutectic Microstructure. Adv. Space Res., Vol. 3, 1983, p. 79.

3-8. Baskaran, V., Eisa, G. F., and Wilcox, W. R.: Influence of Convection on Eutectic Microstructure. Second Intern. Conf. on Computational Methods and Experimental Methods, Queen Elizabeth II, 1984.

3-9. Verhoeven, J. D. and Homer, R. H.: The Growth of Off-Eutectic Composites from Stirred Melts. Met. Trans., Vol. 1, 1970, p. 3437.

3-10. Gelles, S. H., Giessen, B. C., Glicksman, M. E., Margrave, J. L., Markovitz, H., Nowick, A. S., Verhoeven, J. D., Witt, A. F.: Materials Science Experiments in Space. NASA-Lewis Report No. NASA CR-2842, Advanced Copy, April 1977, p. 33.

3-11. Gelles, S. H. and Markworth, A. J.: Agglomeration in Immiscible Liquids, Experiment 74-30. In Space Processing Applications Rocket Project, SPAR II - Final Report, NASA Technical Memorandum 78125, p. VI-5, November 1977.

3-12. Johnston, M. H. and Parr, R. A.: The Influence of Acceleration Forces on Dendritic Growth and Grain Structure. Met. Trans. B, Vol. 13B, 1982, p. 85.

3-13. Mollard, F. R. and Flemings, M. C.: Growth of Composites from the Melt - Part I. Trans. Met. Soc. AIME, Vol. 239, 1967, p. 1526.

3-14. Boettinger, W. J., Biancaniello, F. S., and Coriell, S. R.: Solutal Convection Induced Macrosegregation and the Dendrite to Composite Transition in Off-Eutectic Alloys. Met. Trans A, Vol. 12A, 1981, p. 321.

3-15. Jackson, K. A.: The Dendrite-Eutectic Transition in Sn-Pb Alloys. Trans. Met. Soc. AIME, Vol. 242, 1968, p. 1275.

3-16. Burden, M. H. and Hunt, J. D.: The Extent of the Eutectic Range. J. Crys. Growth, Vol. 22, 1974, p. 328.

3-17. Quenisset, J. M. and Naslain, R.: Effect of Forced Convection on Eutectic Growth. J. Crys. Growth, Vol. 54, 1981, p. 465.

3-18. General Electric Company, Space Sciences Laboratory: Operating Manual for Automated Directional Solidification System. Prepared for NASA under contract NAS8-31536, 1978.

3-19. Pirich, R. G. and Larson, D. J.: The Influence of Gravity on Directional Solidification of Eutectic and Off-Eutectic MnBi Alloys. Annual TMS-AIME Mtg. Louisville, KY, 1981.

3-20. Pirich, R. G., Larson, D. J., and Busch, G.: The Role of Processing Parameters on the Magnetic Properties of Directionally Solidified Bi/MnBi Composites. IEEE Trans. Mag., Vol. MAG-15, 1979, p. 1754.

3-21. Pirich, R. G. and Larson, D. J.: Magnetic and Metallurgical Properties of Directionally Solidified Bi/MnBi Composites: The Effects of Annealing. J. Appl. Phys., Vol. 50, 1979, p. 2425.

3-22. Pirich, R. G., Busch, G., Poit, W., and Larson, D. J.: The Bi-MnBi Eutectic Region of the Bi-Mn Phase Diagram. Met Trans. A., Vol. 11A, 1980, p. 193.

3-23. Coates, P. B. and Smith, A. C. K.: Polynomial Representations of Standard Thermocouple Reference Tables. National Physical Laboratory Report QU 36, 1977.

3-24. Coates, P. B.: Functional Approximations to the Standard Thermocopule Reference Tables. National Physical Laboratory Report QU 46, 1978.

3-25. Personal communicatiosn with authors of Reference 3-4 and 3-5.

SECTION IV

SPAR EXPERIMENT 76-36

SPAR X

COMPARATIVE ALLOY SOLIDIFICATION

Written by Wendy S. Alter

Principal Investigator: Dr. M. H. Johnston

Science Advisor: Mr. R. A. Parr

NOTE: Due to the selection of the Principal Investigator, Dr. Mary Helen Johnston, for the position of Shuttle Payload Specialist, the post-flight analysis and compilation of results for this experiment were conducted by Wendy S. Alter.

BACKGROUND INFORMATION

A series of casting experiments have been performed using the SPAR sounding rocket to investigate the effect of fluid flow during solidification. By comparing convectionless solidification in low-gravity conditions with that which takes place under gravitational or centrifugal acceleration, the change in material characteristics due to convection may be measured.

Early experiments made use of metal-model NH_4Cl-H_2O for optical visualization of the solidification process. Results of these experiments indicated that the absence of gravity-induced acceleration would lead to large-grained, columnar structure and larger, more uniform secondary dendrite arm spacing compared with ground-based freezing [4-1,4-2]. A metal alloy system, tin-15wt%lead, was solidified on SPAR VII. As in the metal-model series, secondary dendrite arm spacing was found to be anomalously larger than that of ground-based samples processed at the same cooling rate. In addition, the grain structure in the flight sample was randomly oriented with equiaxed grains, while the ground-based samples showed a high degree of preferred grain orientation [4-3]. On SPAR VIII, metal alloy tin-3wt%bismuth was solidified in order to investigate the effect of the absence of convection on dendrite remelting. The small grains indicative of remelting were seen only in the last-to-freeze region around the central cavity, with the bulk of the sample consisting of a few large grains. Dendrite arm spacing was comparable to that of the ground-based sample. Some question remains as to whether solidification took place entirely in low-gravity [4-4].

OBJECTIVE OF THE EXPERIMENT

Fluid flow during solidification has been shown to play a major role in the formation of macrosegregation [4-5 to 4-10]. In order to study this phenomenon, a third metal alloy, aluminum-4.5wt%copper, was processed during the SPAR X flight. Under a contract with General Electric Inc. (NAS8-33573), a computer model has been developed to predict macrosegregation under varying solidification conditions. One goal of this flight was to obtain quantitative macrosegregation data for comparison with model predictions. Al-4.5wt%Cu was chosen because the density difference between the constituents could be expected to lead to measurable macrosegregation under the influence of gravitational acceleration, as well as for its representative status of the commercial 2000 series of aluminum alloys.

APPROACH

Calculations which take into account the effects of fluid motion on macrosegregation have achieved good agreement with experimental results for specific experimental setups [4-5 to 4-11]. From 1979 to 1981, two computer models of the solidification of binary alloys (steady-state and nonsteady-state) were developed by G.E.

with particular application to the experimental low-gravity solidification program [4-12, 4-13]. The original models were limited to the calculation of macrosegregation subject to an input thermal field. However, experimental measurement of internal temperatures was an inherently difficult task for the small ingots under investigation; formidably challenging under flight conditions. During the last two years the models have been extended to calculate the heat flow due to both conduction and convection simultaneously with the solidification calculation, so that the only thermal input required is the rate of heat extraction at the chill. This made the flight experiment feasible. A detailed description of the model is contained in "MPS Solidification Model: Final Report, Analysis and Calculation of Macrosegregation in a Casting Ingot," Report No. 83HV004, July 1983, by D. R. Poirier and A. L. Maples [4-14].

PROCEDURE

The Al-4.5wt%Cu alloy was prepared in the form of a master alloy by weighing out and melting, in air, elements of 99.9 percent nominal purity. Ground-based and flight ingots were cast from the master alloy into a cold graphite crucible. Each sample was approximately 60 mm long by 50 mm wide and weighed 100 g. The SPAR flight furnace used to process the samples has been described in previous reports [4-3, 4-4]. The flight sample was remelted prior to liftoff and soaked at 720°C. During liftoff, the molten alloy was subjected to convective mixing. Approximately 5 sec after entry into low gravity, the power was cut to the furnace and the quench was initiated. The sample solidified during the remainder of the low-gravity period. Temperatures from the six thermocouples in the graphite crucible were recorded via telemetry.

Processed samples were photographed (Fig. 4-1), etched to reveal the grain structure, and photographed again (Fig. 4-2). The samples were then cross sectioned as shown in Figure 4-3. Surfaces B11 and B21 were polished and etched (Keller's Etch) to reveal the grain structure (Figs. 4-6, 4-7). Secondary dendrite arm spacings and volume fraction eutectic were obtained from these faces using a Ladd Image Analyzer. Under a contract with the Georgia Institute of Technology Engineering Experiment Station, coring measurements were made by microprobe analysis. Ingot sections B12 and B22 were analyzed by MSFC Materials and Processes Laboratory for macrosegregation by atomic absorption spectroscopy.

OBSERVATIONS AND DATA

Visual appearance as well as flight temperature profile indicate that the flight sample solidified entirely during the low-gravity portion of the flight. The flight cooling rate was 45.4°C/min, compared to the ground-based rate of 55.3°C/min. Both flight and ground-based ingots display a cavity along one face. This is typical for a flight-processed sample, but indicates that the ground-based sample was probably solidified at an angle from the vertical. Grains in the etched flight sample show a more random orientation than those in the ground-based sample.

Porosity is evident in both samples. Although quantitative measurements were not taken, there appears to be either greater or coarser porosity in the ground-based ingot, as seen in Figures 4-4 to 4-7. Secondary dendrite arm spacings were 23 percent larger in low-gravity: flight, 4.93×10^{-3} cm; ground-based, 4.02×10^{-3} cm

(Fig. 4-8). The flight sample was also found to have a smaller volume fraction of eutectic; 9.3 percent as compared to 10.8 percent in the ground-based sample. Microprobe analysis revealed less coring in the flight sample. Solid-solution aluminum dendrites in the flight sample had an average copper content of 3.21 percent with a standard deviation of 0.78, while ground-based dendrites were lower in copper content at 2.80 percent with higher standard deviation of 1.08.

Macrosegregation is shown in Figures 4-9 and 4-10. Copper content in the ground-based sample varied from 5.0%Cu at the upper chill face corner to 4.5%Cu in the center of the ingot, near the shrinkage cavity. The flight sample varied from 5.0%Cu at the lower chill face to 4.3%Cu in the center. There seems to have been more mixing at the center of the ground-based ingot. The flight ingot shows a smooth transition from outside to center.

DISCUSSION

An initial concern in this experiment was the difference in the cooling rate between flight and ground-based runs. Properties could not be legitimately compared if the difference were sufficiently large to affect fluid flow. However, temperature parameters in the model show a strong dependence on cooling rate primarily below 30°C/min, and do not differ significantly at the rates used in this experiment. To confirm this, the velocity field and mass flow predicted by the model for the flight sample was assumed to have the same cooling rate as the ground-based sample (Figs. 4-17, 4-18, 4-21, 4-22). Interdendritic fluid velocity and mass flow theoretically did not differ significantly due to the difference in cooling rates. Thus, acceleration force may be considered the principal variable between the two samples for properties which depend on fluid flow.

Macrosegregation in the flight sample was not as predicted in the model (Fig. 4-15). The model considers a bidirectionally solidified ingot (half of which is shown, the other half assumed symmetrical), and predicts that isoconcentration lines in the low-gravity sample must be vertical. Since telemetry data, visual appearance, and dendrite arm spacing indicate that solidification took place during the low-gravity portion of the flight, the isoconcentration line curvature cannot be attributed to acceleration effects. Most likely the graphite crucible extracted heat at the top and bottom of the ingot as well as at the chill face. Thus, the assumption of bidirectional solidification is a simplification of actual experimental conditions.

Ground-based macrosegregation shows the same tendency for isoconcentration lines to display positive curvature near the top of the ingot. In addition, curvature at the bottom is more pronounced in the actual ingot than the model prediction. This evidence supports the conclusion that heat was lost at the top and bottom of the ingot.

A further departure is seen in both flight and ground-based samples. The model predicts that copper content in the solidifying ingot will drop off sharply approximately 8 mm from the center of the ingot. This corresponds to a porous region resulting from solidification shrinkage. The model assumes that capillary forces, associated with the surface of the interdendritic liquid, are sufficient to prevent vertical drainage through the solid-liquid zone [4-15]. However, the porous region is not seen in the experimental ingots. Shrinkage is manifest as a cavity in the

last-to-freeze region in both flight and ground-based samples. Consequently, copper macrosegregation profiles in the model are higher in the outside region of the ingot and lower in the center region than those seen in the experimental ingots.

CONCLUSIONS

Differences between model predictions and experimental data indicate that the model has not been sufficiently tested within the bounds of its assumptions. A mathematical model must, of necessity, impose simplifying assumptions. This model may be upgraded to take into account interdendritic drainage at the final transient. Modeling nonuniform heat extraction from three crucible walls would be much more difficult. Experimental design could be modified to ensure solidification along one axis only, perhaps by increasing the sample size and changing the mold configuration. At the present time, however, no further SPAR flight experiments in this series are planned.

REFERENCES

4-1. Johnston, M. H., Griner, C. S., Parr, R. A., and Robertson, S. J.: J. of Crystal Growth, Vol. 50, 1980, p. 831.

4-2. Johnston, M. H. and Griner, C. S.: Met. Trans., Vol. 8a, 1977, p. 77.

4-3. Johnston, M. H. and Parr, R. A.: SPAR VII Final Report, NASA TM82535, 1983.

4-4. Johnston, M. H. and Parr, R. A.: SPAR VIII Final Report, to be published.

4-5. Mehrabian, R., Keane, M., and Flemings, M. C.: Met Trans., Vol. 1, 1970, p. 1209.

4-6. Kou, S., Poirier, D. R., and Flemings, M. C.: Proceedings of the Electric Furnace Conference, Iron and Steel Society of AIME, December 1977.

4-7. Flemings, M. C. and Nereo, G. E.: Trans. TMS-AIME, Vol. 239, 1967, p. 1449.

4-8. Flemings, M. C., Mehrabian, R., and Nereo, G. E.: Trans. TMS-AIME, Vol. 242, 1968, p. 41.

4-9. Flemings, M. C. and Nereo, G. E.: Trans. TMS-AIME, Vol. 242, 1968, p. 50.

4-10. Mehrabian, R., Keane, M., and Flemings, M. C.: Met. Trans., Vol. 1, 1970, p. 3238.

4-11. Fujii, T., Poirier, D. R., and Flemings, M. C.: Met. Trans., Vol. 103, 1979, p. 331.

4-12. Maples, A. L. and Poirier, D. R.: Report No. 80HV007, Vol. I - III, General Electric Company, Huntsville, Alabama, 1980.

4-13. Maples, A. L. and Poirier, D. R.: in "Thermal Sciences 16, Proceedings of the 16th Southeastern Seminar," T. Vezinoglie, ed., Hemisphere Publishing Corporation, 1983.

4-14. Poirier, D. R. and Maples, A. L.: Report No. 83HV004, General Electric Company, Huntsville, Alabama, 1983.

4-15. Poirier, D. R. and Maples, A. L.: Report No. 81HV001, Vol. I - II, General Electric Company, Huntsville, Alabama, 1981.

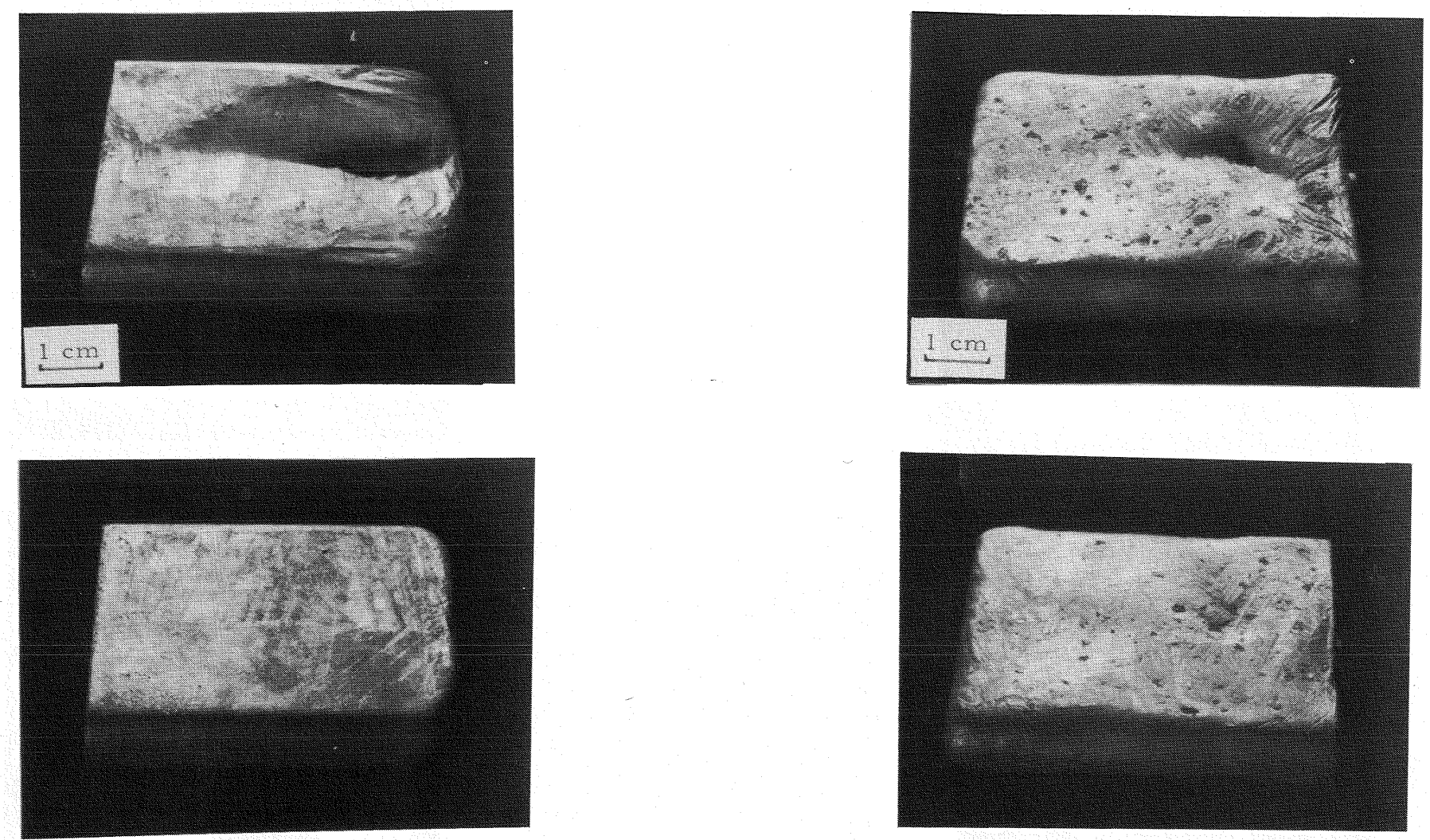

Figure 1. SPAR X flight and ground-based Al-4.5wt% Cu sample, unetched.

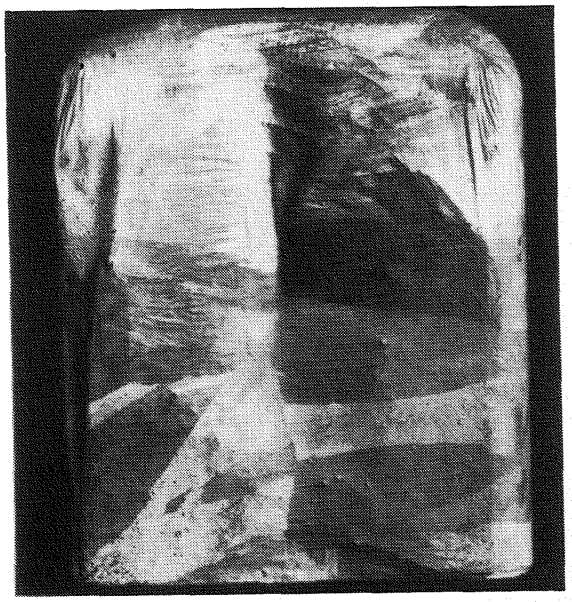

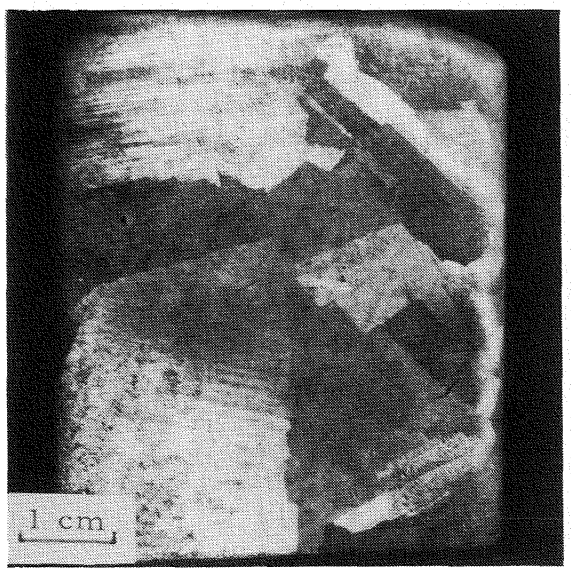

GROUND BASED

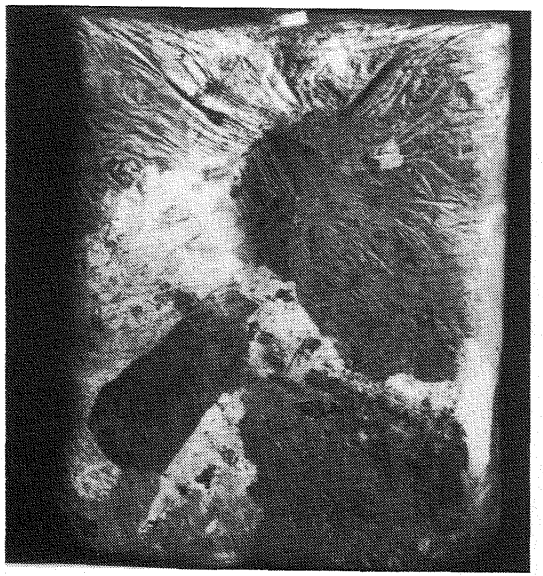

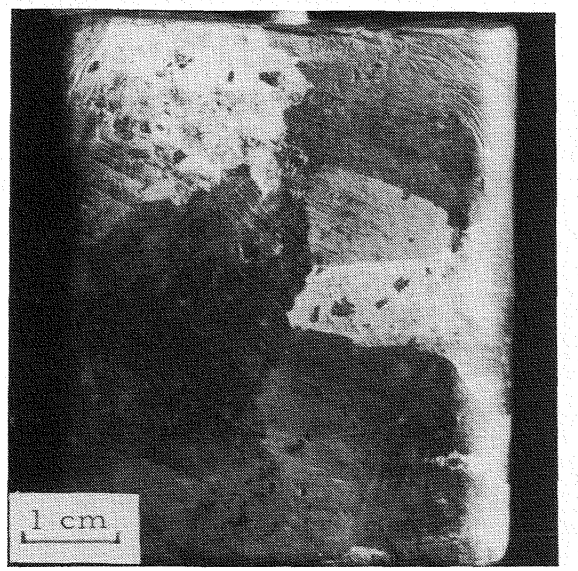

FLIGHT

Figure 2. SPAR X flight and ground-based Al-4.5wt% Cu sample, etched.

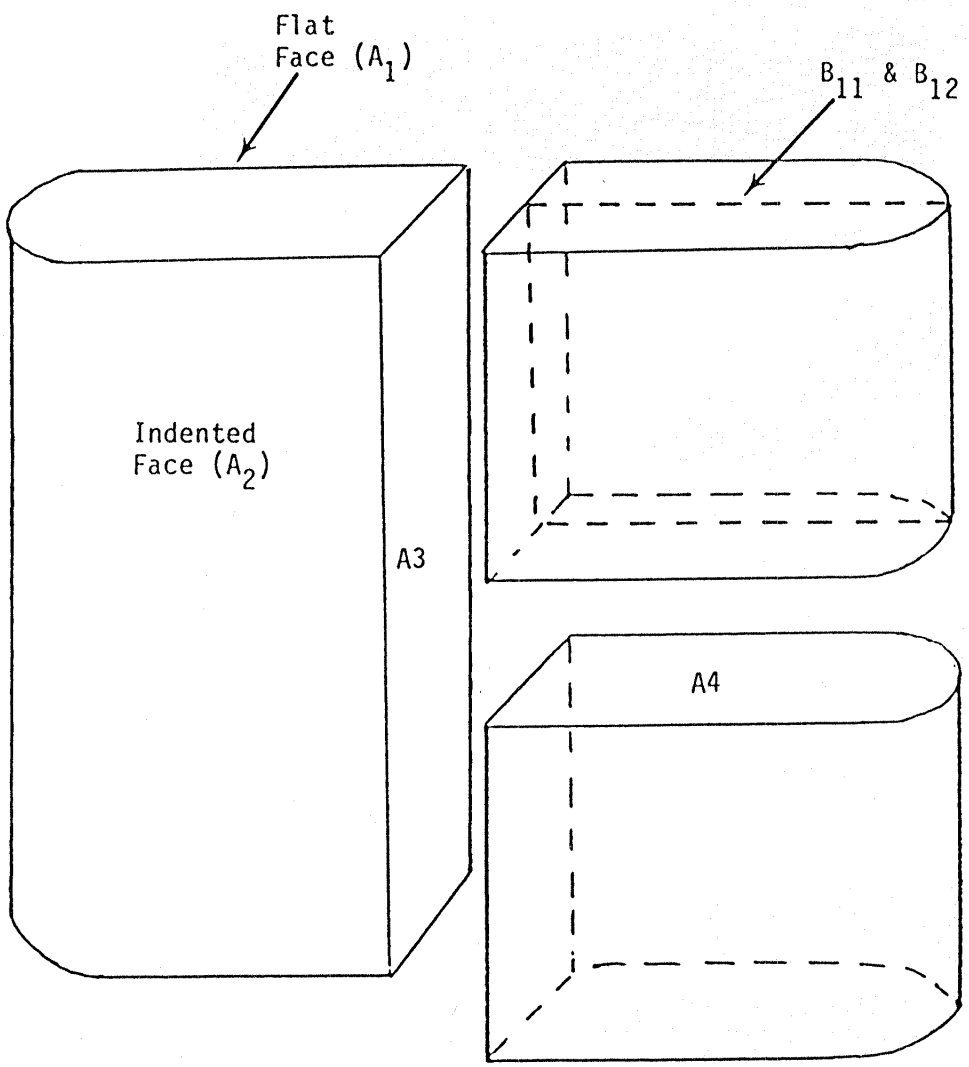

Figure 4-3. Schematic of sectioned sample showing surface designations.

Figure 4-4. SPAR X flight and ground-based samples, face A_3, etched.

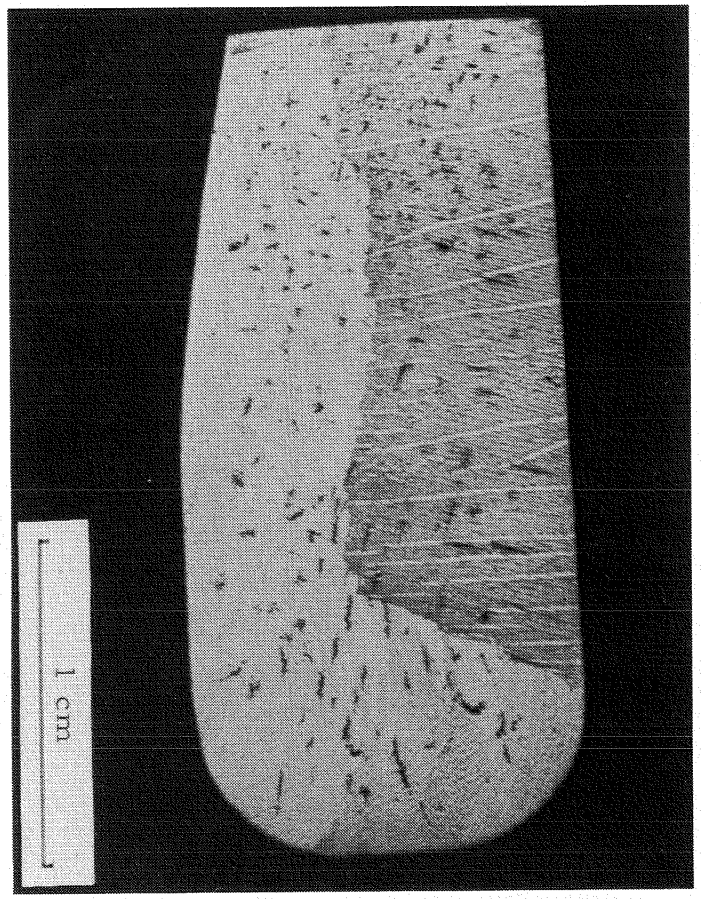

GROUND BASED

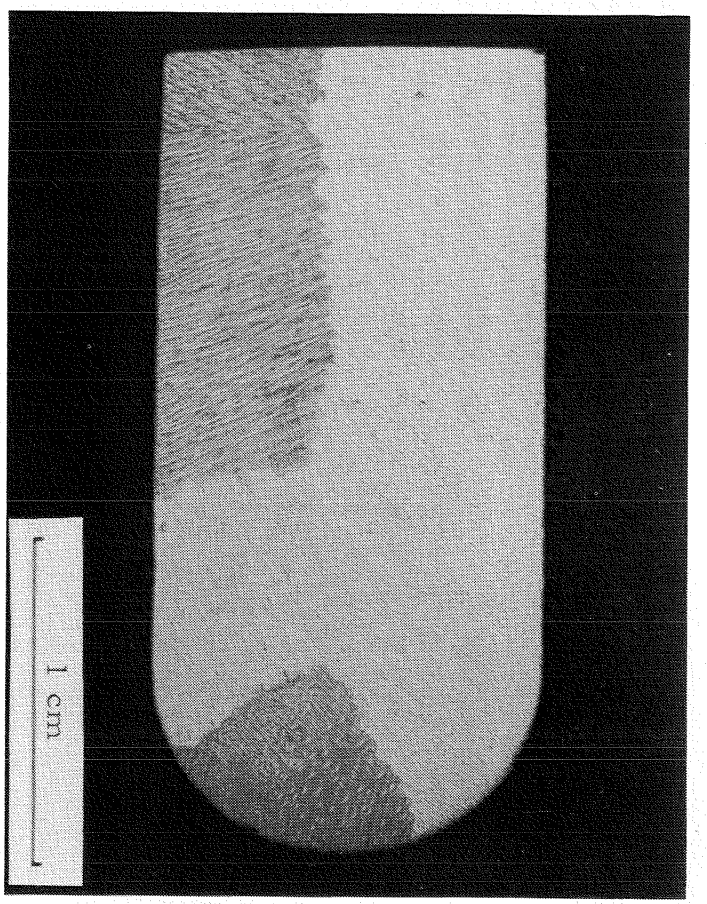

FLIGHT

Figure 4-5. SPAR X ground-based and flight samples, Al-4.5wt%Cu alloy, face A_4, etched.

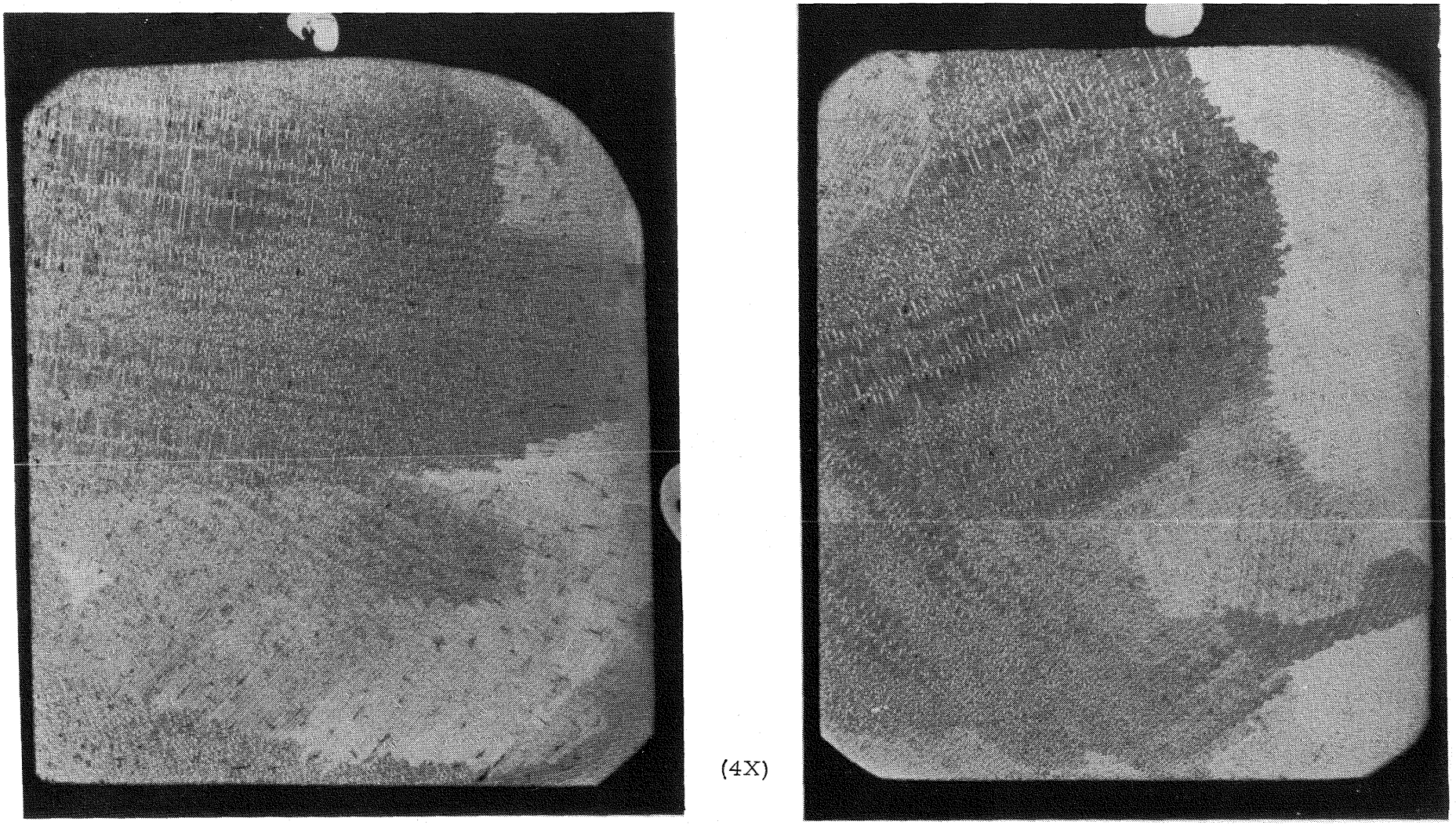

(4X)

Figure 4-6. SPAR X ground based and flight samples, Al-4.5wt%Cu alloy, face B11, etched.

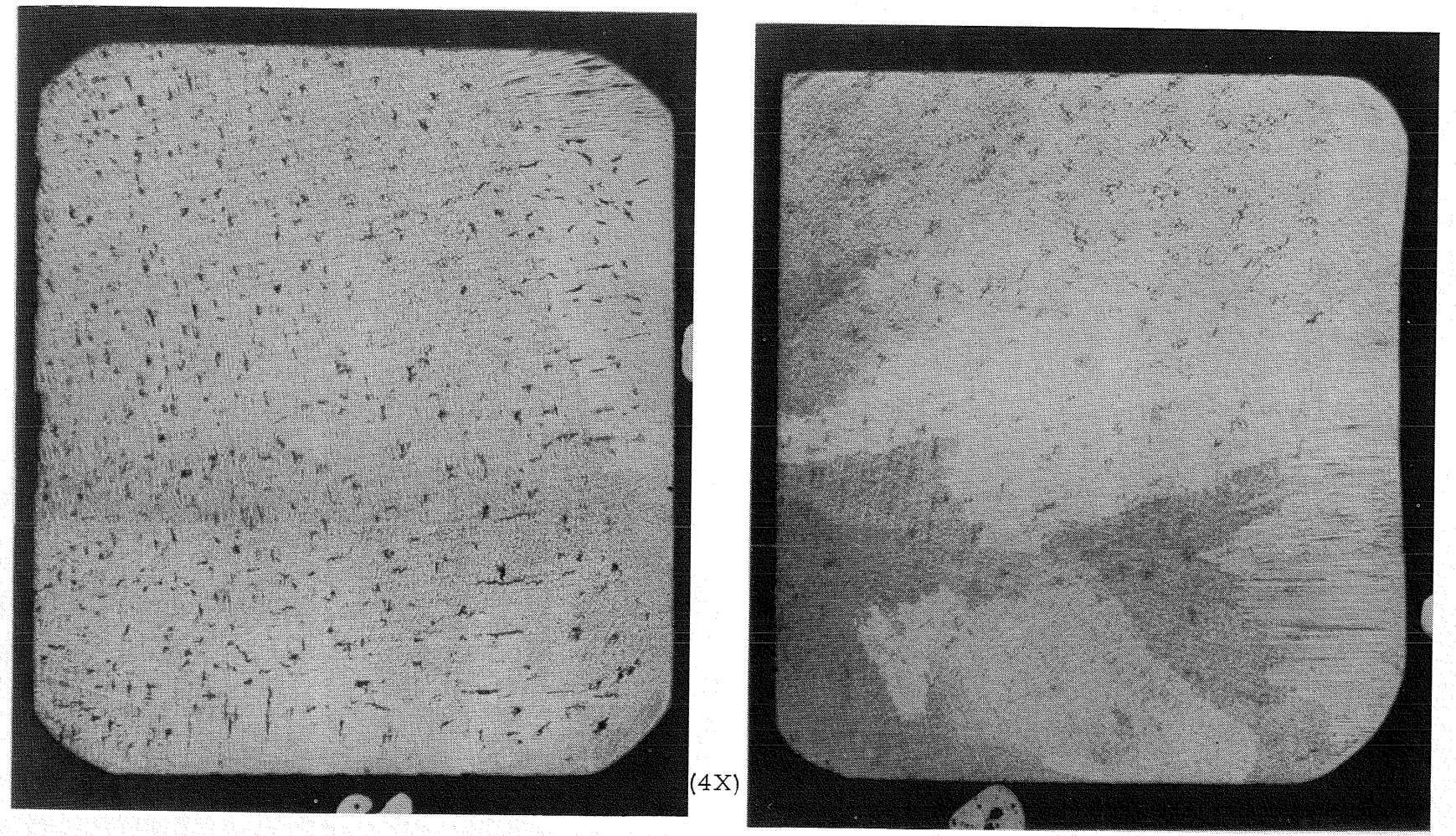

Figure 4-7. SPAR X ground based and flight samples, Al-4.5wt%Cu alloy, face B21, etched.

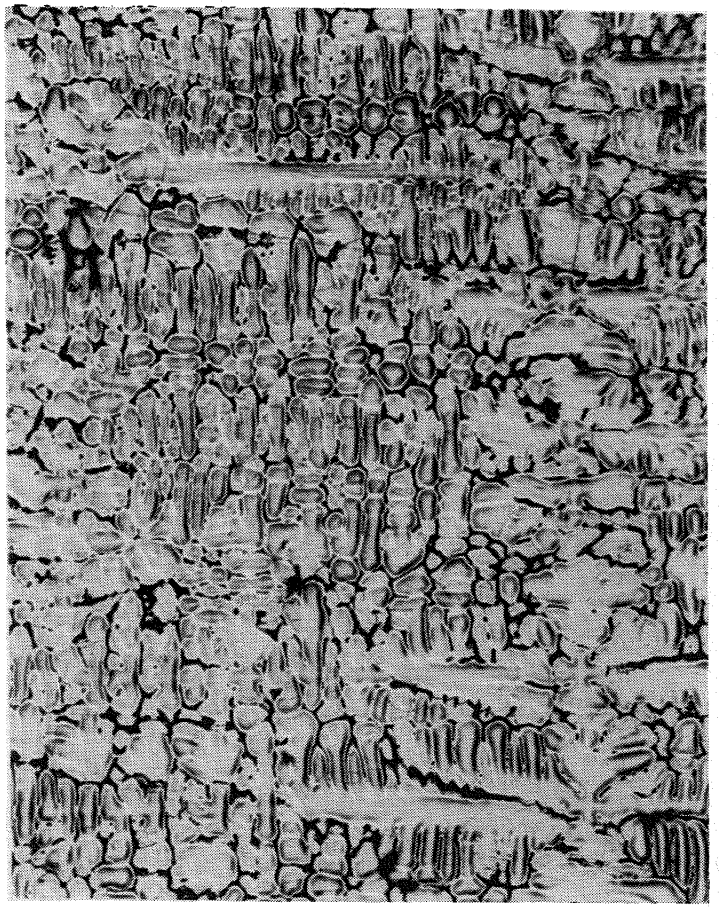

GROUND-BASED

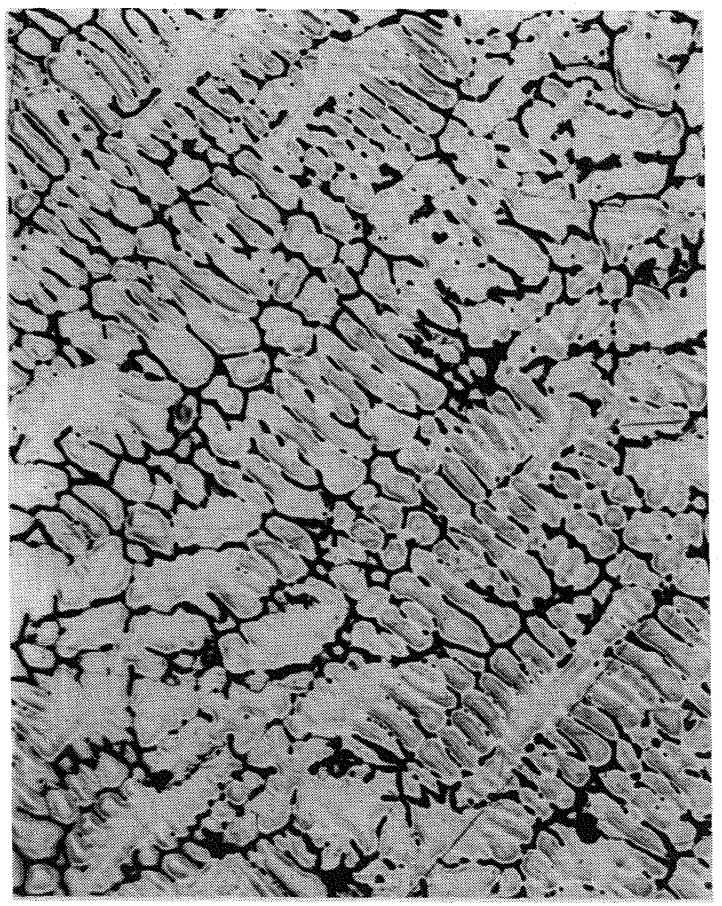

FLIGHT

Figure 4-8. Spar X ground-based and flight samples, Al-4.5wt%Cu alloy, face B11, etched (50X).

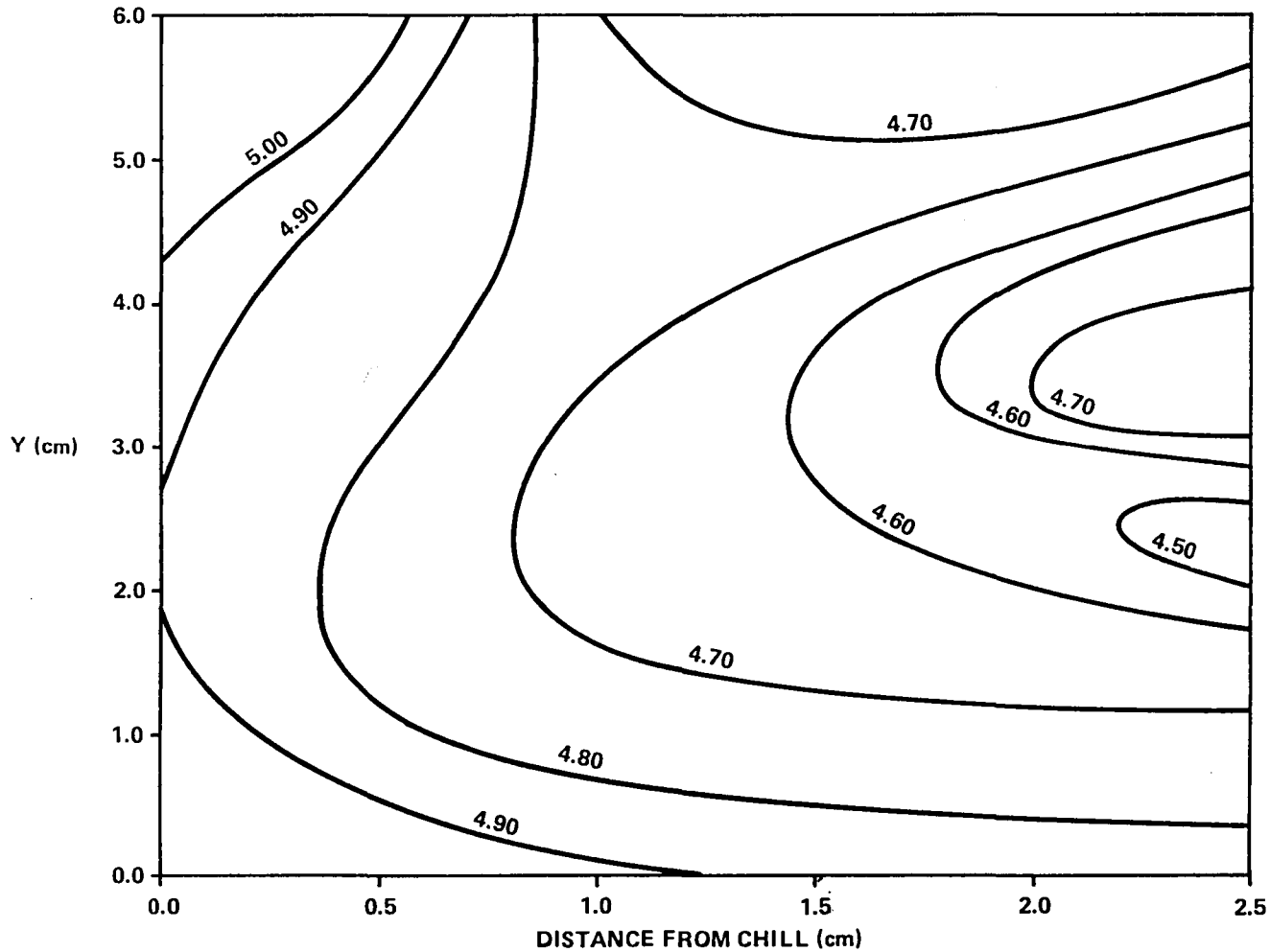

Figure 4-9. Final local average composition, percent Cu, ground-based ingot.

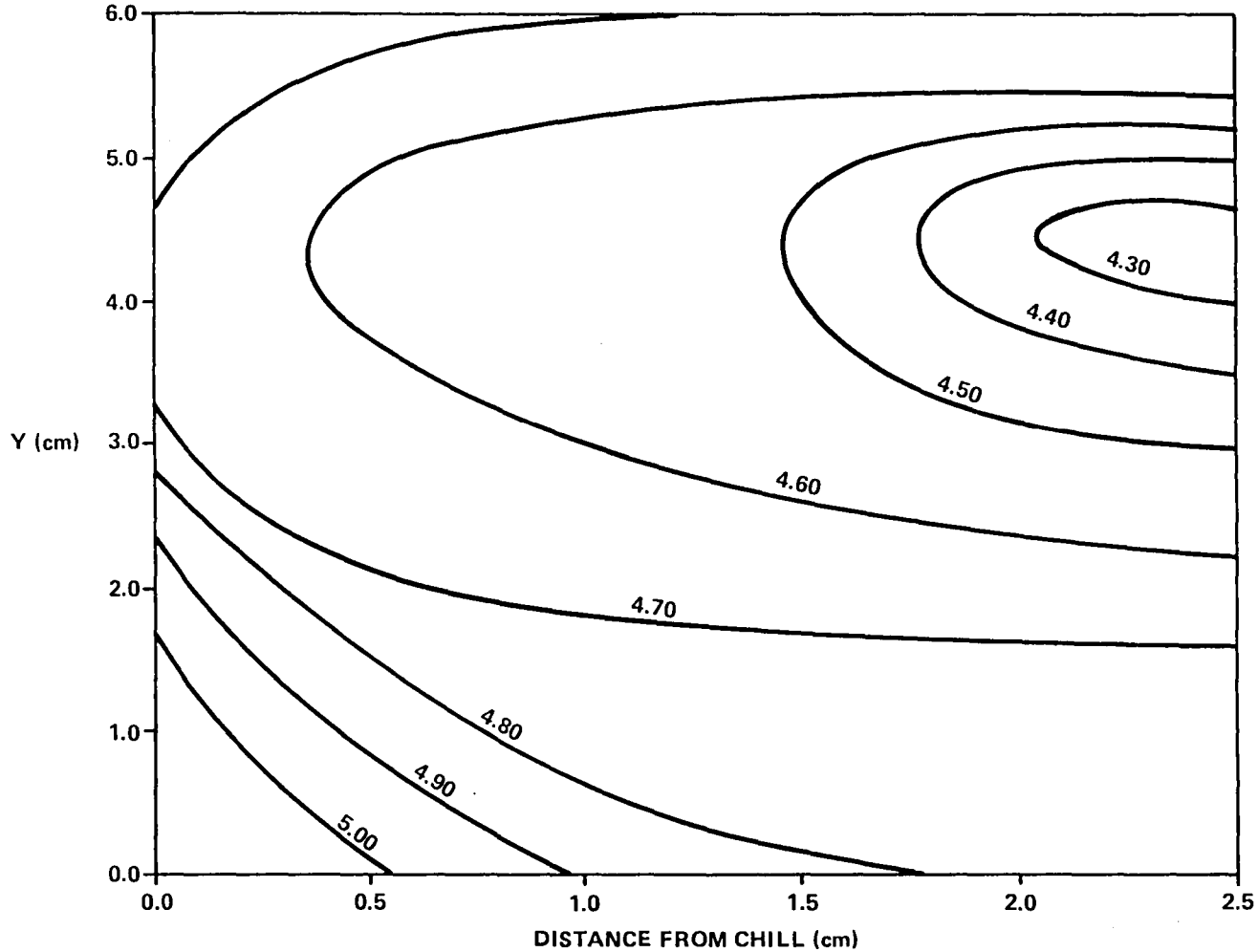

Figure 4-10. Final local average composition, percent Cu, flight ingot.

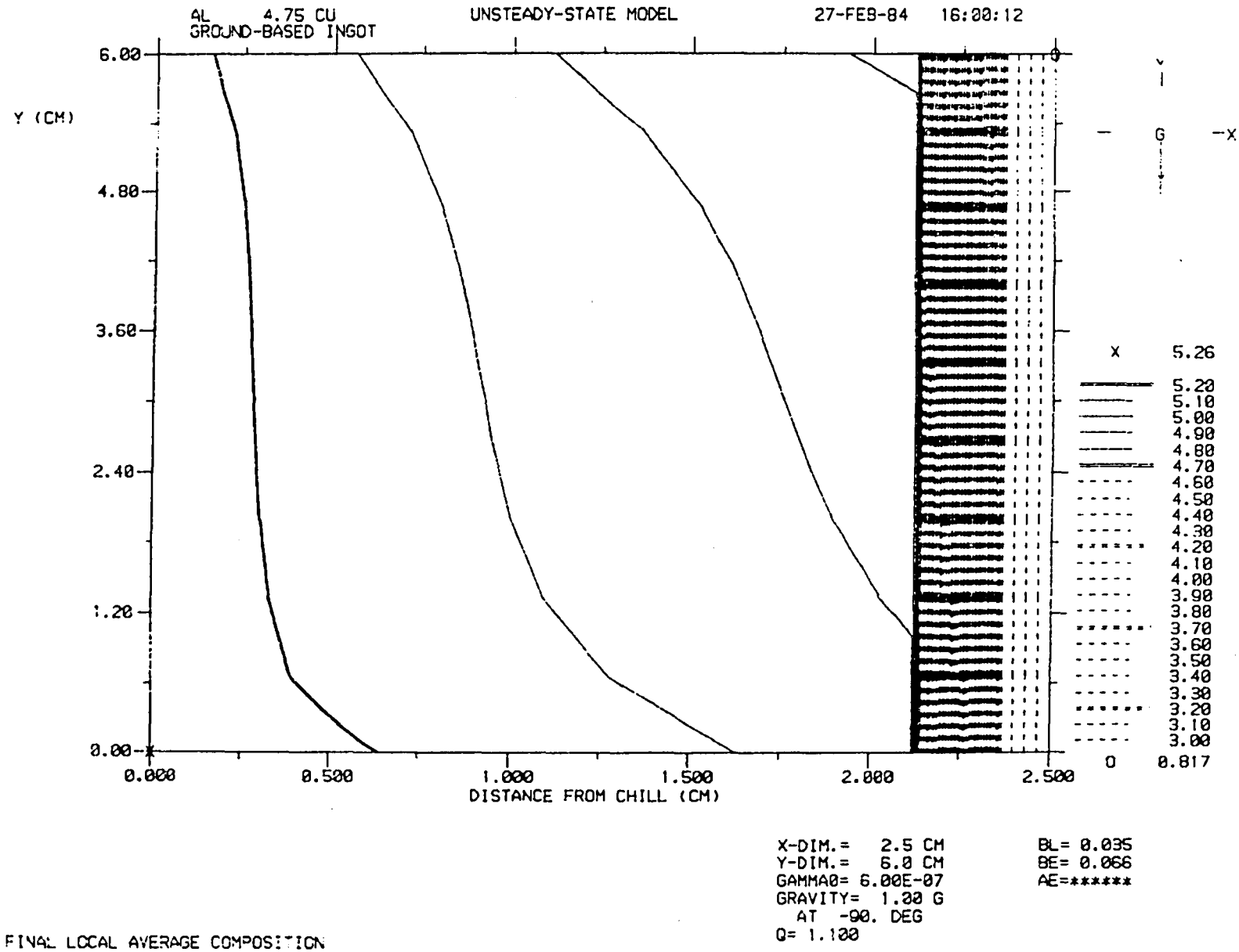

Figure 4-11. Modeled ground-based sample: macrosegregation profiles.

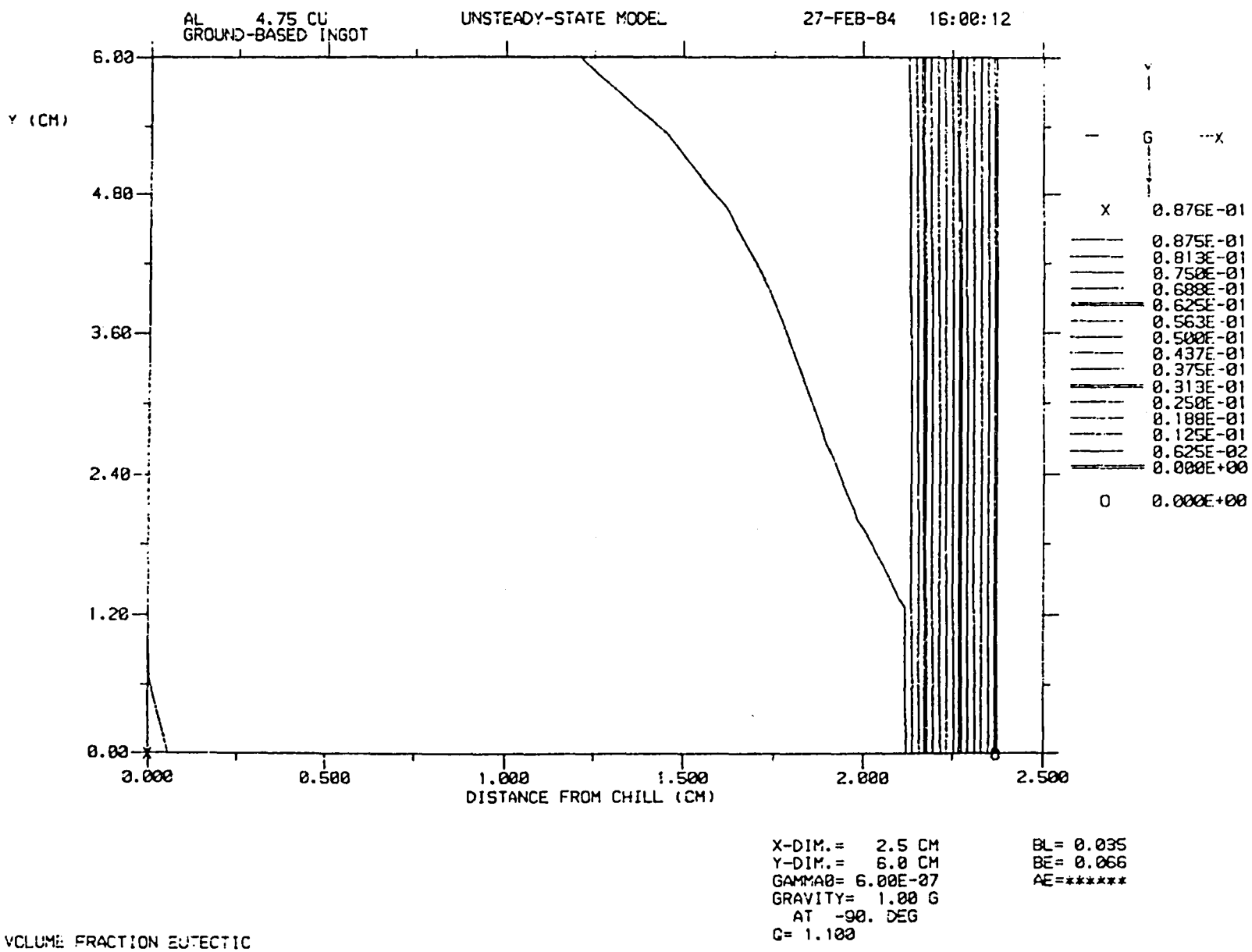

Figure 4-12. Modeled ground-based sample: volume fraction eutectic.

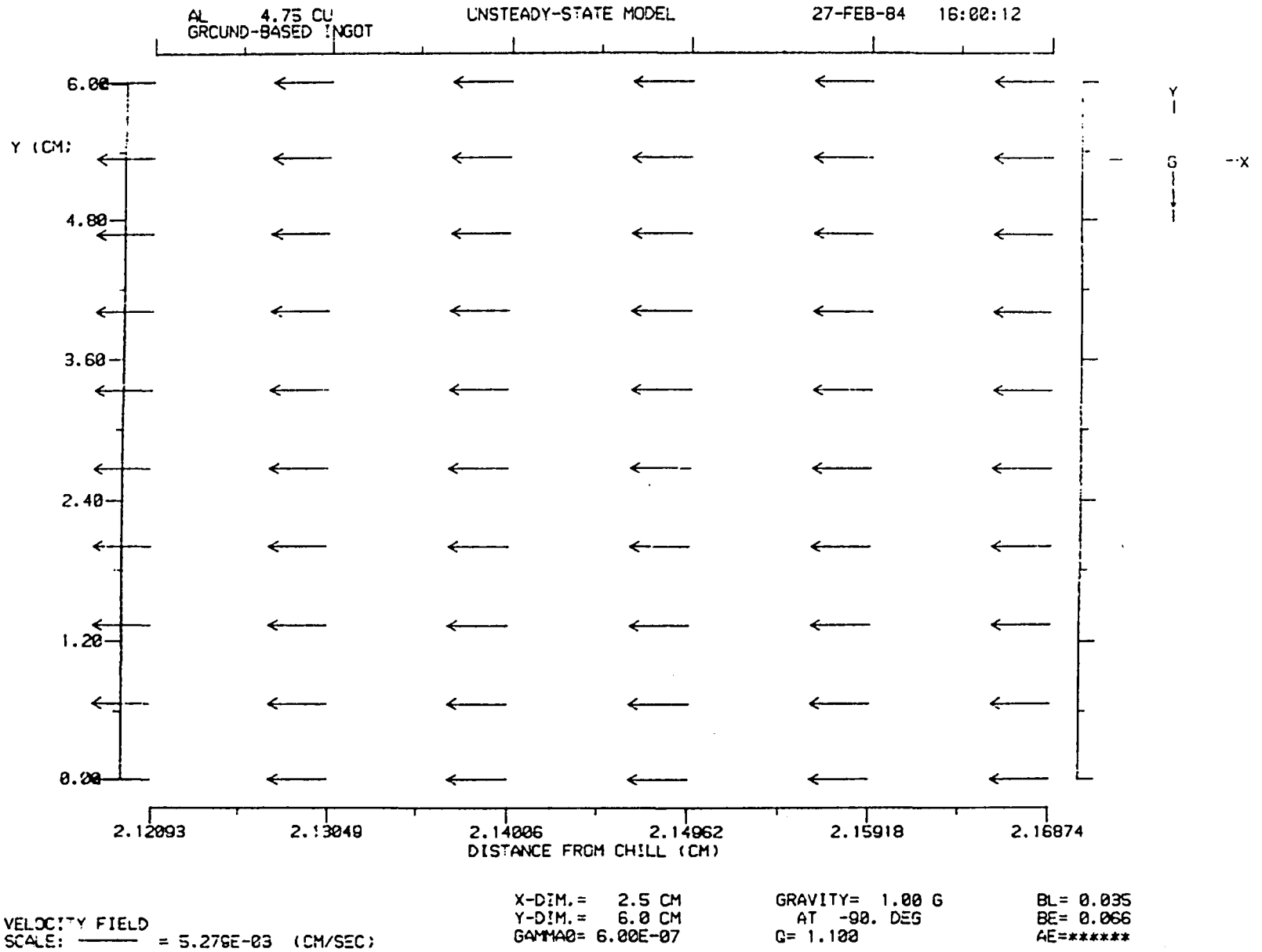

Figure 4-13. Modeled ground-based sample: velocity field.

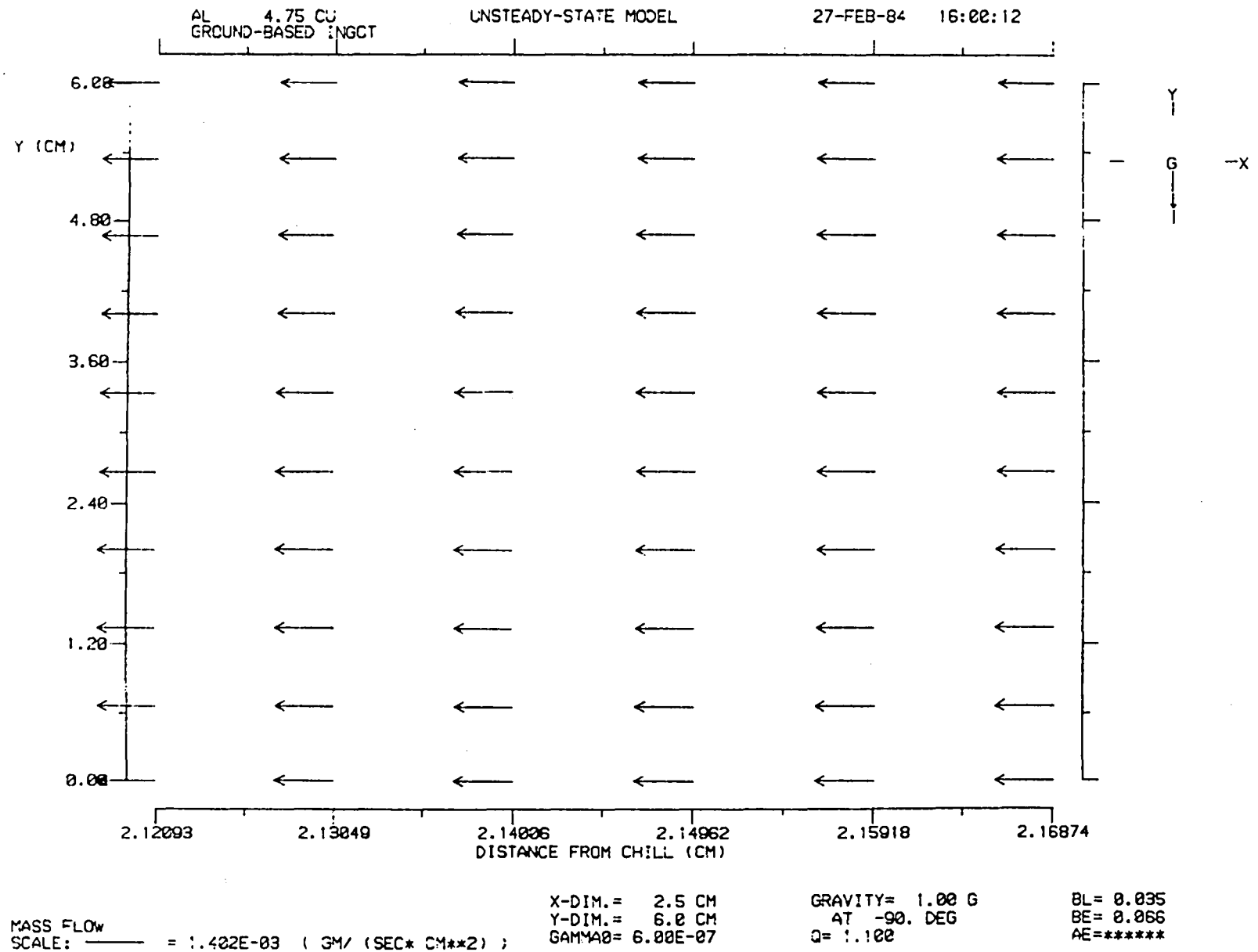

Figure 4-14. Modeled ground-based sample: mass flow.

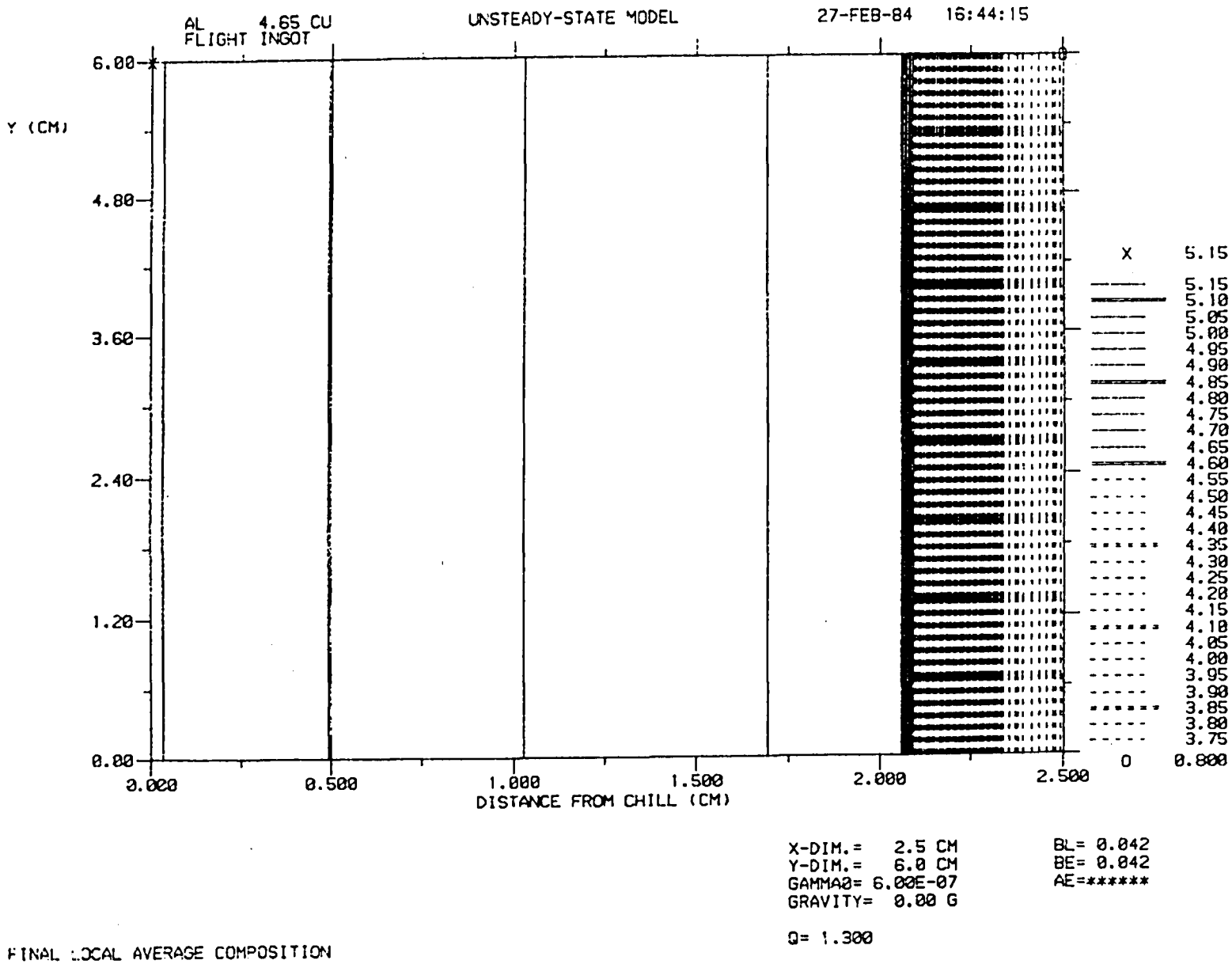

Figure 4-15. Modeled flight sample: macrosegregation profiles.

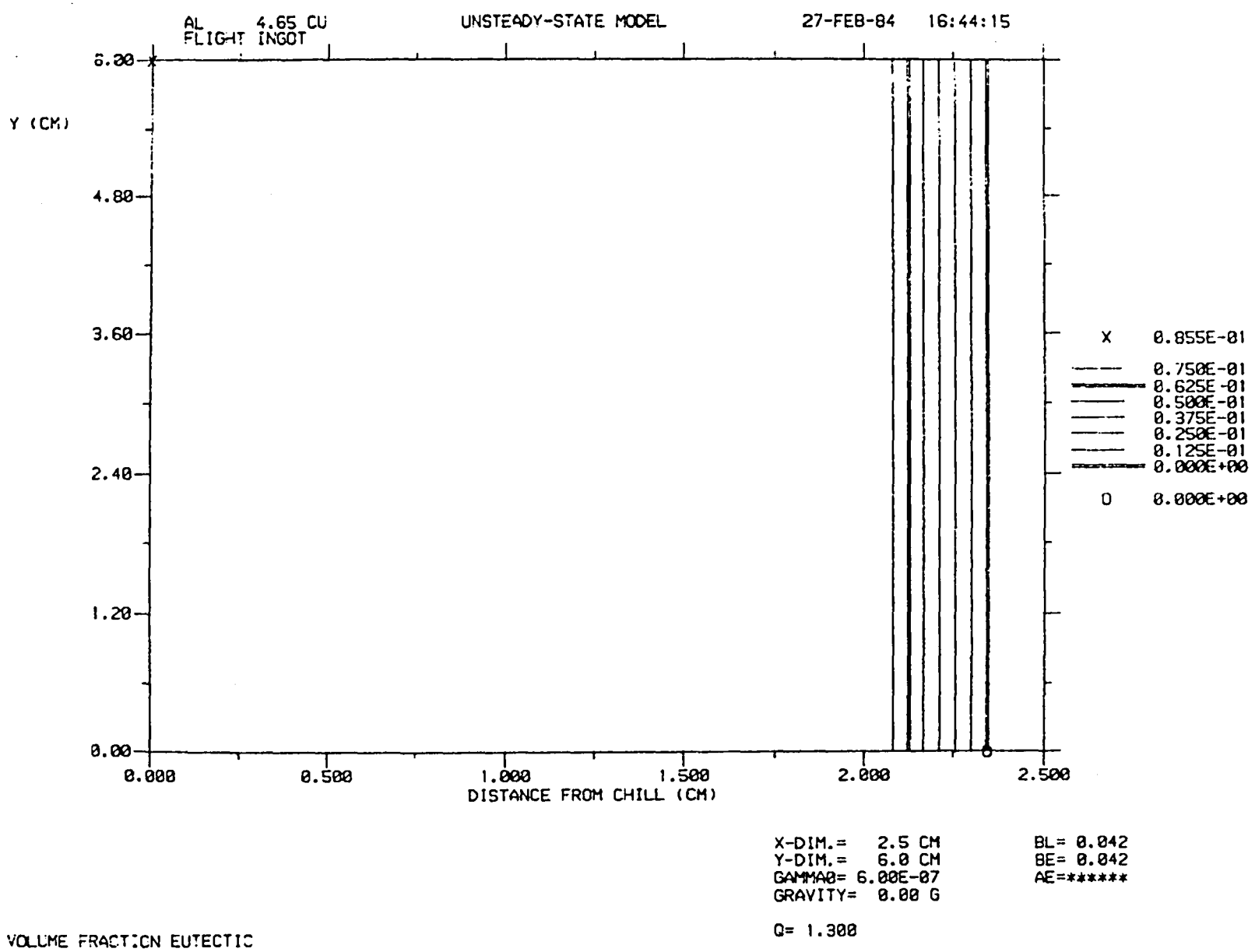

Figure 4-16. Modeled flight sample: volume fraction eutectic.

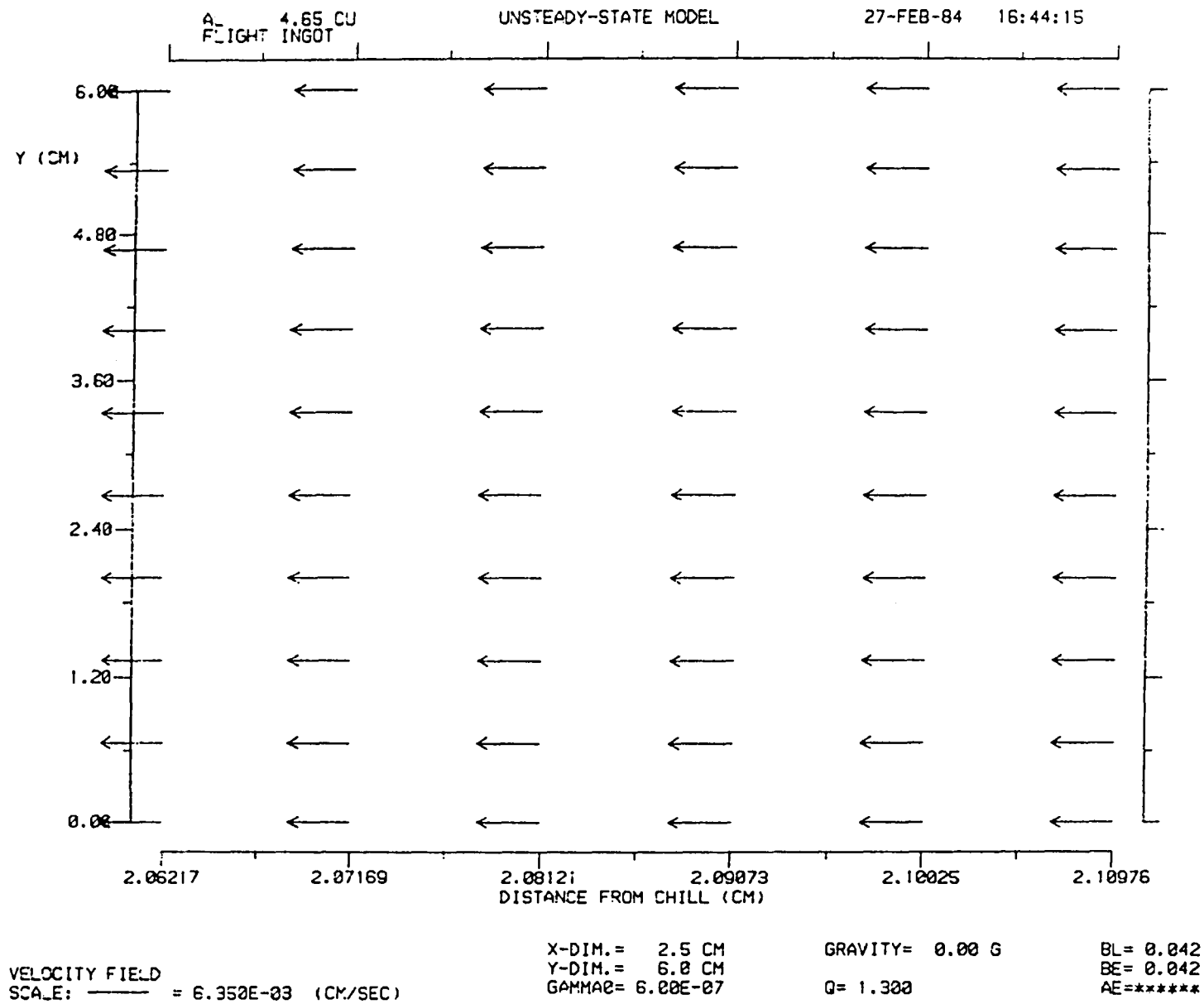

Figure 4-17. Modeled flight sample: velocity field.

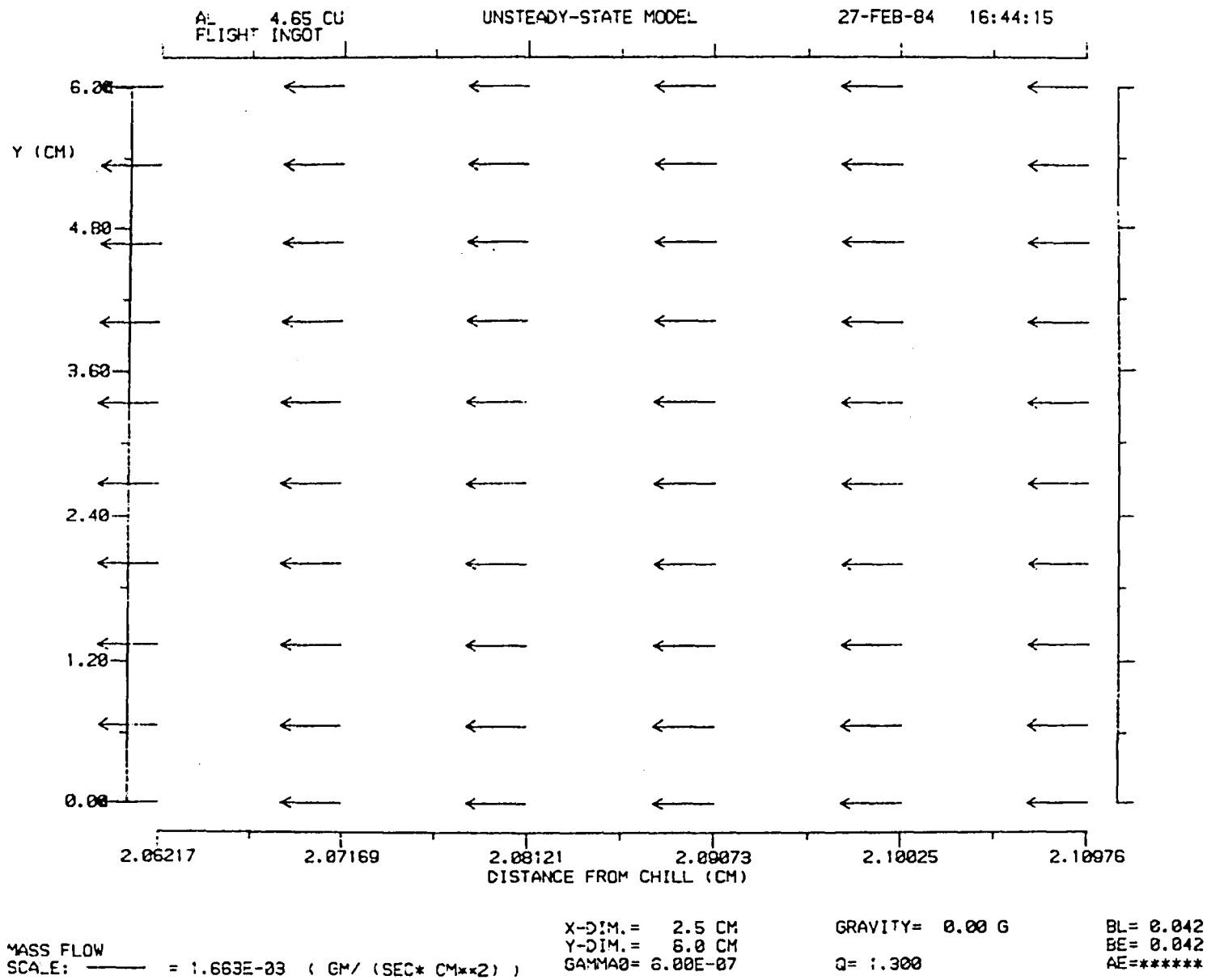

Figure 4-18. Modeled flight sample: mass flow.

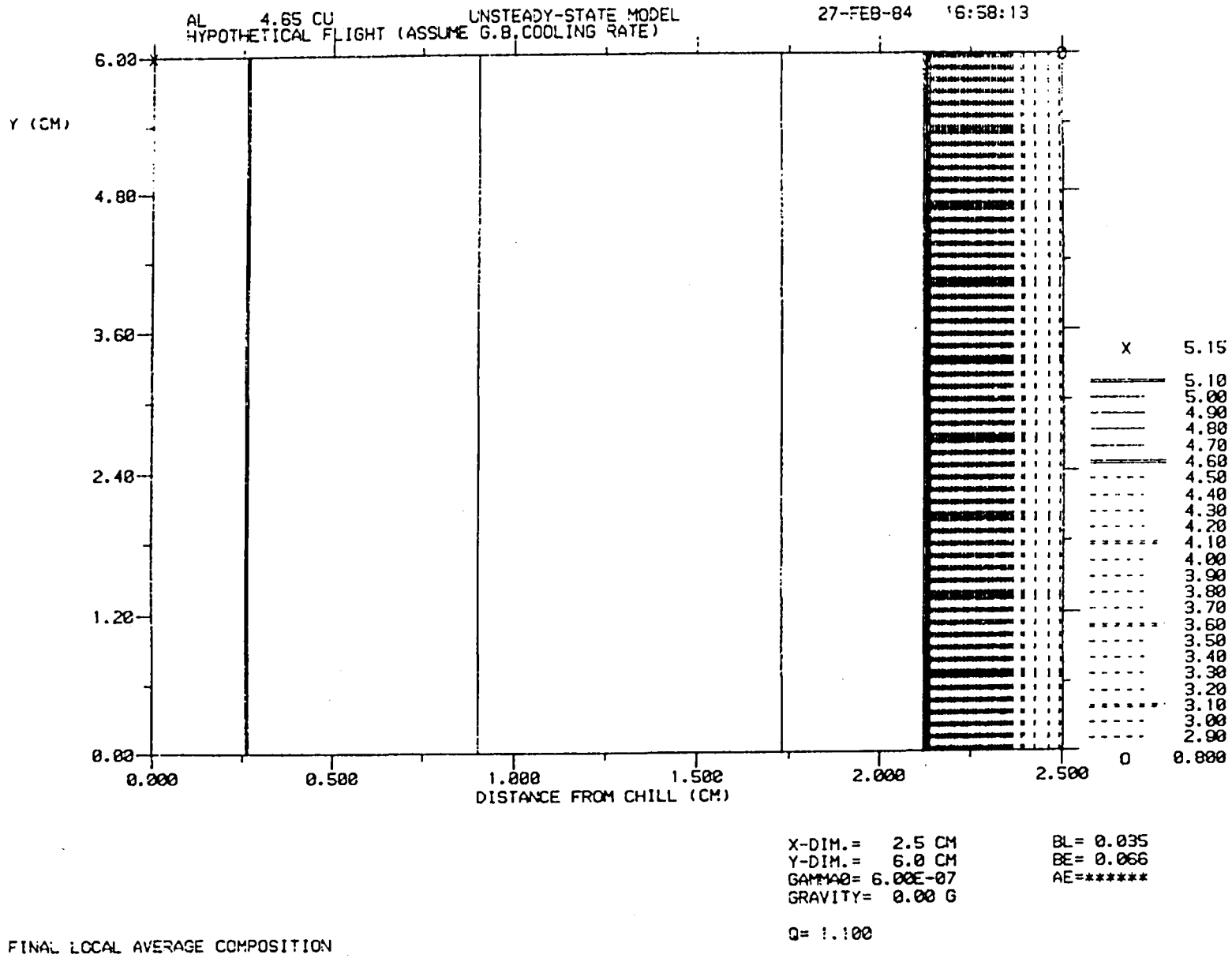

Figure 4-19. Modeled hypothetical flight sample: macrosegregation profiles.

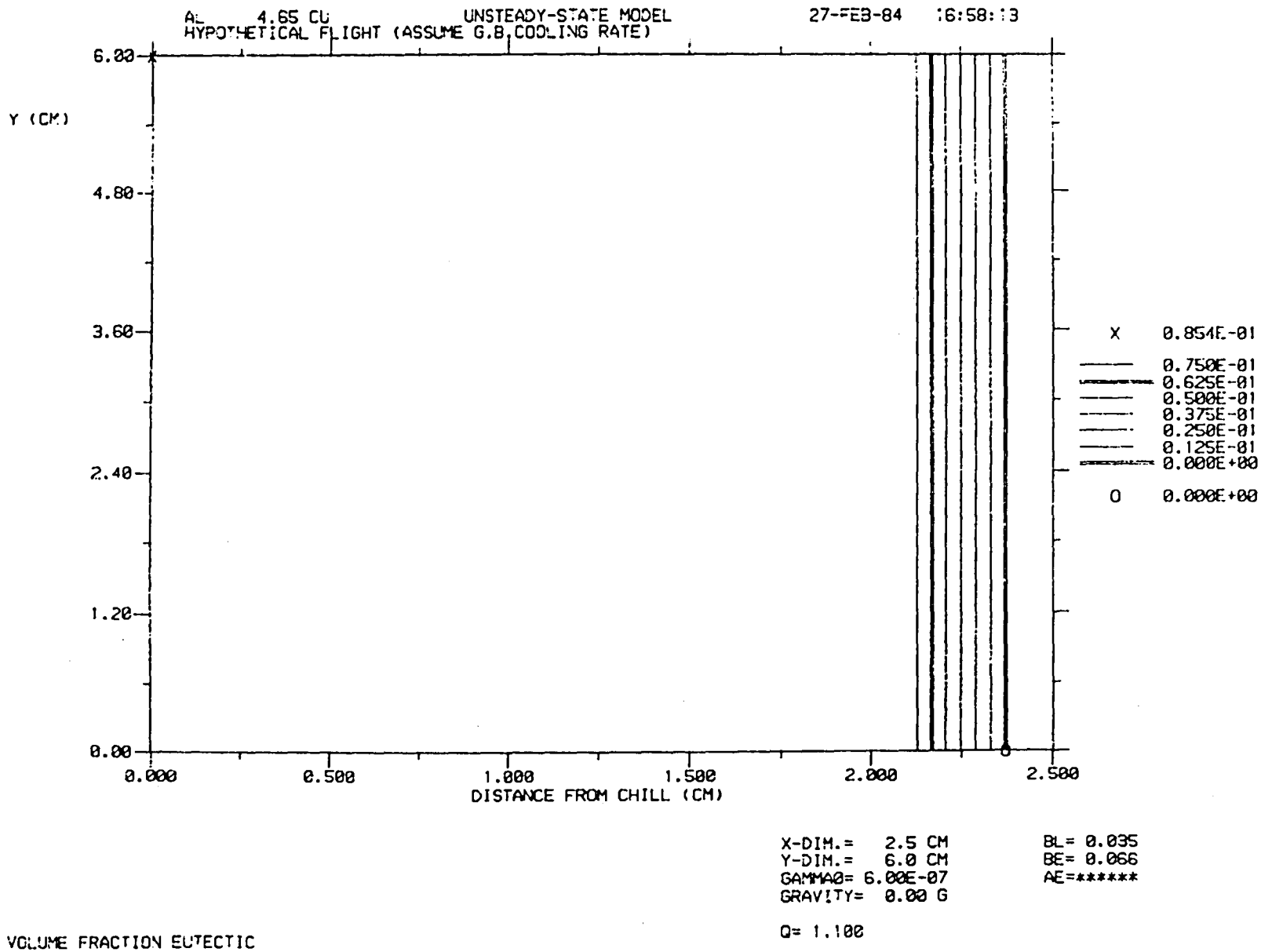

Figure 4-20. Modeled hypothetical flight sample: volume fraction eutectic.

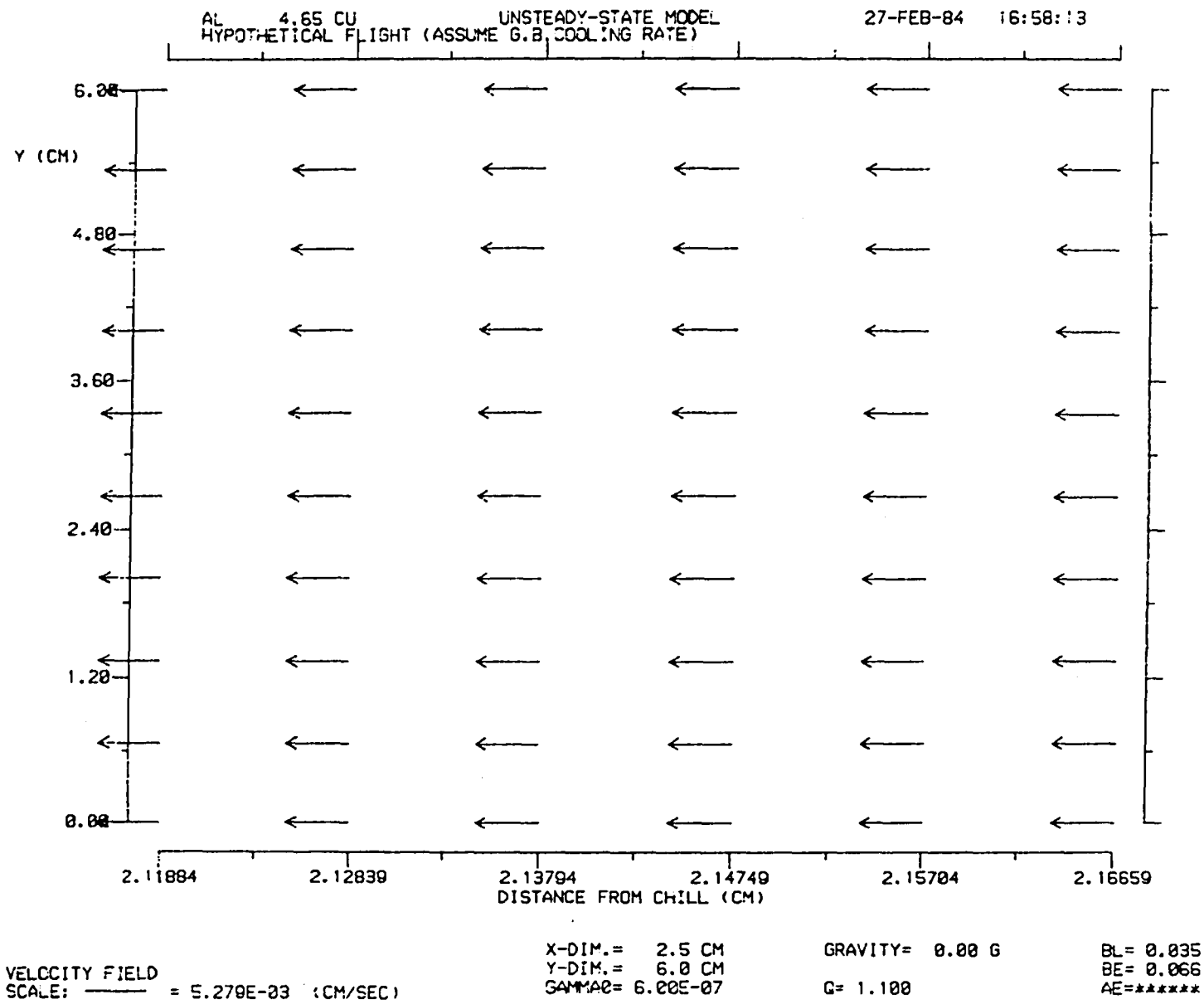

Figure 4-21. Modeled hypothetical flight sample: velocity field.

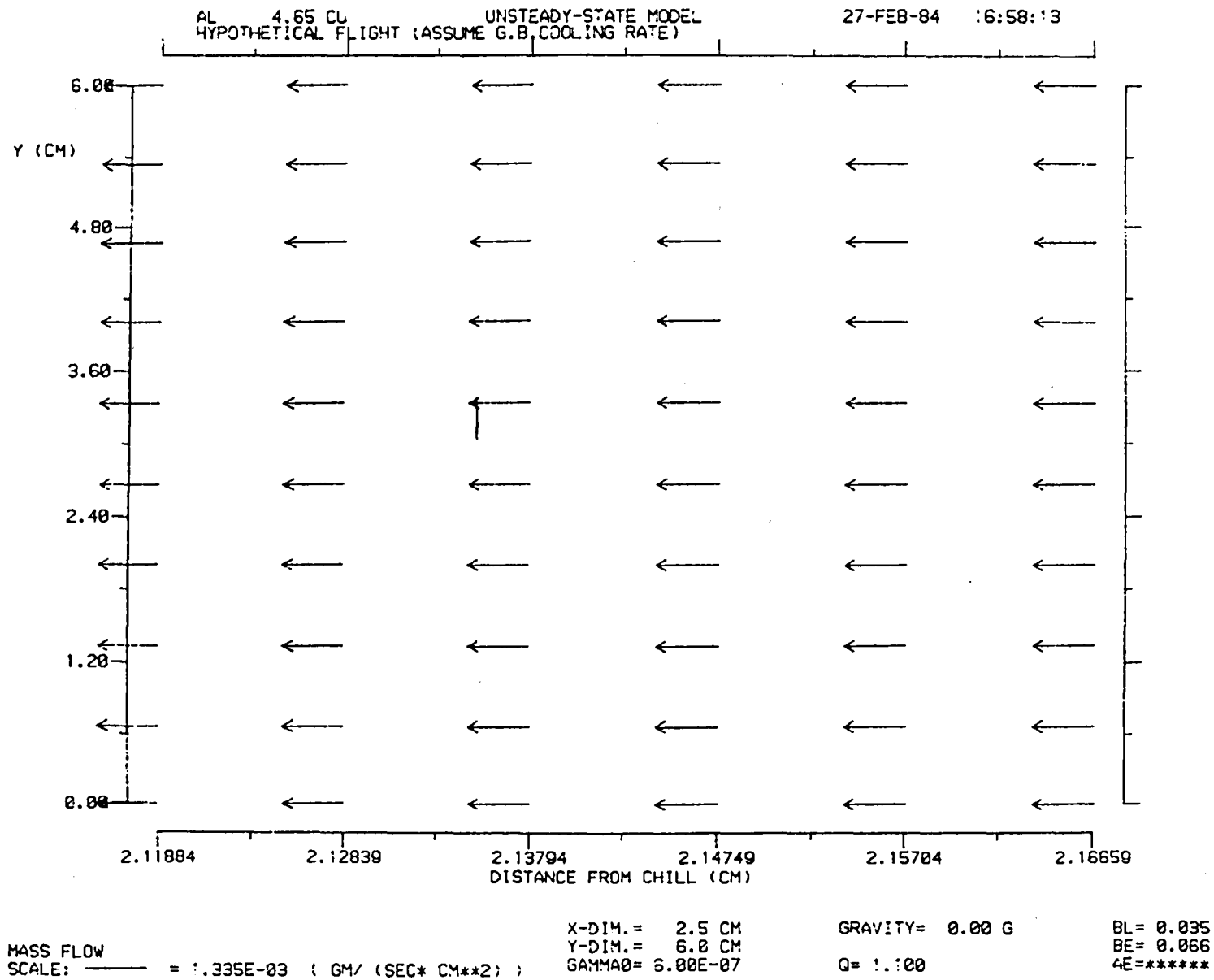

Figure 4-22. Modeled hypothetical flight sample: mass flow.

SECTION V

SPAR EXPERIMENT 77-9/1R

SPAR X

FOAM COPPER

Principal Investigators

Robert B. Pond, Sr.
John M. Winter, Jr.

January 30, 1986

I. INTRODUCTION

The objective of this experiment has been to produce "foam" copper. More accurately, the objective has been to produce "foam" copper alloy, since the copper-copper oxide utilized is really an alloy.

II. FUNDAMENTAL CONSIDERATIONS

First, we shall consider the gas producing reaction.

The fire refining of copper as practiced today has been used for a long time with virtually no change over the years. The molten bath is oxidized until the copper becomes saturated with oxygen, forming "set copper," the slag containing the oxidized impurities is removed, the bath is covered with charcoal and the metal is "poled" to reduce the copper oxide and produce "tough pitch" copper. In "poling," green tree trunks are actually thrust under the surface of the molten metal to promote the reaction;

$$Cu_2O(\ell) + C \text{ (graphite)} \rightarrow 2\,Cu(\ell) + CO\uparrow \qquad (1)$$

and poling continues until the copper reaches the tough pitch stage, when it contains about 0.5wt% Cu_2O, or about 0.05wt% O (monatomic oxygen).

In this investigation, we used the reaction (1) as a means of generating any desired amount of gas in molten copper. The advantage here is that the process is not limited by the solubility of a particular gas in a molten or solid phase. The amount of gas which can be generated is limited only by the reactants, and indeed, as will be discussed, limiting the reactants is the way to control the amount of gas generated. Since copper and oxygen actually form a binary eutectic system [1] in the form of the Cu_2O - Cu eutectic (3.4wt% Cu_2O) system it is possible to prepare a continuous range of copper-oxygen "alloys." This range of compositions can provide more than enough gas by the reaction (1). For example, 1/2 cm^3 of tough pitch copper (0.05wt% monatomic oxygen) could generate 15 cm^3 of CO at 1 atmosphere at 1100°C. The same volume of Cu_2O - Cu eutectic could generate 116 cm^3 of CO at the same temperature and pressure. The same volume of pure Cu_2O could generate more than 2.3 liters of CO at the same temperature and pressure!

There are several additional possibilities one might consider. If one wanted to limit the oxygen available for the reaction, one might "getter" the excess oxygen by using an alloy addition such as aluminum. The result would be a fine dispersion of alumina which could possibly strengthen the matrix. If one wanted an alloy with a lower melting point, one could make ternary (or higher) alloys by additions of metals such as tin. The only limit on the resulting bronze alloys to be considered would be avoiding alloying elements which tie up all the available oxygen.

The fact that the gas-generated reaction has been used in fire refining copper for a very long time stands as proof that the reaction does occur. However, it may be of interest to look at the thermochemistry of the reaction. Using standard tables of thermodynamic constants [2], one computes the Gibbs free energy of reaction (1) as written to be -43,333 gm-calories per mole at 1227°C (1500°K) or -38,261 gm-calories per mole at 1100°C (1373°K). The latter is the solidification temperature for the Cu_2O. There is no doubt that the reaction goes strongly at these temperatures. The fact that CO_2 does not enter into the reaction is apparent when one examines the classic producer-gas reaction;

$$C + CO_2 \rightarrow 2CO \quad . \tag{2}$$

Since the reaction is endothermic, an increase in temperature means an increase in concentration of CO. In fact, it turns out that CO_2 cannot exist at a temperature above 1000°C in the presence of C [3]. Examination of the copper-oxygen phase diagrem [1] shows that CuO does not enter into consideration at these compositions.

Now consider the effect of causing this reaction to proceed in a closed container. It is appropriate to ask what CO pressure would have to develop in order to stop the reaction. (The free energy calculation above assumes, of course, that CO is produced at 1 atmosphere.) The Gibbs free energy change for a process which occurs isothermally may be obtained by integrating the expression for its partial derivative with respect to pressure at constant temperature:

$$\frac{2F}{2P}_T = V$$

$$F_2 - F_1 = \int_{P_1}^{P_2} V(P)\, dP$$

for an ideal gas, take V = RT/P. So,

$$F_2 - F_1 = RT \int_{P_1}^{P_2} \frac{dP}{P} = RT \ln \frac{P_2}{P_1} = \text{work done in isothermal compression}$$

assume that P_2 is that pressure at which the change in free energy from the reaction is zero, so that $F_2 = 0$. Then, using

$$F_1 = -38{,}261 \text{ (gm) cal mole}^{-1}$$

$$P_1 = 1 \text{ atm}$$

$T = 1373°K$

$R = 1.987$ (gm) cal $°K^{-1}$ $mole^{-1}$

$$\ln P_2 = \frac{38,261}{(1987)(1373)} = 14.02$$

$$P_2 = e^{14.02} = 1.2 \times 10^6 \text{ Atm}$$

which is the pressure CO would theoretically attain before the reaction would stop. Since it is certainly clear that the build-up of CO pressure will not slow the reaction, the quantity of reactants will have to be limited to guarantee the pressure will not exceed the strength of the sample cartridge at the operating temperature.

To summarize to this point, the design of the experiment is based on two facts. First, copper and copper oxide form a binary eutectic "alloy" system. Second, these "alloys," when molten, can react with carbon to generate carbon monoxide gas. Taken together, these facts reveal a scheme for generating any desired quantity of gas in molten copper. The quantity can be controlled by controlling either the amount of oxygen available, or the amount of carbon available.

III. EXPERIMENTAL DESIGN CONSIDERATIONS

It is pertinent to examine the evolution of the bubbles of carbon monoxide more carefully.

The only solid phase in reaction (1) is the carbon. Its distribution will determine the distribution of gas bubbles, since it is the nucleating phase for the CO. For this reason, the carbon must be finely dispersed throughout the initial load of copper which is melted in microgravity. This can be accomplished by mixing an appropriate quantity of lamp black into finely powdered copper, and consolidating the result through cold deformation.

Bubbles do not just form by themselves in a melt. Their internal pressure has to be large enough to balance the surface tension of their interface with molten copper (when in equilibrium). The relation is given by:

$$P_1 = \frac{2\sigma}{R} \qquad (1)$$

where

P_1 = internal pressure of the bubble

σ = surface tension of the interface

R = radius of the bubble .

If we equate the increase in volume of the initial load to the product of the bubble volume (as implied in the above relation) and the number of nucleating sites, we get:

$$V_f - V_0 = n V_0 \frac{4}{3} \pi R^3 \qquad (2)$$

where

V_f = final volume of copper bubbles

V_0 = volume of original pellet of copper

n = number of nucleating sites per cm^3 of initial volume.

If we define an expansion ratio,

$$X = \frac{V_f}{V_0} \quad ,$$

and if we then combine equations (1) and (2):

$$n = a_0 \frac{P_1^3}{\sigma^3} [X-1] \quad .$$

We can now define a characteristic separation between nuclei, ℓ;

$$\ell = n^{-1/3}$$

$$P_1 = b_0 \frac{(\sigma)}{\ell} [X-1]^{-1/3} \quad . \qquad (3)$$

It should be noted at this point that the pressure P_1 must not only be the the internal pressure of the bubbles, but also the internal pressure of the container if there is to be equilibrium (and only CO present) when molten in microgravity.

If we assume the cartridge is loaded with a pellet of volume V_0 and then filled with CO at one atmosphere before it is sealed, we can obtain a second relationship by using the ideal gas law. Here we will assume that none of the CO initially present has time to go into the melt, and none of the newly generated CO contributes to the gas trapped in the cavity outside the foam metal, but of course both have to exist at the same pressure to be in equilibrium. Then:

$$\frac{P_0(C-V_0)}{RT_0} = \psi = \frac{P_1(C-XV_0)}{RT_1}$$

or:

$$\frac{P_1}{P_0} = \frac{T_1\,[1-(V_0/C)]}{T_0\,[1-X\,V_0/C)]} \qquad (4)$$

$$0 \leq (V_0/C) \leq X\ (V_0/C) \leq 1 \qquad X \geq 1$$

where

ψ = number of mols of CO initially sealed into the cartridge

P_0, T_0 = pressure, temperature when sealed

P_1, T_1 = pressure, temperature in microgravity

C = interior volume of cartridge .

In the foregoing, we can assume that σ, P_0, T_0, T_1, and C are given. If we then choose a P_1 and an X, equation (4) tells us what the initial load volume must be and equation (3) tells us what the mean separation between nuclei in that load must be.

Finally, we can get an idea of what the effective "ℓ" will be for the specific geometry we intend to use. Assume we have a copper sphere of radius "Q." Assume it is coated with a layer of lamp black which is continuous. Assume the oxygen is homogeneously distributed throughout the copper. Then if the entire sphere contributes oxygen to the reaction (1), the reaction goes to completion, and we have equilibrium. In this case, there exists an internal sphere with radius q_1 such that exactly half of the oxygen has crossed that surface on its way to the surface of sphere Q. The sphere q_1 encloses half the volume of sphere Q. Therefore:

$$q_1^3 = Q^3 - q_1^3$$

$$q_1 = (1/2)^{1/3}\, Q \quad .$$

If the reaction goes only 50 percent to completion, then all the oxygen must be supplied by the portion of the sphere Q which lies outside sphere q_1. In this case there exists a new sphere with radius $q_{0.5}$ such that it divides this new volume in half. Therefore:

$$q_{0.5}^3 = q_1^3 = Q^3 - q_{0.5}^3$$

but

$$q_1^3 = Q^3/2$$

so,

$$q_{0.5} = (3/4)^{1/3} Q \quad .$$

In general, if "α" denotes the fraction of completion of the reaction (i.e., α = 1.0 if 100 percent, α = 0.25 if 25 percent), then we can write:

$$q_x = \left(1 - \frac{\alpha}{2}\right)^{1/3} Q \quad .$$

The mean diffusion distance of oxygen atoms in each of these cases is just the distance between the sphere which half the oxygen atoms cross and the exterior surface. We can define a mean diffusion distance for each degree of completion of the reaction as follows:

$$\langle d_x \rangle = Q - q_x$$

$$\langle d_x \rangle = 1 - \left(1 - \frac{X}{2}\right)^{1/3} Q \quad . \tag{5}$$

And finally we can comment that since we defined the characteristic separation between nuclei as "ℓ," then the effective "ℓ" in this case must be approximately twice the mean diffusion distance:

$$\langle \ell_x \rangle_{\text{effective}} = 2Q \left[1 - \left(1 - \frac{X}{2}\right)^{1/3}\right] \quad . \tag{6}$$

For example, if Q = 5 microns, then we have a relation between the degree of completion of the reaction and $\langle d_x \rangle$ effective, as shown in Table 1.

TABLE 1. EFFECTIVE "ℓ" AS A FUNCTION OF PERCENT COMPLETION OF REACTION

Percent Reaction	$<\ell_X>$ Effective
100	2.1 microns
50	0.9
25	0.4

Where we assume that the oxygen is homogeneously distributed throughout the copper sphere.

IV. GROUND BASED DEVELOPMENT OF APPROPRIATE Cu-Cu_2O-C FLIGHT LOADS (PELLETS)

A water manometer attached to a sample cartridge with suitable arrangements for reusing the seals was used to study rate and quantity of gas evolved during the reaction between copper oxide and carbon. Approximately 80 runs were made, all of which fit chronologically into several categories.

The first category was typically an experiment which monitored gas evolution following abrupt immersion of a room temperature sample cartridge into a 1150°C furnace. These experiments demonstrated excellent reproducibility. They showed appropriate quantities of gas were generated fast enough to be compatible with a 60 sec "soak" time at 1150°C in a flight experiment. They also delineated the difference in peak rates between 44 micron copper powder and 10 micron copper powder (4.7 cm^3/sec and 2.5 cm^3/sec, respectively). These experiments also revealed that the reaction slowed to a very small rate if the carbon distributed in the copper powder was allowed to float to the surface of the molten copper. Maximum rates were measured after refining a method of cartridge loading which involves wedging Mo-30W turnings into the bottom of the cartridge to form a mesh which effectively holds the lampblack submerged once the copper melts. It became obvious that one can ignore the buoyancy of the carbon as it affects rate measurements only if doing the melting in microgravity. For this reason, any ground based experiments which melted loads like those to be used in the flight experiment could not be expected to duplicate the reaction rate expected in microgravity. Indeed, it was difficult to get the reaction to go to completion in hours once the carbon floated to the top in a ground based melting experiment. This meant the ground based sample cartridges were of little use beyond simulating the thermal load which the flight cartridges will impose on the furnace. Recognizing this, but still obligated to deliver these samples, we prepared loads for the ground based cartridges which represented a reasonable guess at the final load which was used for the flight cartridge.

The second category of rate experiments chronologically was to establish limits on allowable preheat times and temperatures. It immediately became clear that the reaction proceeds at very respectable rates at temperatures below the melting point, thus generating the gas too early in the experiment. One could rationalize this by considering the oxygen present on the outside of the copper powder has essentially zero diffusion distance to get to the carbon. However, a careful search for data on diffusion constants for oxygen in pure copper near the melting point of copper revealed very little difference between diffusion in the solid compared to the liquid.

The best data we could establish was about 8 x 10^{-5} cm^2/sec in liquid copper, and 4 to 6 x 10^{-5} cm^2/sec in solid copper, both at the melting point [4].

To circumvent this problem we chose to make use of the fact that Cu_2O melts at a lower temperature than pure copper and the fact that molten Cu_2O has a very low contact angle on copper. (It readily "wets" copper). The idea was to isolate the source of oxygen from the copper until the melting point of copper oxide was exceeded. Thus, the experiment was composed of two "pellets." One was copper and carbon, the other largely copper oxide. This led to the third category of rate experiment.

Pellets of deioxidized copper loaded with a dispersion of lampblack were prepared by mixing nominally 9 gms of 10 micron copper powder with nominally 200 mgs of lampblack, pelletizing at 400°C and 125 ksi, and then "roasting" for 20 minutes at 1000°C. This last step utilizes part of the lampblack to deoxidize the copper. Each of these deoxidized pellets were subsequently loaded into sample cartridges along with a pellet formed from oxidized copper powder. The copper oxide pellets varied in weight. Subsequent gas generation did not scale according to copper oxide pellet weight, which may indicate the gas generating reaction was graphite limited. In three consecutive experiments, each load was "preheated" at 1000°C for various times ranging from 7 to 20 minutes, and then immersed into a 1150°C furnace. Previous measurements indicated it took about 60 seconds for the interior of the cartridge to reach a temperature where melting would begin (1066°C) under these conditions. Two minutes after immersion, the experiments generated 48 ml, 49 ml, and 55 ml of gas, respectively. Five minutes after immersion, they generated 60 ml, 81 ml, and 77 ml, respectively, all three having gone to completion in the gas generating reaction. These gas volumes are at room temperature and (very) slightly above one atmosphere. The experiments showed satisfactory consistency in rate and amount of gas evolved during about one actual minute at 1150°C. The consistency in total gas evolved when the reaction was allowed to go to completion was not as good, but was acceptable. It really does not affect the flight experiment. It does show, however, that if the furnace were to go out of control, the maximum pressure which could be developed would be only about 1.6 times the intended experiment pressure. This would still be well within the safe limits of the cartridge, which should withstand at least 10 to 12 times the intended experiment pressure (which is 20 atmospheres).

For the fourth, and final, category of rate measurement, we rescaled the experiments to produce a nominal 16 ml of gas using a nominally 6 gm copper slug. Two preliminary experiments produced 16 and 17 mls, respectively, a third overshot with 22 ml in the first 2 minutes. The rescaling produced an expansion ratio of about 7.5 with a cartridge pressure of 20 atmospheres. We then prepared samples for another dozen or so runs to better define conditions necessary for consistency.

We switched to a geometry for the copper oxide pellet which permitted fitting an irregular shaped shovel of copper oxide into a cylindrical hole in the copper pellet and crimping the top edges of the hole to trap the copper oxide pellet.

Many more samples were prepared and run (a grand total of 84) to refine the rates and volumes of gas production and to establish a reproducible pattern for sample preparation. The samples selected for the flight experiment were prepared from 6 grams of copper and 60 mg of carbon, ending up with a combined weight of 4.83 gm after pelletizing and hole drilling. The Cu_2O loads weighed 0.47 gms.

V. FLIGHT CARTRIDGE CONSIDERATIONS

It was apparent early in the study that the thin walled stainless steel GFE cartridge (MSFC Dwg 95M19104) would not be adequate. Both different design (for pressure) and a different material were required.

Material Selection Considerations. Any candidate material must have adequate mechanical strength at 2100°F, and not be attacked by molten copper, etc. at 2100°F. It was preferable not to have the container provide a reactant (e.g., graphite) to provide more positive control of the distribution of the gas producing reaction. Thermal conductivity could not be too low if walls were thick. Fabrication capabilities and limitations can dictate design options, and reproducibility of fabrication is important for some materials such as refractory ceramics which are very sensitive to curing and firing schedules. Shock resistance for general handling and launch set-back forces must be considered. Combinations were considered where, for example, the outer shell would provide the pressure strength, an inner liner would provide the corrosion resistance, and an intermediate layer would keep the two from interacting at 2100°F.

A lot of data was collected on high temperature properties of many candidate materials. Among those considered were the austenitic stainless steels, assorted tool steels, nickel based alloys such as Inconel X, 617, and 671, and Hastelloy X and R-235, iron-nickel based alloys such as RA 330, RA 333, and Incalloys, cobalt based alloys such as Haynes 188, Vitallium, Haynes Satellite 27 and 30, tantalum, and molybdenum based alloys such as Mo-30W and TZM. Also in the running were machineable ceramics, plastic refractories (high alumina and high magnesia), castable refractories, quartz, Vycor, and graphite.

The material selected was TZM (Mo-0.5Ti-0.08Zr-0.015C). It has a tensile strength of 53 ksi at 2400°F and a 10-hr rupture strength of 22 ksi at 2400°F. This becomes a 66 ksi tensile strength at 2100°F and an estimated 10-hr rupture strength of 40 ksi at 2100°F. The material has to go above 2500°F to recrystallize, and even if recrystallized (as in the case of a weld of TZM), it has a tensile strength of 35 ksi at 2100°F. Direct experiment with an open cartridge with a 0.812 inch OD and a 0.500 inch ID and closed with a screwed-in plug shows the cartridge should withstand well in excess of 270 atmospheres at 1150°C. In design estimates, the experiment probably ran around 20 atmospheres.

The cartridge had to meet the dimensional requirements set forth by the MSFC furnace engineer. These requirements are an 0.812 inch OD and a nominally 2.75 inch overall length. Tolerance on the former is ±0.005 inches, and on the latter, nominally ±0.1 inch.

Figure 1 shows the cartridge dimensions.

VI. FLIGHT RESULTS

The Cu-Cu_2O-C sample was contained in a TZM capsule having a wall thickness of 0.15 inch which was TIG-welded to maintain the pressure developed during the test. During the flight, the sample was melted and the reaction between the carbon

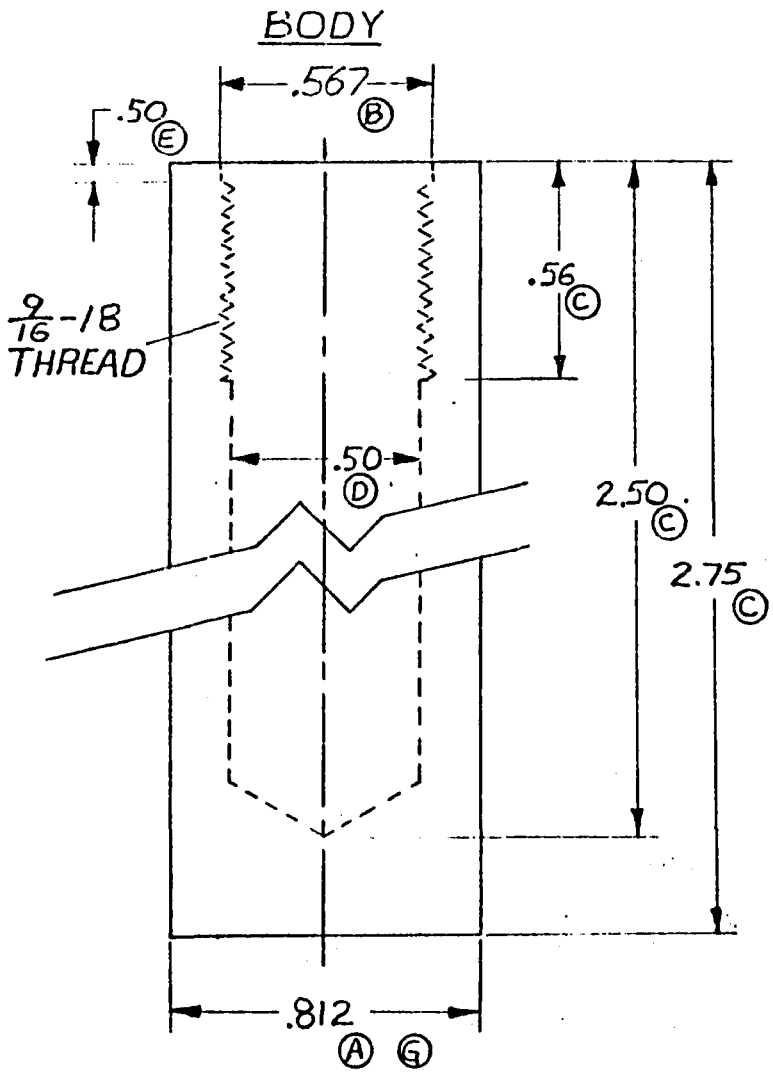

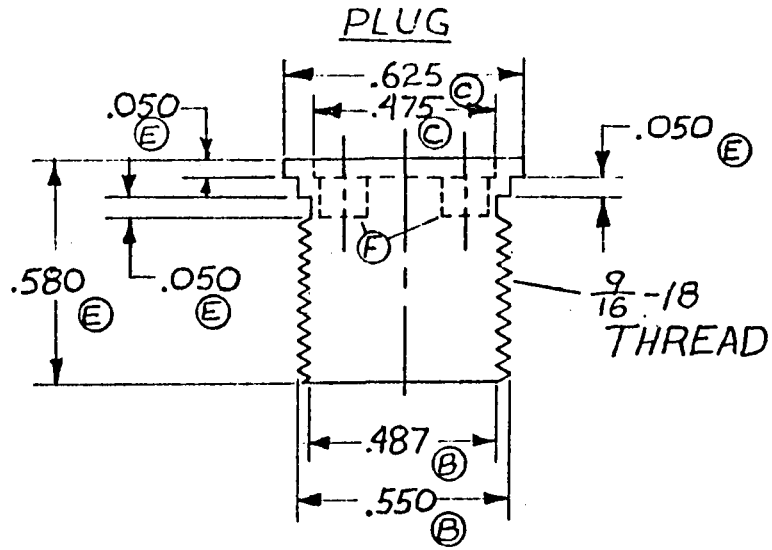

CARTRIDGE 77-9

MATERIAL: "TZM" Mo-0.5 Ti-0.8 Zr-0.015 C cf. AMAX SPEC. METALS

DIMENSIONS ARE IN INCHES

NOTES:

(A) ±.001" (C) ±.05" (E) ±.01"

(B) ±.002" (D) DRILLED HOLE 1/2"

(F) TWO BLIND 1/8" DRILLED HOLES 0.1" DEEP ON 5/16" CTRS.

(G) .812 O.D. SCALE: 2/1

BST 6-20-78

Figure 1.

and the copper-oxide occurred as expected. During the flight, the temperature measurement of the capsule was lost; and therefore, it is not known whether or not the sample solidified before it became affected by the Earth's gravitation. However, the reclaimed capsule provided evidence that a copper foam was developed although it was not maintained.

The metal-carbon sample was positioned at the end of the 2-inch long by 0.5-inch cavity away from the TIG-welded end and was maintained in place by a helical spring to prevent its movement during handling and launching. In the reclaimed capsule, the copper was coated onto three-quarters of the inner surface of the cavity in the half nearest the TIG-welded end. This copper movement could have been the result of its wetting the surface of the TZM or that it developed as a foam which collapsed onto the surface. Isolated in this surface coating are 17 crystals of copper approximately 2 mm on an edge and extending from the surface 2 to 3 mm. This indicates that the pool of copper from which these crystals grew must have been at least 2 to 3 mm thick. Such crystals could not have been developed from a copper sheet generated by wetting but could have developed from a foam. Although this evidence strongly suggests the development of a copper foam, there is no evidence to support a reason for its collapse since the experiment may have been subject to relatively high "g' forces before solidification.

An indepth analysis of the flight results is continuing and it is expected that a further addendum report on this experiment will be published by the principal investigator at a future date.

SECTION VI

SPAR EXPERIMENT 76-20/3

SPAR X

CONTAINERLESS PROCESSING TECHNOLOGY

Principal Investigator

Dr. Taylor Wang, JPL

FINAL REPORT WAS NOT SUBMITTED DUE TO IN-FLIGHT CAMERA FAILURE (See page of SPAR X Post-Flight Engineering Report).

1. REPORT NO.	2. GOVERNMENT ACCESSION NO.	3. RECIPIENT'S CATALOG NO.
NASA TM-86548		

4. TITLE AND SUBTITLE	5. REPORT DATE
Space Processing Applications Rocket (SPAR) Project - SPAR X Final Report	July 1986
	6. PERFORMING ORGANIZATION CODE JA62
7. AUTHOR(S) R. Poorman, Compiler	8. PERFORMING ORGANIZATION REPORT #
9. PERFORMING ORGANIZATION NAME AND ADDRESS	10. WORK UNIT NO. M- 531
George C. Marshall Space Flight Center Marshall Space Flight Center, AL 35812	11. CONTRACT OR GRANT NO.
	13. TYPE OF REPORT & PERIOD COVERED
12. SPONSORING AGENCY NAME AND ADDRESS	Technical Memorandum
National Aeronautics and Space Administration Washington, D.C. 20546	14. SPONSORING AGENCY CODE

15. SUPPLEMENTARY NOTES

Prepared by Spacelab Payload Project Office.

16. ABSTRACT

The Space Processing Applications Rocket Project (SPAR) X Final Report contains the compilation of the post-flight reports from each of the Principal Investigators (PIs) on the four selected science payloads, in addition to the engineering report as documented by the Marshall Space Flight Center (MSFC). This combined effort also describes pertinent portions of ground-based research leading to the ultimate selection of the flight sample composition, including design, fabrication and testing, all of which are expected to contribute to an improved comprehension of materials processing in space.

The SPAR project was coordinated and managed by MSFC as part of the Microgravity Science and Applications (MSA) program of the Office of Space Science and Applications (OSSA) of NASA Headquarters.

This technical memorandum is directed entirely to the payload manifest flown in the tenth of a series of SPAR flights conducted at the White Sands Missile Range (WSMR) and includes the experiments entitled "Containerless Processing Technology," SPAR Experiment 76-20/3; "Directional Solidification of Magnetic Composites," SPAR Experiment 76-22/3; "Comparative Alloy Solidification," SPAR Experiment 76-36/3; and "Foam Copper," SPAR Experiment 77-9/1R.

17. KEY WORDS	18. DISTRIBUTION STATEMENT
Space processing Solidification Containerless processing Foam-Copper	Unclassified - Unlimited Subject Category 15

19. SECURITY CLASSIF. (of this report)	20. SECURITY CLASSIF. (of this page)	21. NO. OF PAGES	22. PRICE
Unclassified	Unclassified	90	A05

For sale by National Technical Information Service, Springfield, Virginia 22161

NASA-Langley, 1986

End of Document